NOVEL QUANTUM PHASES IN ULTRACOLD ATOMS IN OPTICAL SUPERLATTICES

A thesis
submitted for the degree of

Doctor of Philosophy

To
The Department of Physics
Mangalore University

By

Arya Dhar

Indian Institute of Astrophysics
Bangalore - 560 034, India

August 2013

Certificate

This is to certify that the thesis entitled **"Novel Quantum Phases in Ultracold Atoms in Optical Superlattices"** submitted to the Mangalore University by Mr. Arya Dhar for the award of the degree of Doctor of Philosophy in the faculty of science, is based on the results of the investigations carried out by him under my supervision and guidance, at the Indian Institute of Astrophysics. This thesis has not been submitted for the award of any degree, diploma, associateship, fellowship, etc., of any university or institute.

Bangalore
August, 2013

Prof. Bhanu Pratap Das
(Thesis Supervisor)

Declaration

I hearby declare that the thesis titled **"Novel Quantum Phases in Ultracold Atoms in Optical Superlattices"** is the result of the investigations carried out by me at the Indian Institute of Astrophysics, Bangalore under the guidance and supervision of Prof. Bhanu Pratap Das. This thesis has not been submitted for the award of any degree, diploma, associateship, fellowship, etc. of any university or other institutes.

In keeping with the general practice of reporting scientific observations, due acknowledgment has been made whenever the work described is based on the findings of other investigators. Any omission which might have occurred by oversight or error in judgment is regretted.

Bangalore
August, 2013

Arya Dhar
(PhD Candidate)

Dedicated to,

My Parents and My Friends

Acknowledgements

The first person I would like to gratefully acknowledge is my thesis supervisor, Prof. Bhanu Pratap Das. His precious guidance and constant support helped me to achieve this important milestone in my life. His faith on me and the constant belief that he would support me through whatever I do right gave me invaluable confidence to move ahead. The way he gave me independence to do research, while at the same time discussing with me regularly about the progress has truly helped me a lot. There has been so much to learn from him during these years, that it would be futile to list all of them. Those long hours of discussion with him, not only on science, but also on varied other subjects, like politics, history, social issues have enriched me immensely. His sense of judgement always impressed me, and at the same time he never imposed anything on anyone. Instead he gave me the liberty to decide myself, but always guiding me how to take the correct decisions with reasons. He has been a wonderful teacher, showing extraordinary patience in explaining anything. It has been a real honour for me to work with him, and I have thoroughly enjoyed every moment of it. I sincerely thank him for all the love and affection he has shown to me, and I know deep in my heart, that wherever I go in future, I can always come back to him for the right advice and guidance.

I am also very much thankful to Dr. Ramesh V. Pai, for sharing his expertise on ultracold atoms and the different numerical techniques. In the initial stage of my PhD career, he helped me a lot to learn the techniques, especially from the point of view of coding. He generously gave his code for me to use in my PhD thesis, for which I will always be indebted to him. I also thank him for arranging my visit to Goa University twice, from which I have benefitted tremendously. He has been very patient, and always helpful to me. I am deeply grateful for his assistance.

Dr. Tapan Mishra was my senior at IIA, and also in Prof. Das' group. I can never forget his contribution throughout my PhD. Whenever I was stuck at something, I could

freely approach him for his suggestions, and he was always ready to help me. His constant support as well as drive, helped me to be on my toes. I am truly thankful to him for not only his guidance in scientific matters, but also as a friend.

I am also thankful to Dr. Subroto Mukerjee and Dr. Arun Paramekanti for willing to collaborate with our group. Discussions with them have been a real learning experience for me. Their insights in different topics in physics have amazed me a lot.

I would like to thank Dr. Davide Rossini and Prof. Rosario Fazio for inviting me to visit Scuola Normale Superiore, Pisa, Italy twice, and agreeing to start collaborations. I am grateful to them for sharing their codes with our group and I look forward for future projects.

I would like to thank Prof. Diptiman Sen, for giving time to me for intense discussions. His ability to explain things from different perspectives helped me a lot during my research. I am also thankful to Prof. Debashis Mukherjee and Dr. Bijaya Kumar Sahoo for useful scientific discussions and suggestions.

I would like to thank my MSc thesis guide at IIT-Delhi, Prof. D. Ranganathan for his encouragement and support. I would also like to thank Dr. Amruta Mishra, Dr. S. Ghosh, Dr. V. Banerjee at IIT-Delhi for renewing my interests in physics.

I would like to thank Dr. Ananda Dasgupta for his unsurmountable contribution in inspiring me to take up physics as a career option. I am deeply grateful for his invaluable support and encouragement throughout. I still remember those evening sessions at his house during my undergraduate days, where we could ask any question from anywhere in physics, and he would explain to us in his style, clearing all our doubts.

I also want to acknowledge the contributions from my B.Sc. teachers, especially Prof. Albert Gomes, Prof. D. Sengupta, Dr. Shibaji Banerjee, Dr. Tapati Dutta, Dr. Suman Banerjee for their great teaching and also inspiring me for the rest of my life.

I would like to remember and thank all my teachers in my school at St. Xavier's,

Kolkata for shaping me the person I am. The list is too long, and so it won't be possible to name everyone. But one person whose name comes up at this very moment is Late Ms. Mary Chatelier. She was a wonderful teacher, although she never taught me directly in class. She has been an idol for inspiration for me throughout my life. Because of family relations, I was extremely close to her, and hence got the opportunity to learn so much from her.

I still remember my days at the nursery school, Roses' Land in Kolkata. It was the first step outside the house and into this real world. I was fortunate enough to get some extraordinary teachers, such as "Boro" Aunty, Gopadi, Mili Aunty, Kaberi Aunty, and so on. I am truly thankful to them for their caring attitude. Their nurturing at the initial stages has helped me to become what I am today.

Coming to IIA, the one person who deserves special mention is Ramyoo (Ramya P.). She has been truly a unique friend to me, standing beside me through all the difficult times. She was always present there to listen to my problems, and giving me the right advices. I am extremely fortunate to get a friend like her, and I extend my sincere gratitude to her. I am also thankful to her brother, Unni, and her parents for their care and kind hospitality.

I would like to thank my group member, Manpreet Singh, for the interesting discussions. He was always ready to help me, especially in coding aspects.

I would like to sincerely thank Avijeet and Krishna, my roommates, with whom I had spent a wonderful time. After coming back to room after a hard day's work, it was always refreshing to chat with them and get energized.

I would like to thank my batchmates : Ramyoo, Indu, Sindhuja, Hema, Prashanth, Rathnakumar, Dinesh for the wonderful first year we spent together during our coursework. Travelling to IISc and RRI to attend the classes were really very enjoyable moments. Spending nights in the library, solving assignments can never be forgotten.

I would like to thank Sreejith, Avinash and Vaidehi for being such wonderful office-mates, and creating such a pleasant atmosphere in the office. I would like to thank Sajal for his caring nature and being such a nice friend.

I would like to thank Chandrashekhar, Ananthyaa, Vineeth, Arun, Pradeep, Smitha, Sudhakar, Samyaday, Shubham, Sagar, Manogna, Sangeetha, Sowmya, Supriya, Susmita, Joby, Prasanna, Honey, Tanmoy, Sudip, Joice, Mayuresh, Prasanna Deshmukh, Jayashreedidi, Smitha S, Swatididi, Drisya for their friendship which made my life in IIA a memorable one. I would also like to thank my seniors : Nataraj, Veeresh, Girijesh, Blesson, Vigeesh, Anant, Madhulita, Sreeja for their precious advice during my initial days at IIA. It is my great priviledge and honour to have such a wonderful companionship in IIA. The hostel life, where we all stayed together, has been a spectacular experience for me, and I thank the Bhaskara Committee for making our stay at Bhaskara an enjoyable one. I am also thankful to all the members of the play "Heaven abolished" which was performed at IIA. I also enjoyed all the extracurricular activities at IIA, including football, cricket, table tennis, and others. I am also grateful to Sreejith and Joice for taking their time to teach me cycling. The Students' Discussion Forum was a memorable experience where I learnt a lot from my friends and share my views. I am also grateful to all for providing me with the opportunity to run the Friday Movie Club for more than three and a half years. I hope I have been able to entertain all those who came for the movies.

In the last few months at IIA, I was fortunate enough to have a friend like Omelette (Amruta), and I am extremely thankful to her for the wonderful times spent. I am also thankful to John and Estrella for the fun times we had together. I also cannot forget my BSc friends : Amit, Sayan, Beas, Sumitra, Tryambak, Mehuli, and my MSc friends : Sambuddha, Arindam, Kasturi, Sanhita, Shivkant, etc. for the wonderful times spent during college and IIT days. I would also like to thank my dear friend Arpan and Bouthan, whose constant inspiration and support helped me through tough times in my life.

I am thankful to the Director of IIA, the Dean and the Board of Graduate Studies

(BGS) for facilitating all academic matters during my PhD tenure. I am also thankful to Dr. Dipankar Banerjee, Dr. Pravabati Chingangbam, Dr. Preeti Kharb, Dr. Manoj, Dr. D. C. V. Mallik, Dr. Sushma Mallik, Dr. Sivarani, Dr. Ravinder Banyal, Dr. Mousuni Das, Dr. Firoza Sutaria, Dr. Edwin Ebenezer, Prof. Sivaram for their encouragement and valuable discussions. I am also thankful to all the teachers during my coursework in the first year at IIA. I am extremely thankful to Dr. Baba Varghese, Fayaz and Ashok for helping me extensively with computer related issues. I am also thankful to Dr. Rajaguru and Anish for helping me regarding high performance computing issues in the Hydra cluster. I am also extremely thankful to Deepika and Janaki from CDAC for helping me with running jobs in Garuda.

I am grateful to Professor Balakrishna, Professor Dharmaprakash and Professor Bijayakumar of Mangalore Univerisity for providing all kinds of official help. I also thank Ms Anitha of the registrar's office of Mangalore University for helping me by making the official procedure related to my registration smooth.

I would like to thank the administrative people at IIA for their cooperation in all matters. In particular I would like to mention Dr. Kumaresan, Mr. Narasimha Raju, Mr. S. B. Ramesh, Mr. Valsalan, Mr. Parthasarathy, Mr. Lakshmaiah, Mr. Sankar, Ms. Meena, Mr. Rajendran, Mr. Mohan, Mr. Monappa, Ms. Veronica, Ms. Savithri, Mr. Narasimhamurthy, Mr. Murali, Mr. Pranesh, Mr. John, Mr. Iyengar, Mr. Dhananjaya, Mr. Rajan, Ms. Pramila (Director's office), Ms. Malini, Ms. Pramila (Dean's office), Mr. Suresh for their kind help and support, which enabled me to proceed through administrative activities without any hassles.

I would like to take this opportunity to thank Karabi, without whom it would have been impossible to sustain this long. Her constant support, encouragement and affection were indispensable. I would also like to thank her parents for the care and amiable hospitality shown to me.

I am fortunate enough to belong to a family, where we are still connected with everyone. This strong bond rescues us from loneliness. I am happy to have so many relatives whose blessings and well wishes always surround me. The list is so long that I will not even dare to start writing, but I sincerely thank each and everyone of them for being there beside me.

I would also like to thank to all those people who came into my life briefly and contributed significantly. It has been a collective contribution from everyone that I am here.

Let me end this long acknowledgement with the people without whom I would not be standing on this planet, "baba" and "ma", my father and mother. Thanks would be too small a word to account for their immense contributions in my life. Hailing from a middle-class family in Kolkata, they never imposed anything on me. In fact, at a time when studying engineering was an obvious choice, and I chose to study physics, not once did they object. On the contrary, they encouraged and supported me throughout, and they are still doing it withour faltering even once. Their love and affection has been a constant driving force and I hope it never stops.

Arya Dhar

Abstract

Ultracold atoms is one of the most rapidly expanding fields of modern science. Its applications are not restricted to just atomic and molecular physics, but also to condensed matter physics, astrophysics, quantum information, and many more areas. This has become possible because of the unprecedented advances on the experimental front, where various physical quantities characterising a system can be exquisitely controlled to very high precision. The focus of the thesis is on the existence of different quantum phases and transitions between them in a system of ultracold bosonic atoms loaded in an optical superlattice.

Using two different numerical techniques, the mean-field theory and the density matrix renormalisation group (DMRG) method, this system has been analysed in details, revealing novel quantum phases depending on the densities and the values of the system parameters. This novel quantum phase, which has a periodic variation in the number occupancy in the sites, have been named as the superlattice induced Mott insulator (SLMI). This phase arises in addition to the usual Mott insulator (MI) and superfluid (SF) phases. Results from both the numerical methods are in qualitative agreement with each other. The effects of the three-body interaction on these quantum phases and the critical points of various quantum phase transitions are studied. At higher densities, it is found that the insulating lobes get enlarged in the presence of the three-body interaction. Apart from this, it is also seen that the SF phase shifts in the phase diagram when three-body interaction is included. A possible experimental scneario is proposed which can be employed to measure the three-body interaction strengths.

Ultracold atoms in different lattice geometries are very interesting to explore since they contain rich physics in it. Two such cases are studied in this thesis. First an optical superlattice with nearest and next-nearest hopping is considered. Such a model can be mapped exactly into a zig-zag ladder with different potential depths along the two chains. Using finite-size DMRG method, a detailed analysis is performed for hard-core bosons at half-filling, spanning a wide range of values of the next-nearest hopping amplitudes in both positive and negative directions. In the positive region, it is found that the system exhibits two phases, the SLMI phase and the SF phase, and there is a phase transition to the latter as the magnitude of the next-nearest tunneling amplitude is increased. On the negative side, in the absence of the superlattice potential, the system goes from the SF phase to the bond-ordered (BO) phase because of the geometric frustration induced in the system. The BO phase has a finite bond order parameter, which distinguishes it from the other phases. However, for finite values of the superlattice potential, the system enters the gapped SLMI phase, and hence the transition to the BO phase occurs at a more negative value of the next-nearest hopping amplitude.

Secondly, a two-leg Bose ladder is considered with inter- and intra-chain hopping such that it induces a net flux of π in each of the plaquette. For low values of interaction, the system is in the gapless phase, with a finite loop current order in each plaquette. This phase is called the chiral superfluid (CSF). At high values of the repulsive interaction, the system resides in the gapped MI phase with no loop current order. However, there lies an intermediate range of interaction values where the the system is gapped, but simultaneously supports staggered loop currents which spontaneously breaks time-reversal symmetry. This unique phase is named as the chiral MI (CMI). The transition from CSF to CMI falls to the Berezinskii-Kosterlitz-Thouless type whereas CMI to MI transition

belongs to the Ising class.

Having studied the time-independent properties of the optical superlattice, the dynamics of ultracold atomic gases in optical superlattice is then pursued. The superlattice potential is made a function of time (linear in nature), such that the system passes through two critical points. Such a time evolution will generate defects. The scaling of these defects formed with the rate of quenching is studied and the validity of Kibble-Zurek mechanism is tested.

List of Publications

Following is the list of my publications till date. It is written in the format; title, authors, journal, volume number, page number, year of publication, arxiv source where ever available.

1. *Quantum phases of ultracold bosonic atoms in a one-dimensional optical superlattice.*
   Arya Dhar, Tapan Mishra, Ramesh V. Pai, and B. P. Das
   Physical Review A **83**, 053621 (2011).

2. *Mean-field analysis of quantum phase transitions in a periodic optical superlattice.*
   Arya Dhar, Manpreet Singh, Ramesh V. Pai, and B. P. Das
   Physical Review A **84**, 033631 (2011)

3. *Bose-Hubbard model in a strong effective magnetic field: Emergence of a chiral Mott insulator ground state.*
   Arya Dhar, Maheswar Majhi, Tapan Mishra, R. V. Pai, Subroto Mukerjee, Arun Paramekanti
   Physical Review A (Rapid Communication) **85**, 041602 (2012).

4. *Three-body on-site interactions in ultracold bosonic atoms in optical lattices and superlattices.*
   Manpreet Singh, **Arya Dhar**, Tapan Mishra, R. V. Pai, B. P. Das
   Physical Review A (Rapid Communication) **85**, 051604 (2012).

5. *Chiral Mott insulator with staggered loop currents in the fully frustrated Bose Hubbard model.*

   Arya Dhar, Tapan Mishra, Maheswar Majhi, R. V. Pai, Subroto Mukerjee, Arun Paramekanti

   Physical Review B **87**, 174501 (2013).

6. *Hardcore bosons in a zig-zag optical superlattice.*

   Arya Dhar, Tapan Mishra, R. V. Pai, Subroto Mukerjee and B. P. Das

   arXiv:1307.4053 (Submitted in Physical Review A).

7. *Quasi-adiabatic dynamics in one-dimensional optical superlattices.*

   Arya Dhar, Davide Rossini, B. P. Das and Rosario Fazio

   To be submitted soon.

List of Presentations

Oral Presentations

1. *Novel Quantum Phases in Ultracold Atoms*

   Presented in IIA In-house Scientific Meeting, April 9, 2010, IIA, Bangalore, India.

2. *Computation of Phases of Ultracold Atoms in Optical Superlattices*

   Invited talk at the 5th GARUDA Partners' Meet, Bangalore, India.

3. *Quantum phases of Ultracold Atoms in a 1-D Optical Superlattice*

   Invited talk at the Indian Asscociation for the Cultivation of Science, Kolkata, India, December 6, 2010

4. *Three-body on-site interactions in ultracold bosonic atoms in optical lattices and superlattices*

   Invited talk at the Scuola Normale Superiore, Pisa, Italy, June 25, 2012

Poster Presentations

1. *Quantum Phases in One-Dimensional Optical Superlattice*

   Presented in Workshop on "Physics of Strong Correlations", Harish-Chandra Research Institute, Allahabad, India.

2. *Quantum Phases in One-Dimensional Optical Superlattice*

   Presented in Conference on "Research Frontiers in Ultra-Cold Atomic and Molecular Gases", Goa, India

3. *Quantum Phases of Ultracold Bosonic Atoms in a One Dimensional Optical Superlattice*

   Presented in Workshop on "Frontiers in Ultracold Fermi Gases", Abdus Salam International Center for Theoretical Physics, Trieste, Italy.

4. *Study of time-dynamics in a one dimensional optical superlattice*

   Presented in Workshop on "Quantum Simulations with Ultracold Atoms", Abdus Salam International Center for Theoretical Physics, Trieste, Italy.

Contents

List of Figures

List of Tables

Chapter 1

Introduction

In 1924-25, following the work of Satyendranath Bose, Albert Einstein predicted a unique state of matter, which can be obtained if a system of dilute gas of *bosons* are trapped and cooled to temperatures very near to absolute zero [1, 2]. Under these conditions, a large fraction of the bosons occupy the lowest single particle quantum state. This phenomenon of a macroscopic number of particles condensing to one state came to be known as Bose-Einstein Condensation (BEC). But the experimental observation of this state of matter eluded the scientists for seventy long years. Extensive developements in the cooling and trapping techniques in the the 1970's and 80's [3, 4, 7, 6, 7] paved way for the first experimental observation of BEC in the laboratory in 1995 [8, 9, 10, 11]. The Nobel Prize in Physics was given for this landmark achievement in 2001. This discovery led to detailed studies of the properties exhibited by BEC in various forms [12, 13].

A new field was emerging in parallel with the experiments on atomic BEC. It started with the theoretical analysis of the Bose-Hubbard model by Fisher *et al* in 1989 [14]. A phase transition from the Mott insulator (MI) to the superfluid (SF) phases was predicted in their seminal paper. Then in 1998, Jaksch *et al* proposed the idea of observing this quantum phase transition using ultracold atoms in optical lattices [15, 16]. Following the advances in the creation of optical lattices using laser beams and trapping ultra-

cold atoms in these systems, Greiner *et al* in 2002 were successful for the first time to observe this quantum phase transition [17, 18]. This astounding feat opened the doors of an exciting field whereby ultracold atoms of different species can be trapped in a variety of lattice geometries and their properties studied both theoretically and experimentally [16, 19, 20, 21, 22, 23, 24]. The unique features of these systems are that they are nearly defect free, the interaction strengths (both magnitude and signs) and other lattice parameters can be controlled and tuned to very high degree of accuracy. Regimes that were not accessible earlier are now within experimental reach via ultracold atoms, which have become testbeds to study and verify various phenomena from different branches of physics. The applications of these systems have grown over the years, and these range from simulating a host of condensed matter systems such as low dimensional systems [25, 26, 27, 28, 29, 30, 31], spin systems [32, 33, 34, 35, 36], disordered systems [37, 38, 39, 40, 41, 42], high T_c superconductivity [43, 44, 45], BCS-BEC crossover [46, 47, 48, 49, 50, 51], quantum magnetism [52, 53] to problems in astrophysics [54] and quantum field theory [55, 56]. Ultracold atoms in optical lattices have also emerged as a possible candidate for quantum computers [57, 58]. The field of ultracold atoms is therefore clearly one of the areas in the forefront of modern physics [59, 60]. The present thesis addresses some problems of current interest in this field.

1.1 Quantum Phase Transitions

We frequently encounter phase transitions in our everyday life, the most common being ice melting to water, and water boiling off to steam. These phase transitions are driven by changes in temperature, and are called classical phase transitions (also called thermal phase transitions). The classical phase transitions occur due to competition between the energy of the system and the entropy of its thermal fluctuations. But there exists another class of transitions which occur at temperature, $T = 0$. This transition takes place by tuning a non-temperature parameter, and are called quantum phase transitions

(QPT) [61]. The underlying source for QPT are quantum fluctuations, unlike thermal ones for the classical phase transitions. Quantum fluctuations are characterised by the quantity $\hbar\omega$ whereas for thermal fluctuations, it is k_BT. So even at finite temperatures, when $\hbar\omega > k_BT$, the properties of the system will be dominated by quantum fluctuations, and so we expect to see remnants or traces of the QPT even at low enough finite temperatures. At high enough temperatures, the system enters the classical regime, which is dominated by classical (thermal) fluctuations.

1.1.1 Quantum Phases in an Optical Lattice

The simplest way to form a one-dimensional optical lattice is by superposing two counter propagating laser beams, each having the same frequency. An electron in an atom in the presence of an oscillating electric field, $E(r,\mathrm{t})$ of the laser attains a time-dependent dipole moment, d. When the field frequency is far off from resonance, the induced dipole moment follows the laser field oscillations. The energy of an atom thus gets shifted, and this energy shift may be regarded as an external potential, V acting on the atom. This is given by

$$V = -\frac{1}{2}\alpha'(\omega)\langle E(r,t)^2\rangle_t \tag{1.1}$$

where α' is the real part of the dynamical polarizability of the atom, which can be expressed in terms of the dipole moment, d, the ground state and excited state energies, the frequency of the laser beam and the lifetime of the excited state. $\langle E(r,t)^2\rangle_t$ is the square of the electric field, averaged over a time much longer than the period of the wave. Therefore to make a lattice potential, it is necessary to construct an electric field such that $\langle E(r,t)^2\rangle_t$ is periodic in space, which is provided by the counter propagating laser beams. The height of the energy barrier depends on the intensity of the lasers and the real part of the polarizability. Higher dimensional lattice potentials can be constructed

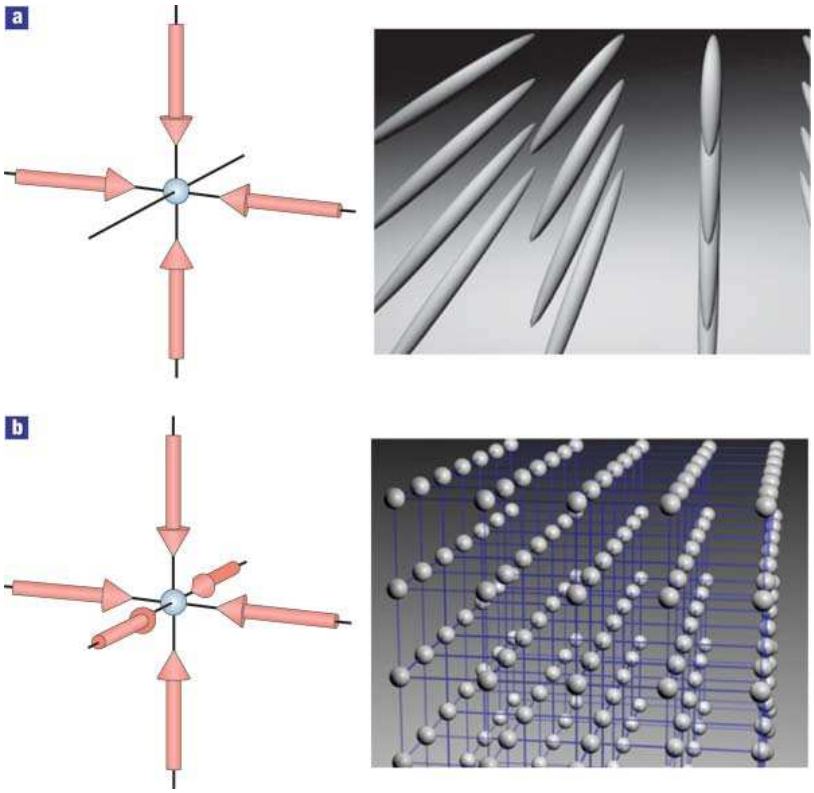

Fig. 1.1: Schematic illustration of two dimensional (a) and three dimensional optical lattice (b)

by superimposing more than two beams with different wave vectors.

The system of ultracold atoms loaded in an optical lattice can be best described by the Bose-Hubbard model given by

$$H = -t \sum_i a_i^\dagger a_{i+1} + h.c. + \frac{U}{2} \sum_i n_i(n_i - 1) \tag{1.2}$$

In the above equation, $a_i^\dagger$ (a_i) creates (destroys) a particle at site i. They obey the commutation relation for bosons : $[a_i^\dagger, a_j] = \delta_{ij}$. The number operator at a particular site i is given by operator n_i. The tunneling probability amplitude is given by t. Since the hopping probability decreases exponentially with distance, hopping is typically assumed to occur between nearest neighbouring sites. The on-site inter-atomic repulsive interaction is given by U. This interaction is usually short-range, similar to van der Waals forces.

When the interaction between atoms is weak compared to the tunneling probability

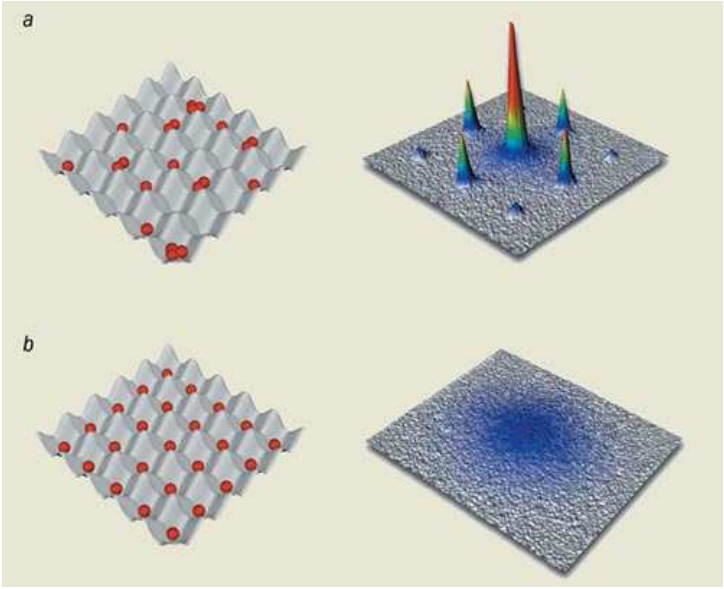

Fig. 1.2: By changing the lattice potential depth, one can undergo a quantum phase transition from SF (a) to MI (b) transition. SF phase is characterised by zero gap with fluctuating number of atoms at each site, whereas MI phase has a fixed number of atoms at all the sites. The left panel shows schematically the two phases whereas the right panel denotes the interference peaks observed in experiments

amplitude, the states of the many-atom system can be approximated as superpositions of single-atom Bloch states. In the ground state, all atoms occupy the Bloch state with lowest energy. This corresponds to a Bose-Einstein condensed state with perfect correlations between the phases of the condensate wave function on different sites, although the number of atoms on each site is not fixed. The atoms are mobile, and respond to weak force. This corresponds to the situation for electrons in metals. In this state, the system is gapless in nature, and such a phase of matter is called the superfluid (SF) phase.

On the other extreme, when hopping amplitude is negligible compared to the on-site interaction energy, the atoms cannot move from one site to another. The ground state of the hamiltonian in this scenario will have an integer number of atoms on each site and there are no phase correlations between different sites, the reason being that the energy is independent of the phases of the wave function. In particular, each site has equal number of atoms in this phase. If in this state, one atom is removed from the system, then one site has one less atom, while one site will have one additional atom. This will result in

a finite amount of change in interaction energy. Consequently, there is an energy gap between the ground state and the lowest excited state. This gapped phase is called as the Mott insulator (MI). As the ratio of the tunneling matrix element to the repulsive energy increases, the system undergoes a phase transition from MI to SF phase.

1.1.2 Experimental Detection of the Quantum phase transition between MI and SF phases

Greiner *et al* in 2002 first provided the experimental evidence for the SF-MI transition [17]. The basic concept behind the experiment is to suddenly switch off the lattice potentials and all other trapping potentials, and let the cloud of atoms expand. This will result in sharp interference peaks if there is coherence between the phases of the atoms on different sites, as in the SF phase, whereas there will be smooth distribution of atoms, with a blurred interference pattern, if there is no coherence as in the case of MI state. They had performed the experiment in a three dimensional optical lattice, and so in the superfluid regime, where all the atoms are delocalized over the entire lattice with equal relative phases between different sites, a high contrast three-dimensional interference pattern was obtained as shown in Fig.(1.3). Tuning the laser intensity leads to the transition into the MI phase, where no interference pattern is visible at all, implying the complete loss of phase coherence as shown in Fig.(1.3).

They also probed into the excitation spectrum to distinguish between the two phases. The lowest lying excitation in the MI phase is the creation of a particle-hole pair, where an atom is removed from a lattice site and added to a neighbouring site. Due to the presence of doubly occupied site, the energy of the system will be raised by an amount equal to U, the on-site repulsive interaction, above the state with singly occupied site. Therefore, to create an excitation, the finite amount of energy U is required. This is provided by tilting the lattice potential through the application of a potential gradient. This allows tunneling if the energy difference between neighbouring lattice sites due to

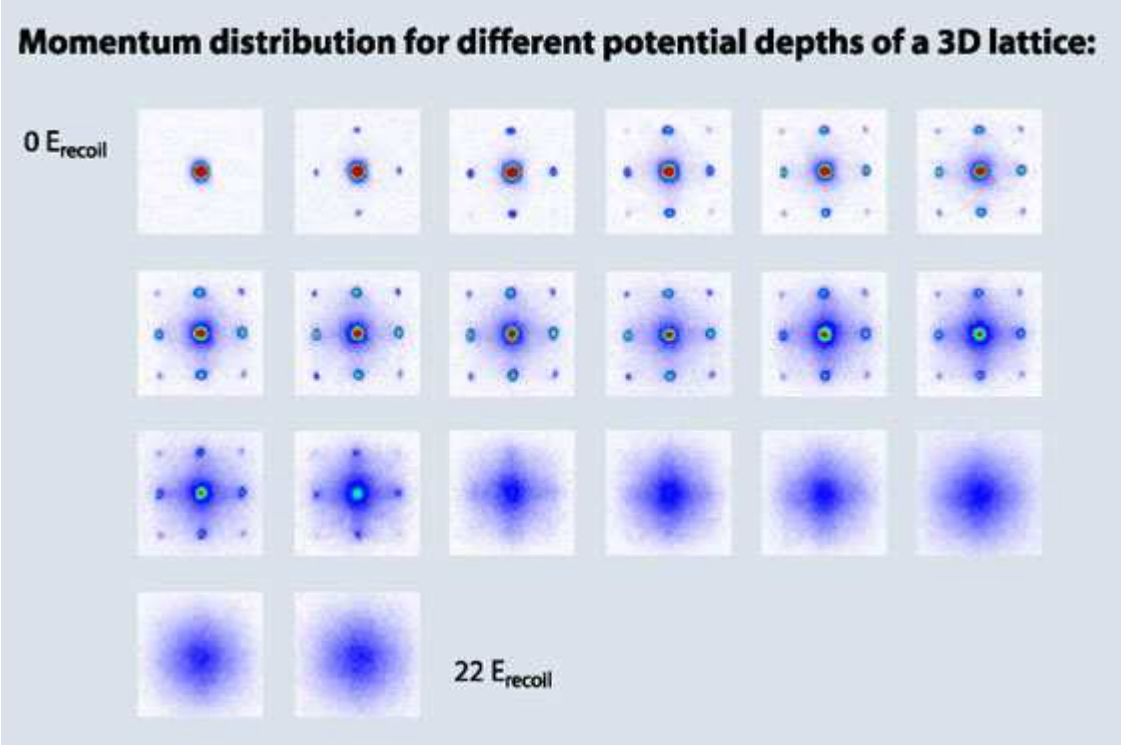

Fig. 1.3: Absorption images of multiple matter wave interference patterns. These were obtained after suddenly releasing the atoms from the lattice potentials of various depths ranging from 0 E_R to 22 E_R, where E_R is the recoil energy.

the potential gradient is equal to U, the on-site interaction energy. Two narrow resonance peaks are clearly visible on top of an otherwise completely flat excitation probability. The first resonance peak can be attributed to the creation of a particle-hole pair in the MI phase, and directly proves that one has entered the MI regime. The second resonance, which is weaker and has exactly twice the energy difference compared to the first, can happen due to a number of reasons :

- Simultaneous tunneling of two particles in a MI phase with $n > 1$ atoms.
- Second order process, in which two particles-hole pairs are created simultaneously
- Tunneling process occurring between lattice sites with $n = 1$ atom next to lattice sites with $n = 2$ atoms.

1.1.3 Outline of the forthcoming chapters

Having given an introduction to the optical lattice, and the possible basic quantum phases, we now outline the forthcoming chapters in this thesis. In the next chapter, the different theoretical methods used in this thesis, such as the Mean-Field Decoupling Approximation, density matrix renormalisation group (DMRG) method and the matrix product states (MPS) method are described in detail. The third chapter is concerned with the mean-field and the DMRG treatments of an optical superlattice with soft-core bosons. The different phases such as the superfluid (SF) and the Mott insulator (MI) phases along with a novel quantum phase with a periodic variation in the occupation, which is called as the superlattice induced Mott insulator (SLMI) are presented and discussed. The complete phase diagram is obtained for density one, with other relevant physical quantities needed to distinguish between the phases. Chapter 3 ends with the inclusion of three-body on-site interaction in the Bose-Hubbard hamiltonian modified for optical superlattice, and analyses the shifts in the transition points that occur because of this interaction. An experiment is also proposed at the end of the Chapter 3 to detect the

three-body interaction. Chapter 4 contains frustrated ladded systems, and is divided into two parts. The first part deals with the nearest and next-nearest neighbour hopping in an optical superlattice. The phase diagram is plotted for this system along with different signatures for the phase transitions. The second part deals with a two-leg Bose ladder, with inter- and intra-chain hopping amplitudes having signs such that it induces an effective π flux in each of the plaquettes. A detailed analysis reveals a very remarkable phase sandwiched between the conventional MI phase and SF phase with currents. This phase is gapped, while simultaneously supporting staggered loop currents, and is called chiral Mott insulator (CMI) phase. In Chapter 5, we move over from the static to the dynamic regime. By considering the superlattice potential as a function of time, the effect of quenching through two quantum critical points are studied rigorously. The defect generation, which is proportional to the residual energy, is found to have a power law dependence on the quench rate. Finally, Chapter 6 summarizes our findings, and concludes with future directions.

References

[1] S. Bose, Z. Phys. **26**, 178 (1924)

[2] A. Einstein, *Sitzungsberichte der Preussischen Akademie der Wissenschaften, Physikalisch-mathematische Klasse* (1924), p. 261; (1925), p.3.

[3] S. Chu, Rev. Mod. Phys. **70**, 685 (1998).

[4] C.N. Cohen-Tannoudji, Rev. Mod. Phys. **70**, 707 (1998).

[5] W.D. Phillips, Rev. Mod. Phys. **70**, 721 (1998).

[6] H.J. Metcalf and P. van der Straten, *Laser Cooling and Trapping*, (Springer, Berlin, 2001).

[7] P. Meystre, *Atom Optics*, (American Institute of Physics, Ridge, NY, 2001).

[8] M.H. Anderson, J.R. Ensher, M.R. Matthews, C.E. Wieman, and E.A. Cornell, Science **269**, 198 (1995).

[9] K.B. Davis, M.O. Miewes, M.R. Andrews, N.J. van Druten, D.S. Durfee, D.M. Kurn, and W. Ketterle, Phys. Rev. Lett. **75**, 3969 (1995).

[10] E.A. Cornell and C.E. Wieman, Rev. Mod. Phys. **74**, 875 (2002).

[11] W. Ketterle, Rev. Mod. Phys. **74**, 1131 (2002).

[12] L. Pitaevski and S. Stringari, *Bose-Eisntein condensation*, (Clarendon Press, Oxford, 2003).

[13] C. J. Pethick, and H. Smith, *Bose-Einstein Condensation in Dilute Gases*, (Cambridge University Press, Cambridge, 2008).

[14] M.P.A. Fisher, P.B. Weichman, G. Grinstein, and D.S. Fisher, Phys. Rev. B **40**, 546 (1989).

[15] D. Jaksch, C. Bruder, J. I. Cirac, C. W. Gardiner, and P. Zoller, Phys. Rev. Lett. **81**, 3108 (1998).

[16] D. Jaksch, H.-J. Briegel, J. I. Cirac, C. W. Gardiner, and P. Zoller, Phys. Rev. Lett. **82**, 1975 (1999).

[17] M. Greiner, O. Mandel, T. Esslinger, T. W. Hänsch and I. Bloch, Nature **415**, 39 (2002).

[18] I. Bloch, Physics World **17**, 25 (2004).

[19] M. Köhl, H. Moritz, T. Stöferle, K. Günter, and T. Esslinger, Phys. Rev. Lett. **94**, 080403 (2005)

[20] L. Fallani, J. E. Lye, V. Guarrera, C. Fort, and M. Inguscio, cond-mat/0603655.

[21] S. Ospelkaus, C. Ospelkaus, O. Wille, M. Succo, P. Ernst, K. Sengstock, and K. Bongs, Phys. Rev. Lett. **96**, 180403 (2006).

[22] K. Günter, T. Stöferle, H. Moritz, M. Köhl, and T. Esslinger, Phys. Rev. Lett. **96**, 180402 (2006.)

[23] T. Volz, N. Syassen, D. M. Bauer, E. Hansis, S. Dürr, and G. Rempe, Nature Phys. **2**, 692 (2006).

[24] K. Winkler, G. Thalhammer, F. Lang, R. Grimm, J. Hecker-Denschlag, A. J. Daley, A. Kantian, H. P. Büchler, and P. Zoller, Nature **441**, 853 (2006).

[25] F.H.L. Essler, H. Frahm, F. Göhmann, A. Klümper, and V. E. Korepin, *The One-Dimensional Hubbard Model*, (Cambridge University Press, Cambridge, 2005).

[26] Th. Giamarchi, *Quantum Physics in One Dimension*, (Oxford University Press, Oxford, 2004)

[27] U. Schollwöck, Rev. Mod. Phys. **77**, 259 (2005).

[28] M.A. Cazalilla, J. Phys. B- Atom. Molec. Phys. **37**, S1 (2004).

[29] A. Recati, P.O. Fedichev, W. Zwerger, and P. Zoller, Phys. Rev. Lett. **90**, 020401 (2003).

[30] B. Paredes and J.I. Cirac, Phys. Rev. Lett. **90**, 150402 (2003).

[31] C. Kollath, U. Schollwöck, and W. Zwerger, Phys. Rev. Lett. **95**, 176401 (2005).

[32] D. Jaksch and P. Zoller, Ann. Phys. (N.Y.) **315**, 52 (2005).

[33] J. J. García-Ripoll, M.A. Martin-Delgado, and J.I. Cirac, Phys. Rev. Lett. **93**, 250405 (2004).

[34] L. Santos, M.A. Baranov, J.I. Cirac, H.-U. Everts, H. Fehrmann, and M. Lewenstein, Phys. Rev. Lett. **93**, 030601 (2004).

[35] L.-M. Duan, E. Demler, and M.D. Lukin, Phys. Rev. Lett. **91**, 090402 (2003).

[36] U. Dorner, P. Fedichev, D. Jaksch, M. Lewenstein, and P. Zoller, Phys. Rev. Lett. **91**, 073601 (2003).

[37] B. Damski, J. Zakrzewski, L. Santos, P. Zoller, and M. Lewenstein, Phys. Rev. Lett. **91**, 080403 (2003).

[38] R. Roth and K. Burnett, J. Opt. B: Quantum Semiclass. Opt. **5**, S50 (2003).

[39] R. Roth and K. Burnett, Phys. Rev. A **68**, 023604 (2003).

[40] A. Sanpera, A. Kantian, L. Sanchez-Palencia, J. Zakrzewski, and M. Lewenstein, Phys. Rev. Lett. **93**, 040401 (2004).

[41] V. Ahufinger, L. Sanchez-Palencia, A. Kantian, A. Sanpera, and M. Lewenstein, Phys. Rev. A **72**, 063616 (2005).

[42] J. Wehr, A. Niederberger, L. Sanchez-Palencia, and M. Lewenstein, cond-mat/0604063.

[43] W. Hofstetter, J.I. Cirac, P. Zoller, E. Demler, and M.D. Lukin, Phys. Rev. Lett. **89**, 220407 (2005)

[44] A.O. Koetsier, D.B.M. Dickerscheid, H.T.C. Stoof, Phys. Rev. A **74**, 033621 (2006).

[45] T. Stöferle, H. Moritz, K. Günter, M. Köhl, and T. Esslinger, Phys. Rev. Lett. **96**, 030401 (2006)

[46] S. Inouye, M.R. Andrews, J. Stenger, H.-J. Miesner, D.M. Stamper-Kurn, and W. Ketterle, Nature **392**, 151 (1998).

[47] S.L. Cornish, N.R. Claussen, J.L. Roberts, E.A. Cornell, and C.E. Wieman, Phys. Rev. Lett. **85**, 1795 (2000).

[48] E. Timmermans, P. Tommasini, M. Hussein, and A. Kerman, Phys. Rep. **315**, 199 (1999).

[49] M.W. Zwierlein, J.R. Abo-Shaeer, A. Schirotzek, C.H. Schunck, and W. Ketterle, Nature **435**, 1047 (2005).

[50] M.W. Zwierlein, A. Schirotzek, C.H. Schunck, and W. Ketterle, Science **311**, 492 (2006).

[51] G.B. Partridge, W.H. Li, R.I. Kamar, Y.A. Liao, and R.G. Hulet, Science **311**, 503 (2006).

[52] D. Stamper-Kurn and W. Ketterle, cond-mat/0005001, Proceedings of Les Houches 1999 Summer School, Session LXXII.

[53] E. Demler and F. Zhou, Phys. Rev. Lett. **88**, 163001 (2002).

[54] A. Gezerlis and J. Carlson, arXiv:1109.4946v1.

[55] K. Osterloh, M. Baig, L. Santos, P. Zoller, and M. Lewenstein, Phys. Rev. Lett. **95**, 010403 (2005).

[56] J. Ruseckas, G. Juzeliunas, P. Öhberg, and M. Fleischhauer, Phys. Rev. Lett. **95**, 010404 (2005)

[57] A. Kitaev, Ann. Phys. (N.Y.) **321**, 2 (2006).

[58] B. Douçot, M.V. Feigelman, L.B. Ioffe, A.S. Ioselevich, Phys. Rev. B **71**, 024505 (2005).

[59] M. Lewenstein, A. Sanpera, V. Ahufinger, B. Damski, A. Sen De, U. Sen, Advances in Physics Vol. **56** Nos. 1-2, January-April 2007, 243-379

[60] M. Lewenstein, A. Sanpera, and V. Ahufinger, *Ultracold atoms in Optical Lattices*, (Oxford University Press, Oxford, 2012).

[61] S. Sachdev, *Quantum Phase Transitions*, Cambridge University Press, Cambridge (1999).

Chapter 2

Numerical Methods

The different quantum phases that we have studied in this thesis are in the framework of Bose-Hubbard model or modifications to it. In this chapter, we shall discuss three different methods for determining the ground state wavefunction and the energy of the Bose Hubbard hamiltonian. These quantities are used in evaluating the signatures of the different phases. As can be seen from Eqn.(1.2), BH model is expanded in the second quantized form, and so it is convenient to work in the occupation number basis.

2.1 Mean Field Theory

A closer look at the hamiltonian described in Eqn.(1.2) would show that there are two types of terms in it. The first type contains operators defined at a single site, whereas the second type has operators defined in different sites, for our case, the neighbouring ones. The presence of these types of multi-site terms that makes it impossible to solve such a hamiltonian. The Mean-Field theory attempts to decouple such terms, so that the hamiltonian can be expressed in terms of single-site operators only.

To demonstrate the mean-field theory we first consider the Bose-Hubbard model for

optical lattice and then move on to optical superlattice. We write the operators a_i and $a_i^\dagger$ as a sum of some mean value and small fluctuations about this mean.

$$a_i = \langle a_i \rangle + \tilde{a_i}; \quad a_i^\dagger = \langle a_i^\dagger \rangle + \tilde{a_i^\dagger} \tag{2.1}$$

where $\langle a_i \rangle$ is the expectation value of the operator a_i with respect to the ground state wavefunction. This approach is similar to that of solving a system of electrons, where the motion of one electron is governed by all the other electrons and vice-versa. In such a situation, a mean-field is considered which is generated by all the other electrons, and the electron moves in such an effective field.

Without loss of generality, we consider $\langle a_i \rangle$ to be real, and so we can replace $\langle a_i \rangle = \langle a_i^\dagger \rangle = \phi_i$, where ϕ_i is also called the superfluid order parameter. Substituting the above expression in the kinetic energy part of Eqn.(1.2), we get :

$$\begin{aligned} -t \sum_{\langle i,j \rangle} (a_i^\dagger a_j + h.c) &= -t \sum_{\langle i,j \rangle} (\tilde{a}_i^\dagger \tilde{a}_j + \tilde{a}_i \tilde{a}_j^\dagger) \\ &\quad -t \sum_{\langle i,j \rangle} (\tilde{a}_i^\dagger \phi_j + \tilde{a}_j \phi_i + \tilde{a}_i \phi_j + \tilde{a}_j^\dagger \phi_i + 2\phi_i \phi_j) \end{aligned} \tag{2.2}$$

The first term is neglected, since it is second order in fluctuations. Such an approximation is valid when t, the hopping amplitude is small compared to other terms in the hamiltonian, such as U, λ, and μ. We then define $\bar{\phi_i} = \frac{1}{z} \sum_\delta \phi_{i+\delta}$, δ being summed over $z = 2d$ nearest neighbours, and get the following mean-field hamiltonian,

$$\begin{aligned} H^{MF} &= -tz \sum_i [\bar{\phi_i}(\tilde{a}_i^\dagger + \tilde{a}_i) + \bar{\phi_i}\phi_i] \\ &\quad + \frac{U}{2} \sum_i n_i(n_i - 1) - \sum_i \mu_i n_i \end{aligned} \tag{2.3}$$

Now substituting back from the relation, $\tilde{a}_i = a_i - \phi_i$, we get the following

$$\begin{aligned} H^{MF} &= -tz\sum_i[\bar{\phi}_i(a_i^\dagger + a_i) - \bar{\phi}_i\phi_i] \\ &\quad + \frac{U}{2}\sum_i n_i(n_i-1) - \sum_i \mu_i n_i \end{aligned} \tag{2.4}$$

Thus, for a homogeneous case in an optical lattice, μ_i, ϕ are the same for all sites, and so we are in a position to write the full hamiltonian as a sum of single-site hamiltonian in the mean-field approximation, i.e., $H^{MF} = \sum_i H_i^{MF}$, and dividing throughout by zt to make the hamiltonian and other parameters dimensionless we get the single site hamiltonian as

$$H_i^{MF} = -\bar{\phi}_i(a_i^\dagger + a_i) + \bar{\phi}_i\phi_i + \frac{\tilde{U}}{2}n_i(n_i-1) - \tilde{\mu}_i n_i \tag{2.5}$$

where $\tilde{U} = U/zt$, $\tilde{\mu}_i = \mu_i/zt$ are dimensionless on-site interaction and chemical potential respectively.

Having written the single-site mean-field hamiltonian, we can solve it in two different ways. The first one is the perturbative approach [12]. In cases where U is much larger than other hamiltonian parameters, the system will be in the MI state with a fixed number of atoms at every site. In such cases, the first two terms in the above equation (the hopping part) may be considered as the perturbation. We can now apply various orders of corrections, to get the wavefunction and energy. Looking at the structure of the perturbative terms, it is evident that only even order corrections will survive.

The second method does not rely on the assumption of an initial ground state. Instead, one assumes an initial value of ϕ_i, and the hamiltonian is expressed in some convenient basis. It is then diagonalised, and with the ground state eigenvector, ϕ_i is evaluated. We then put this value of ϕ_i in the hamiltonian, and keep on iterating till convergence is achieved.

2.2 Density Matrix Renormalisation Group Method

As seen in the previous section, the mean-field theory excludes the fluctuations, or the correlations among atoms present in different sites. Consequently its accuracy is much limited. Hence we use another numerical technique, the density matrix renormalisation group (DMRG) method to evaluate the ground state wavefunction and energy, and eventually other physical quantities of interest.

The basics of DMRG was first developed by S. White in 1992 [2, 3]. Since then, it has become a powerful numerical technique that has been widely used in low dimensional strongly correlated fermionic and bosonic systems. Based on the concepts of renormalisation method, the algorithm begins with a small size of quantum chain, and solving the hamiltonian to find the ground state wavefunction and energy. After this operation, the size of the system is iteratively increased, which also increases the size of the Hilbert space exponentially. As a result, a truncation is done on the Hilbert space at every iteration, thus keeping the states with highest contribution to the ground state of the system. This is continued till the desired length of the system is reached. The details of the DMRG algorithm will be explained elaborately in the following subsections.

2.2.1 Basics of DMRG

Historically DMRG originated from the works of White and Noack in 1992 [2], when they were analysing the failure of the real-space renormalisation group (RSRG) method to give physically relevant solutions of low-energy ground state properties in quantum many-body systems. The principle idea of the DMRG method is based on the concept of density-matrix projection where we consider a small system, embedded in a larger system, so as to mimic a very large system [4, 5, 6, 7, 8]. The information of the '*environment*' (E) is automatically included in the information content of the reduced density-matrix of the small system (S). This will help us to decide the relevant states to be considered

when enlarging the size of the small system to some desired length, L.

Let us consider a scenario where the size of the system has reached l sites, with the size of the Hilbert space being M^S, and the states being denoted as $\{|\omega^S\rangle\}$. Now consider adding one more site to this system. Then the size of the Hilbert space will become $M^S \times N_{site}$, where N_{site} is the size of the Hilbert space of one individual site. Thus the basis states of the combined system and the added single site becomes $\{|\omega^S\sigma^S\rangle\} = \{|\omega^S \otimes \sigma^S\rangle\}$, where $|\sigma^S\rangle$ are the N_{site} basis states of a single site. To get rid of the strong boundary effects, the system (S) is embedded in an environment (E) which is constructed in a similar way. The basis states of E will thus be $\{|\omega^E\sigma^E\rangle\}$. Thus the two parts, the system and the environment blocks, together form the superblock which is of length $2l+2$. The main aim of density-matrix projection is to select a set of m^S states, such that it represents quite accurately certain state, ψ, e.g. the ground state (also called the target state) of the superblock

$$\begin{aligned} |\psi_0\rangle &= \sum_{\omega^S=1}^{M_S}\sum_{\sigma^S=1}^{N_{site}}\sum_{\omega^E=1}^{M_E}\sum_{\sigma^E=1}^{N_{site}} \psi_{\omega^S\sigma^S\omega^E\sigma^E}|\omega^S\rangle|\omega^E\sigma^E\rangle \\ &= \sum_{i,j=1}^{N_S,N_E} \psi_{i,j}|i\rangle \otimes |j\rangle \end{aligned} \tag{2.6}$$

where $|i\rangle = |\omega^S\sigma^S\rangle$ and $|j\rangle = |\omega^E\sigma^E\rangle$ are the basis states of the system (the size of the Hilbert space being $N_S = M_S \times N_{site}$) and environment (the size of the Hilbert space being $N_E = M_E \times N_{site}$) respectively. We now want to obtain a variational wave function, $|\hat{\psi}_0\rangle$, defined in an optimally reduced Hilbert space, generated by the m^S system vectors ($m^S < N^S$) as follows :

$$|\alpha\rangle = \sum_{i=1}^{N_S} u_{\alpha i}|i\rangle \tag{2.7}$$

Thus the variational wavefunction can be written as :

$$|\hat{\psi}_0\rangle = \sum_{\alpha=1}^{m} \sum_{j}^{N_E} a_{\alpha j} |\alpha_j\rangle |j\rangle \tag{2.8}$$

We now try to minimize the modulus of the difference between this trial wave function, and the true wavefnction, with respect to the variational parameters, $a_{\alpha j}$

$$| \, |\psi_0\rangle - |\hat{\psi_0}\rangle \, |^2 \tag{2.9}$$

Substituting the forms of $|\psi_0\rangle$ (Eqn.(2.6)) and $|\hat{\psi_0}\rangle$(Eqn.(2.8)) in Eqn.(2.9), and minimizing lead to the following expression :

$$| \, |\psi_0\rangle - |\hat{\psi_0}\rangle \, |^2 = 1 - \sum_{\alpha,j,i,i'} \psi_{ij} u_{\alpha i} \psi_{i'j} u_{\alpha i'} \tag{2.10}$$

Now, the density matrix for a pure state of the universe is defined as

$$\rho = |\psi_0\rangle\langle\psi_0|$$

But the reduced density matrix of the system is defined as :

$$\begin{aligned} \rho_{ii'} &= \sum_{j} \rho_{ij,i'j} \\ &= \sum_{j} \langle j|\langle i|\psi_0\rangle\langle\psi_0|i'\rangle|j\rangle \\ &= \sum_{j} \psi_{ij}\psi_{i'j} \end{aligned} \tag{2.11}$$

It should be kept in mind that the eigenvectors of the reduced density matrix are in fact $|\alpha\rangle$, with the corresponding eigenvalues being ω_α. Thus after doing all the proper substitutions, we arrive at the following expression :

$$| \, |\psi_0\rangle - |\hat{\psi_0}\rangle \, |^2 = 1 - \sum_{\alpha} \omega_\alpha \tag{2.12}$$

This important result clearly states that the error involved in using the approximate wavefunction by using the truncated Hilbert space is exactly equal to the sum of the discarded eigenvalues of the reduced density matrix of the system. This also implies that to improve the accuracy of this approximation, we should keep those eigenstates of the reduced density matrix, which correspond to the highest eigenvalues, as these states contribute the most to the ground state of the system.

2.2.1.1 Infinite-Size DMRG Algorithm

The infinite size DMRG is used to compute the ground state properties of a quantum chain in the thermodynamic limit, where the length of the chain tends to infinity, i.e. $L \to \infty$. The algorithm consists of the following iterative steps :

1. The hamiltonian $H_{BB'}$ is defined for the superblock (also called the universe), which is formed by putting the two blocks of system [**B**], environment [**B'**] and two added sites [a] and [a']. The non-primed and primed blocks usually have similar structures, but it can vary, for which we need to use finite-size DMRG, as described in the next section.

2. The total Hilbert space of this superblock can be written as the direct product of individual basis of **B**, a, a' and **B'**. The size of the total Hilbert space will be $(mn)^2$, where m and n are the sizes of Hilbert space of the block and one site respectively. But it should be kept in mind that if there are some constraints on the system (e.g. fixed density), then the total size is much less than $(mn)^2$.

3. The hamiltonian, $H_{BB'}$ is diagonalised to obtain the ground state, $|\psi_0\rangle$ using some standard algorithms like the Lanczos or Davidson's. $|\psi_0\rangle$ is called the target state.

4. Using this ground state, the reduced density matrix of the system block, is computed

:

$$\rho_{ii'} = \sum_j \psi_{0,ij}\psi_{0,i'j}$$

where $|\psi_{0,ij}\rangle = \langle i \otimes j|\psi_0\rangle$, and $|i\rangle$, $|j\rangle$ denote the basis states of system block and environment block respectively.

5. The reduced density matrix of the system block is then diagonalised, and the eigenstates corresponding to 'm' highest eigenvalues are retained.

6. A qualitative description of the accuracy can be calculated from the expression $1 - \sum_{\alpha=1}^{m} \omega_\alpha$, where ω_α are the eigenvalues of the reduced density matrix.

7. With these 'm' states, a rectangular matrix 'O' is formed, which is used to transform all the operators in the system block in this new basis, including the hamiltonian.

8. Similar steps are carried out for the system block also, and then [**B** a], [**B'** a'] are renamed as [**B**] and [**B'**] respectively.

9. Two new sites, a and a' are now added and the new superblock [**B** a a' **B'**] is formed.

10. This iteration is continued until the desired length is achieved.

11. If there are more than one target states, then the reduced density matrix is defined as :

$$\rho_{ii'} = \sum_l p_l \sum_j \phi_{l,ij}\phi_{l,i'j}$$

where p_l is the probability of finding the system in the target state, $|\phi_l\rangle$.

2.2.1.2 Finite-Size DMRG

Many a times, infinite-size DMRG do not yield correct resuts. The reason for such behaviour can be attributed to the fact that simulating the final system size may not turn out to be correct by using a small environment block in the early stages of DMRG. Also, if the system is inhomogeneous, or contains impurities randomly distributed, then

infinite-size DMRG cannot take into account such effects, since the total hamiltonian is not known in the intermediate steps. Finite size DMRG attempts to eliminate such problems to a very large extent and also to reduce the truncation error. The flow of the finite-size DMRG algorithm is as follows :

1. The infinite-size algorithm is stopped at some pre-selected size of the superblock, L.

2. Now, instead of simultaneous growth of both the blocks, one of the blocks is grown, at the expense of the other block, thus keeping the total length of the superblock fixed.

3. Reduced basis transformations are performed only for the growing block.

4. Once we reach one end of the superblock by this process, we interchange the blocks which grows, and which shrinks, and the process is continued till it reaches the other end of the superblock.

5. A complete shrinkage and growth sequence of both the blocks is called a *sweep*.

6. Sweeping is continued till the energy values converge.

Such a process will increase the accuracy of the ground-state wavefunction, and the energy, as well as optimize all the operators in the blocks.

2.2.2 Matrix Product States

In this section we introduce one more numerical technique, the Matrix Product states (MPS) method to solve hamiltonians described on a 1-dimensional lattice. The connection between DMRG and MPS, was first pointed out by Rommer and Östlund [9], where they stated that the thermodynamic limit of DMRG can be mapped into a position-independent matrix product wavefunction. From the computational aspect, MPS came

to the spotlight with the help of quantum information perspectives, which led to algorithms to describe periodic boundary problems and finite temprature effects. In the next subsection, we would show how any arbitrary quantum state can be decomposed into the MPS form followed by the variational ansatz of minimizing the energy [10, 11, 12].

2.2.2.1 Expressing a quantum state as MPS

Let us consider a lattice of L sites, with each site described by a local Hilbert space of size d, denoted by $\{\sigma_i\}$, where $i = 1, 2, ...L$. A general state on such a lattice can be written as

$$|\psi\rangle = \sum_{\sigma_1,...\sigma_L} c_{\sigma_1,...\sigma_L} |\sigma_1, ...\sigma_L\rangle, \tag{2.13}$$

with the number of coefficients $c_{\sigma_1,...\sigma_L}$ being exponentially large (d^L to be exact). The idea is to find a notation which gives a more local notion of the state, but at the same time preserves the quantum non-local charateristics of the state. We first rewrite the d^L coefficients in the form of a matrix of dimensions $d \times d^{L-1}$, with the components related as :

$$\Psi_{\sigma_1,(\sigma_2...\sigma_L)} = c_{\sigma_1...\sigma_L}. \tag{2.14}$$

We now perform Singular Value Decomposition (SVD) on the matrix Ψ, which gives

$$\begin{aligned} c_{\sigma_1,...\sigma_L} = \Psi_{\sigma_1,(\sigma_2...\sigma_L)} &= \sum_{a_1,b_1}^{r_1} U_{\sigma_1,a_1} S_{a_1,b_1} (V^\dagger)_{b_1,(\sigma_2...\sigma_L)} \\ &= \sum_{a_1}^{r_1} U_{\sigma_1,a_1} c_{a_1\sigma_2...\sigma_L} \end{aligned} \tag{2.15}$$

In the last equality, S and $V^\dagger$ have been multiplied and reshaped into the vector. The rank $r_1 \leq d$, is essentially equivalent to the truncation in DMRG method. The matrix

U is now decomposed into d row vectors called A^{σ_1} with components related through $A^{\sigma_1}_{a_1} = U_{\sigma_1,a_1}$. At the same time, the vector $c_{a_1\sigma_2\ldots\sigma_L}$ is written in the form of the matrix $\Psi_{(a_1\sigma_2),(\sigma_3\ldots\sigma_L)}$ of dimension $r_1 d \times d^{L-2}$ as follows :

$$c_{\sigma_1\sigma_2\ldots\sigma_L} = \sum_{a_1}^{r_1} A^{\sigma_1}_{a_1} \Psi_{(a_1\sigma_2),(\sigma_3\ldots\sigma_L)} \tag{2.16}$$

This matrix Ψ is now subjected to SVD, such that we have

$$\Psi_{(a_1\sigma_2),(\sigma_3\ldots\sigma_L)} = \sum_{a_2,b_2}^{r_2} U_{(a_1\sigma_2),a_2} S_{a_2,b_2} V^{\dagger}_{b_2,(\sigma_3\ldots\sigma_L)} \tag{2.17}$$

S and V are multiplied, and reshaped back into a row vector, $c_{a_2\sigma_3\ldots\sigma_L}$, such that

$$c_{\sigma_1\sigma_2\ldots\sigma_L} = \sum_{a_1,a_2}^{r_1,r_2} A^{\sigma_1}_{a_1} U_{(a_1\sigma_2),a_2} c_{a_2\sigma_3\ldots\sigma_L} \tag{2.18}$$

We now replace U by a set of 'd' matrices, $A^{\sigma_2}_{a_1,a_2}$ of dimensions $r_1 \times r_2$, given by

$$A^{\sigma_2}_{a_1,a_2} = U_{(a_1\sigma_2),a_2} \tag{2.19}$$

Therefore we get,

$$c_{\sigma_1\sigma_2\ldots\sigma_L} = \sum_{a_1,a_2}^{r_1,r_2} A^{\sigma_1}_{a_1} A^{\sigma_2}_{a_1,a_2} c_{a_2,(\sigma_3\ldots\sigma_L)} \tag{2.20}$$

The above procedure is continued till we reach the L-th site, where we replace U_{a_{L-1},σ_L} by a set of column vectors $A_{a^{\sigma_L}_{L-1}}$. Thus we have arrived to a stage where we can write the coefficients as a product of matrices :

$$c_{\sigma_1 \ldots \sigma_L} = \sum_{a_1, a_2, \ldots a_{L-1}}^{r_1, r_2 \ldots} A^{\sigma_1}_{a_1} A^{\sigma_2}_{a_1, a_2} \ldots A^{\sigma_{L-1}}_{a_{L-2}, a_{L-1}} A^{\sigma_L}_{a_{L-1}} \tag{2.21}$$

Hence we can now write the general wavefunction of the system in the MPS form as :

$$|\psi\rangle = \sum_{\substack{a_1, a_2, \ldots a_{L-1} \\ \sigma_1, \sigma_2 \ldots \sigma_L}} A^{\sigma_1}_{a_1} A^{\sigma_2}_{a_1, a_2} \ldots A^{\sigma_{L-1}}_{a_{L-2}, a_{L-1}} A^{\sigma_L}_{a_{L-1}} |\sigma_1 \sigma_2 \ldots \sigma_L\rangle \tag{2.22}$$

which can be more compactly written as

$$|\psi\rangle = \sum_{\sigma_1, \sigma_2 \ldots \sigma_L} A^{\sigma_1} A^{\sigma_2} \ldots A^{\sigma_{L-1}} A^{\sigma_L} |\sigma_1 \sigma_2 \ldots \sigma_L\rangle \tag{2.23}$$

One of the properties of these A-matrices is that they are left normalised, that is,

$$\sum_{\sigma_L} A^{\sigma_L^\dagger} A^{\sigma_L} = 1 \tag{2.24}$$

It should be noted that the MPS form derived above is not unique, in the sense that a gauge degree of freedom exists. The R.H.S. of the Eqn.(2.23) will remain unchanged under the following transformation on A matrix :

$$A^{\sigma_k} \rightarrow A' \sigma_k = V^{[k]} \cdot A^{\sigma_k} \cdot W^{[k \oplus 1]} \tag{2.25}$$

where $\oplus$ stands for the sum modulus L, and where $V^{[1]}, V^{[2]}, ..., V^{[L]}$ and $W^{[1]}, W^{[2]}, ..., W^{[L]}$ represent two sets of (not necessarily quadratic) matrices which fulfill the isometry condition $W^{[k]} \cdot V^{[k]} = I$, with I being identity matrix.

Indeed, one can also start from the right most site, or even mix the decomposition by starting from left and right. In reality, one must understand that the degree of non-uniqeness is much higher, each having their own advantages and disadvantages. The gauge degrees of freedom can be used cleverly to decrease the manipulations significantly.

2.2.2.2 MPS Variational Method

In the approach mentioned in the earlier section, consider the parameters from SVD, $r_1, r_2...$ be all equal ($= m$), called the *bond link* of the MPS. It can be shown with the help of the area law [13], that ground states for 1D systems can be accurately described even with a bond link dimension, m which does not scale with the system length. Such a representation will thus decrease drastically the amount of needed sources from exponential to polynomial growth with the system size.

Having known the MPS structure, the best approximation to the ground state in an MPS-like form of a given hamiltonian, H can be obtained by applying the variational principle, which will minimize the energy function, under the normalisation constraint.

$$E := \varepsilon/N = \frac{\langle\psi|H|\psi\rangle}{\langle\psi|\psi\rangle} \tag{2.26}$$

Consider an hamiltonian describing a 1D lattice of finite size, N, of the form :

$$H = \sum_{k=1}^{N} \sum_{\alpha,\beta} h_k^{(\alpha,\beta)} O_k^{\alpha} \otimes O_{k+1}^{\beta} \tag{2.27}$$

where O_k^{α} denotes some operators defined at site k, and $h_k^{(\alpha,\beta)}$ are the respective coupling strengths. For any site, k, let us define the so-called *transfer matix*, $E^{[k]}[O_k]$ of dimensions $m^2 \times m^2$:

$$E^{[k]}[O_k] = \sum_{\sigma_k,\sigma_k{}'=1}^{d} \langle\sigma_k{}'|O_k|\sigma_k\rangle (A^{\sigma_k{}'})^* \otimes A^{\sigma_k} \tag{2.28}$$

Hence the expectation value of the hamiltonian, H, can be written as :

$$\begin{aligned} \varepsilon &= \langle\psi|H|\psi\rangle \\ &= \sum_{k=1}^{N}\sum_{\alpha,\beta} h_k^{\alpha\beta}\langle E^{[1]}E^{[2]}\cdot\ldots\cdot E^{[k]}[O_k^\alpha]\cdot E^{[k+1]}[O_{k+1}]^\beta\cdot E^{[k+2]}\cdot\ldots\cdot E^{[N]} \end{aligned} \quad (2.29)$$

In the above expression, the abbreviation $E^{[k]}[\mathbb{1}_k] := E^{[k]}$ is used to describe the transfer matrix of identity operator, $\mathbb{1}_\mathbb{k}$ and $\langle\cdots\rangle := Tr[...]$ denotes Trace operation. The algorithm deals with sequentially minimizing the energy with respect to all the A's by fixing all of them except the ones defined at a given site k. It is essentially a single-site optimization process, compared to DMRG, which is a two-site optimization method. As is apparent from the above equation, the dependence on A^{σ_k} is quadratic in nature. The minimization of energy thus involves minimizing a quadratic polynomial ε with quadratic constraints N which essentially boils down to solving the eigenvalue equation :

$$H_k x_k = \lambda_k N_k x_k \quad (2.30)$$

Here the unknown coeffiecients of the $m \times m$ matrix, A^{σ_k} (where $\sigma_k = 1...d$), is mapped onto a column vector, x_k of dimensions dm^2, whereas the matrices H_k and N_k have dimensions $dm^2 \times dm^2$, called the "*effective hamiltonian*" and the "*effective norm operator*" respectively, are formed by similar mapping. Once the optimization of A^{σ_k} associated with the k-th site is over, the next step involves the optimization of $A^{\sigma_{k+1}}$. We continue the iteration until we reach the rightmost end of the lattice, i.e. site N. Then, the process is repeated, this time going from the rightmost site to the leftmost site, which is essentially called sweeping. At each step, the matrices associated with a particular site is computed, until the energy value converges to a minimum.

Having computed the ground state wavefunction, various quantities such as overlaps between wavefunctions, expectation values and general matrix elements can be evaluated

in quite a straightforward way. In fact there exists a graphical representation of MPS which makes all these calculations much simpler.

2.2.3 DMRG leading to MPS

Assume a block represented by a chain of $L-1$ sites [14]. If d is the size of the local Hilbert space defined on each site, then the size of the Hilbert space of the entire block, if we were to treat it exactly, would be d^{L-1}. Now assuming an approximation made in the previous iterations aiming to describe ground-state properties, the chain can be represented by a smaller number of states labelled by $|\beta\rangle_{L-1}$. The number of states in this basis is m, with $m \leq d^{L-1}$. We now add a single site to the chain. The new block will now have L sites with $d \times m$ states in its basis. The basis states are now given as the direct product of the basis of the single site and the block : $\{|s_L\rangle \otimes |\beta\rangle_{L-1}\}$. We now generate a new truncated basis with typically m states using a projection operator A_L. These m states represent the most important states of the new block. So, we can write a relation between the basis of $L-1$ and L sites in a simple manner by the recursion relation of the following form :

$$|\alpha_L\rangle = \sum_{\beta, s_L} A_L^{\alpha,(\beta,s_L)} |s_L\rangle \otimes |\beta\rangle_{L-1} \tag{2.31}$$

Here the initial state, $|\beta\rangle_0$ should be given beforehand. The matrices A_L are the variational parameters of MPS method, as described in the previous section. Determining these matrices are the central problem to solve in MPS. DMRG actually provides a convenient way to determine these parameters by keeping the largest eigenvalues of the density matrix.

We now perform a simple change in notation $A_L^{\alpha,\beta}[s_L] \equiv A_L^{\alpha,(\beta,s_L)}$ and write the $m \times (md)$ matrix as a set of d $m \times m$ matrices. If we now recursively apply the renormalisation step in the previous equation, the state of the chain of length L sites takes the form :

$$|\alpha_L\rangle = \sum_{s_L,\ldots,s_1} (A[s_L]A[s_{L-1}]\ldots A[s_1])^{\alpha,\beta} |s_L s_{L-1}\ldots s_1\rangle \otimes |\beta\rangle_0 \tag{2.32}$$

We thus see that the renormalisation procedure results in a wavefunction which can be written in a matrix-product form.

References

[1] D. van Oosten, P. van der Straten, and H. T. C. Stoof, Phys. Rev. A **63**, 053601 (2001).

[2] S. R. White, Phys. Rev. Lett. **69**, 2863 (1992).

[3] S. R. White, Phys. Rev. B **48**, 10345 (1993).

[4] U. Schollwöck, Rev. Mod. Phys. **77**, 259 (2005).

[5] K. Hallberg, Theoretical Methods for Strongly Correlated Electrons, CRM Series in Mathematical Physics, Springer, New York, 2003, arXiv:cond-mat/0303557v1.

[6] A. L. Malvezzi, Brazilian Journal of Phys. vol. **33**, no. 1, March, 2003.

[7] G. De Chiara, M. Rizzi, D. Rossini, S. Montangero, arXiv:cond-mat/0603842v2

[8] G. Chan, J. Dorando, D. Ghosh, J. Hachmann, E. Neuscamman, H. Wang, T. Yanai, arXiv:0711.1398v1 [cond-mat.str-el]

[9] S. Östlund and S. Rommer, Phys. Rev. Lett. **75**, 3537 (1995).

[10] U. Schollwöck, Annals of Physics **326**, 96 (2011).

[11] D. Rossini, V. Giovannetti, R. Fazio, J. Stat. Mech. (2011) P05021.

[12] F. Verstraete, J. I. Cirac, V. Murg, Adv. Phys. **57**, 143 (2008).

[13] J. Eisert, M. Cramer and M. B. Plenio, Rev. Mod. Phys. **82**, 277 (2010).

[14] Hamed Saberi, *Matrix-product states for strongly correlated systems and quantum information processing*, PhD. Thesis (München, 2008).

Chapter 3

Quantum Phases in Optical Superlattice

3.1 Introduction

In this chapter, we present a detailed analysis of the phases exhibited by a system of soft-core bosons loaded in an optical superlattice. Two different numerical methods, as described in Chapter 2, are used for this purpose. An optical superlattice is created by superposing two optical lattices of different frequencies, resulting in the formation of an interference pattern. In particular, if the frequency of one of the optical lattices is double that of the other, then it will produce a two-period optical superlattice, as shown in Fig.(3.1). The neighbouring sites get displaced with respect to each other, and it seems as if a bias has been provided at alternate sites. Such a modification in the geometry corresponds to an extra term in the Bose-Hubbard model as shown below :

$$H = -t \sum_{\langle i,j \rangle} a_i^\dagger a_j + \frac{U}{2} \sum_i n_i(n_i - 1) + \sum_i \lambda_i n_i \tag{3.1}$$

Here $a_i^\dagger$ is the creation operator for bosons, n_i is the number operator. The last term in Eqn.(3.1) is due to the optical superlattice, and the difference in the minimas of the

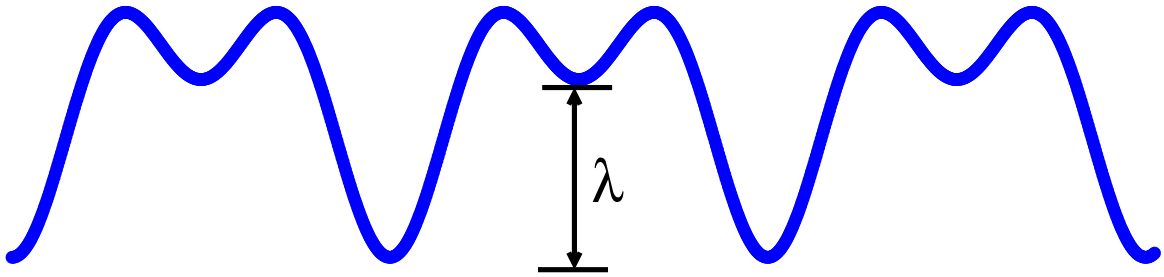

Fig. 3.1: Schematic diagram of a two-period optical superlattice, with the superlattice potential denoted by λ

adjacent sites is denoted by λ_i, which is called the superlattice potential. For a 2-period optical superlattice, $\lambda_i = 0$ for even sites, and λ for odd sites. The competition between the parameters in the above hamiltonian will give rise to various novel phases, which is quite distinct from the existing phases exhibited by the Bose-Hubbard model in an optical lattice. Previously it has been shown using exact diagonalisation, quantum Monte Carlo, and the mean field decoupling approximation methods that ultracold bosonic atoms loaded in optical superlattices exhibit different phases. Apart from the usual Mott insulator (MI) and superfluid (SF) phases, different charge-density-wave orders were found to be present [1, 2, 3, 4]. In the presence of a disordered and quasiperiodic potential, it has been shown that the system exhibits, in addition to MI and SF phases, the quasi-Bose glass phase and the incommensurate charge-density-wave phases [5, 6]. Various experiments on this subject have been proposed and carried out in different laboratories [7, 8, 9]. The mean-field analysis of the above system is presented below and it is followed by the DMRG treatment.

3.2 Mean-Field analysis

There have been a number of versions of mean-field theory which have been applied to the study of ultracold atoms [10, 11]. For example the Bogoliubov approximation [11], the Gutzwiller approach [12, 13, 14], and the mean-field decoupling approximation [15]. The Bogoliubov approach is useful when the interactions between the atoms are weak.

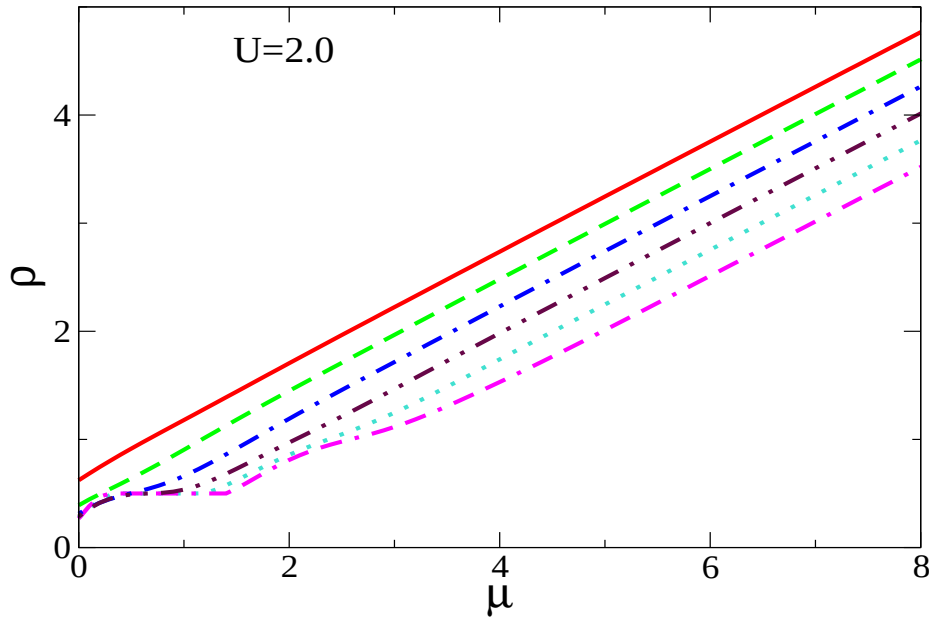

Fig. 3.2: Variation of average density ρ as a function of the chemical potential μ for U=2, but for different values of λ starting from 0.5 (red solid curve) to 5.5 (magenta double dash dot curve) at the intervals of 1.0.

However, the SF-MI transition cannot be studied by such a method since it takes place in the strong interaction regime. The mean field theory in the decoupling approximation decouples the Bose-Hubbard hamiltonian into a sum of single-site hamiltonians. This resulting mean-field equation can be solved either analytically using a perturbative approach, or numerically by diagonalising the matrix expressed in some convenient single site basis in a self consistent manner. In this thesis, the decoupling approach has been applied to a d-dimensional system of optical superlattice with a periodicity of two sites.

As shown in the previous chapter, after decoupling, the single site mean-field hamiltonian looks like (from Eqn.(2.5)):

$$H_i^{MF} = -\bar{\phi}_i(a_i^\dagger + a_i) + \bar{\phi}_i\phi_i + \frac{\tilde{U}}{2}n_i(n_i - 1) - \tilde{\mu}_i n_i \tag{3.2}$$

where $\tilde{U} = U/zt$, $\tilde{\mu}_i = \mu_i/zt$ are dimensionless on-site interaction and chemical potential respectively. For the optical superlattice with a periodicity of two sites, the unit cell will consist 2^d sites, with alternate sites having an energy shift of λ_i. To take this

into account, we consider the on-site chemical potential as $\mu_i = \mu - \lambda_i$, where μ is the chemical potential of the system, and λ_i being the superlattice potential. Since the entire system can be constructed using the unit cell comprising two neighbouring sites, and all dimensions are equivalent, we can work on any one such direction, and hence we denote the two neighbouring sites by 1 and 2. The mean-field hamiltonian of this unit cell, in the presence of superlattice potential can be written as :

$$\begin{aligned} H_{uc}^{MF} &= -\bar{\phi_2} a(a_1^\dagger + a_1) - \bar{\phi_1}(a_2^\dagger + a_2) + 2\bar{\phi_1}\phi_2 + \frac{\tilde{U}}{2}[n_1(n_1-1) + n_2(n_2-1)] \\ &\quad -\tilde{\mu}[n_1 + n_2] + \tilde{\lambda_1} n_1 + \tilde{\lambda_2} n_2 \end{aligned} \tag{3.3}$$

We express all the operators in the above hamiltonian in the occupation number basis, and starting with initial guess values of the superfluid order parameters, ϕ_1 and ϕ_2, the matrix H_{uc}^{MF} is diagonalised using the Jacobi method to obtain the ground state energy and the corresponding wavefunction. The superfluid order parameter, ϕ_i, as mentioned in the previous chapter is defined as $\phi_i = \langle a_i \rangle$. So, using the ground state wavefunction, the expectation values are calculated, and substituted back into H_{uc}^{MF}. The process is iterated, until the values of ϕ_1 and ϕ_2 converge to 10^{-6}. The analysis of the various phases are carried out using the values of these superfluid densities.

3.2.1 Results

Considering the two-period optical superlattice, we can simplify by taking $\lambda_1 = 0$, and $\lambda_2 = \lambda$, where λ is the difference between the neighbouring potential minimas, called the superlattice potential. We investigate a wide range of λ, densities ρ, and four characteristic values of the on-site repulsive interaction, U, so as to cover an extensive part of the phase-diagram. Throughout our analysis, we have taken $zt = 1.0$, so all the quantities such as U, λ and μ are expressed conveniently in units of zt. As for the size of the Hilbert space on a particular site, we have truncated it to $n_{max} = 10$, i.e. each site can accommodate a

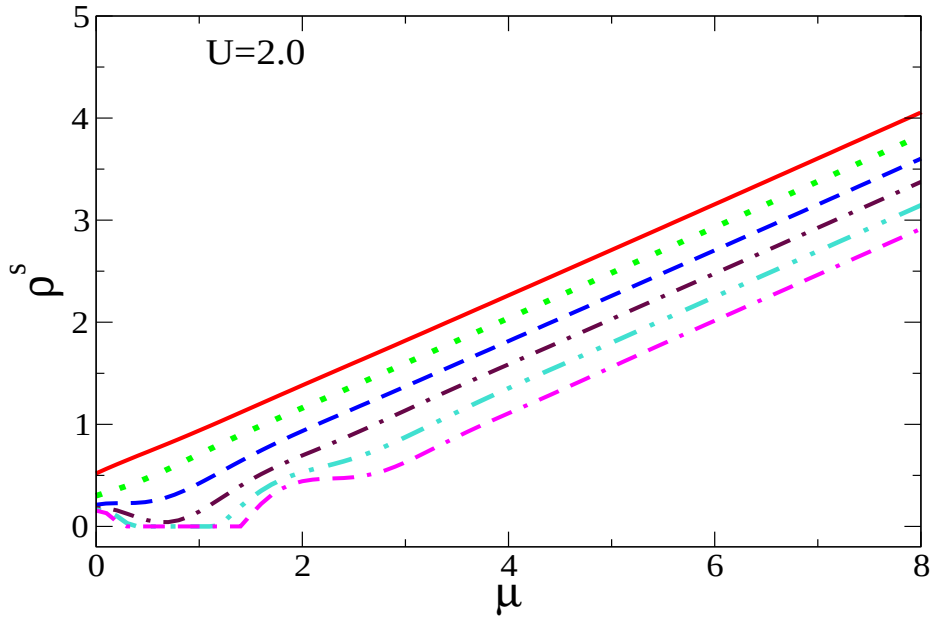

Fig. 3.3: Variation of average superfluid density ρ^s as a function of μ for the same set of parameters as in Fig. 3.2.

maximum of 9 bosons.

We first investigate the effect of superlattice potential on the superfluid (SF) phase. We start with $U = 2.0$ in Figs.(3.2) and (3.3) which show the plots of average density, ρ and the superfluid density, ρ^s for a range of values of chemical potential, μ, for different values of λ starting from 0.5 to 5.5 at intervals of 1.0. It should be noted that ρ and ρ^s are respectively the average density and the superfluid density of the unit cell, defined as $\rho = (\rho_1 + \rho_2)/2$ and $\rho^s = (\phi_1^2 + \phi_2^2)/2$. For $U = 2.0$, in the absence of any superlattice potential, the system will be always in the SF phase.

Figs.(3.2) and (3.3) show that density ρ increases with an increase in μ for non-zero but small values of λ. The superfluid density, ρ^s continues to be finite, indicating the SF phase throughout for $\lambda = 0$. But as λ increases further, say for example 4.5, the density, ρ remains constant at 0.5, forming a plateau sort of structure for a range of μ values as can be seen in Fig.(3.2). This signifies a finite gap in the energy spectrum, for this range of μ values, with a vanishing compressibility, $\kappa = \frac{\partial \rho}{\partial \mu}$. Fig.(3.3) also indicates vanishing superfluid density for the same range of μ. For all other densities, $\rho \neq 1/2$, including

at integer densities, the superfluid density remains finite. The above two features clearly imply that for $U = 2$, model described in Eq.(3.1) exhibits SF phase for all values of $\rho \neq 1/2$, for all values of λ. However, for $\rho = 1/2$, there is a transition from SF to an insulator phase as λ increases.

Table 3.1: $U = 2.0$

λ	ρ	μ	ρ_1^s	ρ_2^s	n_1	n_2
0.5	0.620	0.00	0.58	0.45	0.73	0.51
0.5	1.022	0.70	0.87	0.75	1.12	0.92
0.5	2.017	2.60	1.72	1.57	2.13	1.91
1.5	0.490	0.20	0.52	0.21	0.77	0.21
1.5	1.020	1.20	0.98	0.62	1.32	0.71
1.5	2.020	3.10	1.87	1.41	2.34	1.69
2.5	0.490	0.47	0.39	0.08	0.91	0.08
2.5	1.030	1.71	1.11	0.49	1.53	0.53
2.5	2.030	3.61	2.02	1.26	2.57	1.49
3.5	0.500	0.70	0.07	0.01	0.99	0.01
3.5	1.020	2.10	1.14	0.33	1.70	0.34
3.5	2.030	4.10	2.16	1.10	2.79	1.28
4.5	0.500	0.40	0.00	0.00	1.00	0.00
4.5	1.000	2.40	1.08	0.19	1.82	0.19
4.5	2.000	4.50	2.24	0.91	2.96	1.03
5.5	0.500	0.30	0.00	0.00	1.00	0.00
5.5	1.000	2.60	0.89	0.10	1.91	0.10
5.5	2.000	5.00	2.36	0.77	3.18	0.84

This insulator is not the same as the conventional Mott insulator (MI), which arises due to strong on-site interactions, U. The MI phase is not expected for as low a value as $U = 2$. The cause of the above mentioned insulator phase is the superlattice potential, and to distinguish it from the MI, we label it as the superlattice induced Mott insulator (SLMI). In order to get an idea of the SLMI phase, the distribution of bosons in a unit cell in this phase is listed in Table 3.1, along with other relevant quantities. As discussed earlier, the unit cell consists of 2^d sites, and we choose one of the directions consisting of two sites, labelled as 1 and 2. The values of the on-site occupancy, ρ_1 and ρ_2 and superfluid densities, ρ_1^s and ρ_2^s are listed in the table for different values of λ, for $U = 2$. For $\lambda < 3.7$, the on-site superfluid densities ρ_1^s and ρ_2^s remain finite for all densities.

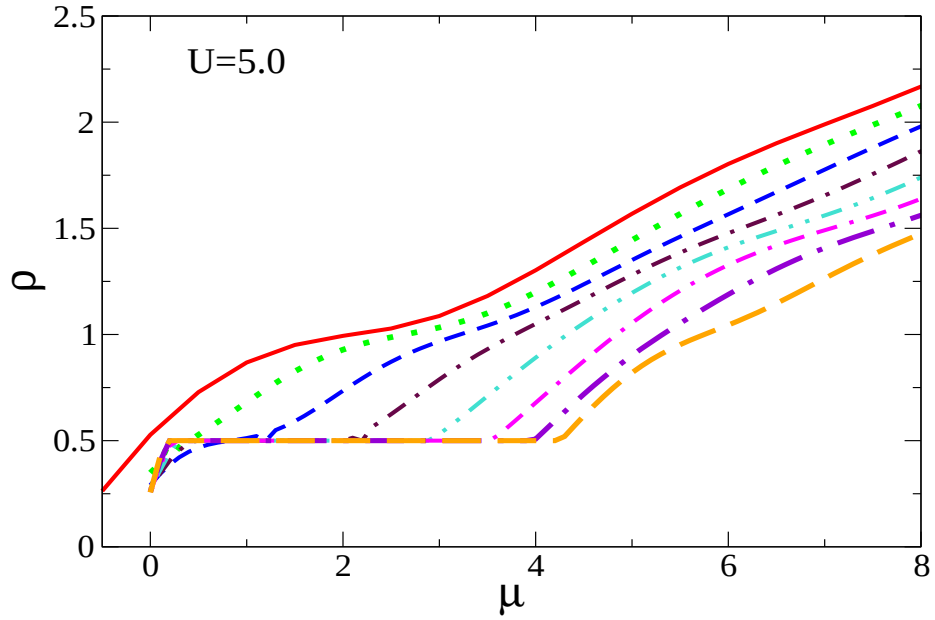

Fig. 3.4: Variation of average density of a unit cell ρ as a function of the chemical potential μ for U=5, but for different values of λ starting from 0.2 (red solid curve) to 7.2 (orange large dashed curve) at intervals of 1.0.

However for $\lambda \geqslant 3.7$, and average density $\rho = 1/2$, we find $\rho_1^s = \rho_2^s = 0$ and $\rho_1 = 1$, $\rho_2 = 0$. This means that within the unit cell, one site is occupied, whereas the other is empty. Since this unit cell can be repeated in all directions to construct the entire lattice, the system has every alternate site occupied, and the other being empty, similar to a charge density wave (CDW) phase, which normally arises in the presence of the nearest neighbour interactions [16] . However, the appearance of this CDW-like density distribution is because of the superlattice potential, and the nearest neighbour interactions are not involved. This distribution of atoms of the form [1 0 1 0 1 0 ...] is called the SLMI-I phase. Table 3.1 also confirms that there is no insulating phase at integer densities.

Results for $U = 5$ is very similar to the $U = 2$ case, since both of them exhibit the SF phase for $\lambda = 0$. Figs.(3.4) and (3.5) respectively show plots of the density and the superfluid density as a function of μ for various values of λ. The system is in the SF phase at $\rho = 1/2$ and $\rho = 1$ initially for low values of λ (< 2.6). But as λ is increased beyond 2.6, a plateau develops at $\rho = 1/2$, indicating a gap in the energy spectrum. Consequently the

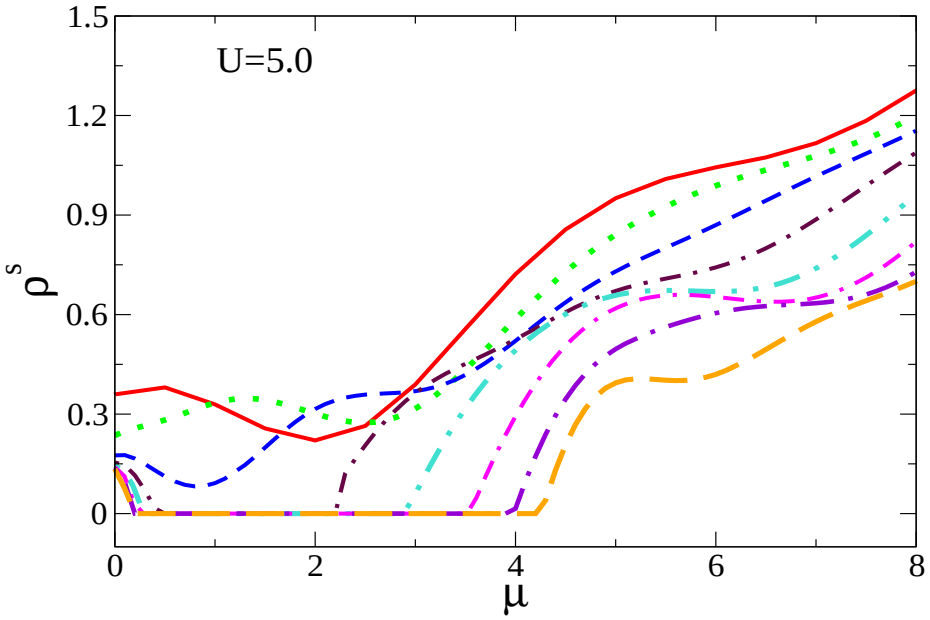

Fig. 3.5: Variation of average superfluid density of a unit cell as a function of μ for the same set of parameters as in Fig. 3.4.

SF density vanishes in this region (Fig.(3.5)). As λ is increased, the extent of the plateau structure increases. However, the system remains in the SF phase at $\rho = 1$ for all the values of λ that have been considered. Table 3.2 has the values of the on-site density and the SF density within the cell. We thus conclude that the transition from SF to SLMI-I takes place at $\lambda = 2.6$, when the SF density vanishes, and the occupancy configuration takes the form [1 0 1 0 ...]. But at all other values of ρ, and for all values of λ, the SF densities, ρ_1^s and ρ_2^s remain finite.

Results for $U = 10$ show a marked difference from that of the $U = 5$ case. The reason for this is that as discussed in Chapter 1, there is a MI-SF transition for integer densities in the Bose-Hubbard model. For $\rho = 1$, the mean-field decoupling theory predicts the critical U value, $U_c \sim 5.8$ [10]. So for $U = 10$ (greater than U_c), the system will be in the MI phase for $\rho = 1$, when $\lambda = 0$. Figs.(3.6) and (3.7) show respectively the plots of density ρ and SF density, ρ^s as a function of μ for various values of λ. It can be seen that a plateau exists at $\rho = 1$ for small values of λ (Fig.(3.6)), and the SF density vanishes in the same range of μ, confirming the expected MI phase. The system remains in the

Table 3.2: $U = 5.0$

λ	ρ	μ	ρ_1^s	ρ_2^s	n_1	n_2
0.2	0.523	0.0	0.370	0.35	0.57	0.48
0.2	1.030	2.5	0.270	0.26	1.03	1.02
0.2	2.080	7.5	1.190	1.17	2.09	2.06
2.2	0.500	0.9	0.110	0.06	0.95	0.06
2.2	1.010	3.3	0.433	0.36	1.13	0.90
2.2	2.000	8.1	1.250	1.09	2.19	1.81
3.2	0.500	0.5	0.000	0.00	1.00	0.00
3.2	1.000	3.8	0.570	0.42	1.22	0.78
3.2	2.010	8.7	1.350	1.08	2.30	1.73
4.2	0.500	0.2	0.000	0.00	1.00	0.00
4.2	0.990	5.3	0.790	0.29	1.65	0.34
4.2	2.010	10.2	1.540	0.91	2.62	1.40
7.2	0.500	0.2	0.000	0.00	1.00	0.00
7.2	1.010	5.8	0.620	0.18	1.82	0.20
7.2	2.020	10.7	1.54	0.83	2.73	1.30

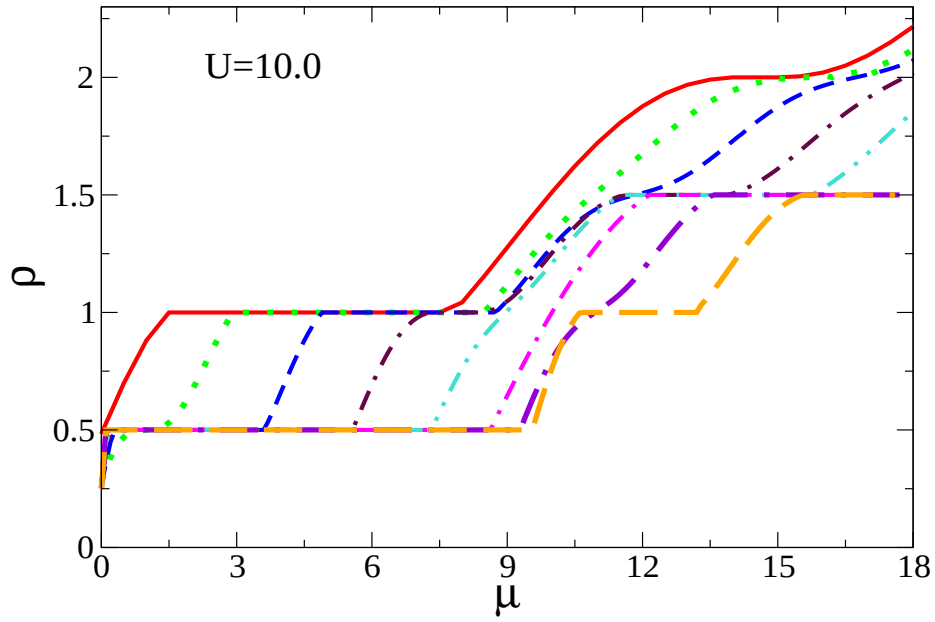

Fig. 3.6: Variation of average density of a unit cell ρ as a function of the chemical potential μ for U=10, but for different values of λ, varying from 0.2 (red solid curve) to 14.2 (orange large dashed curve) at intervals of 2.0

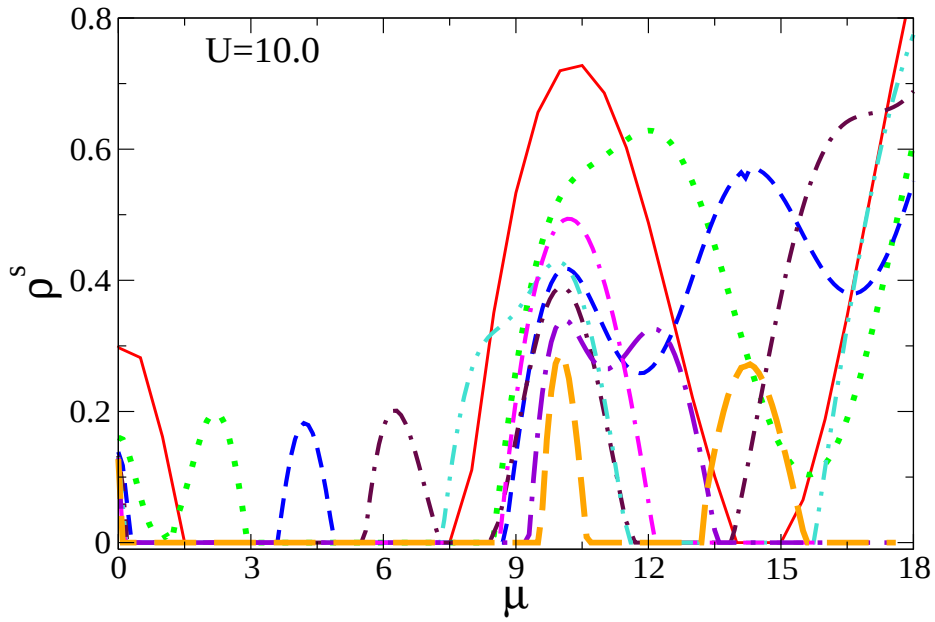

Fig. 3.7: Variation of average superfluid density of a unit cell as a function of μ for the same set of parameters as in Fig. 3.6.

SF phase for all other densities. However as λ is increased, the plateau at $\rho = 1$ starts shrinking, leading to its complete disappearance, and again it reappears as λ is increased further.

At $\rho = 1/2$, a plateau develops for $\lambda > 2.3$, and for $\rho = 3/2$, the transition takes place for $\lambda > 5.3$. From the values as listed in Table 3.3, we can infer that the insulator at $\rho = 1/2$, is the same as SLMI-I with the occupancy configuration [1 0 1 0 ...]. But at $\rho = 3/2$, the values indicate that the configuration is [2 1 2 1 ...], which we call SLMI-III. At $\rho = 1$, there are two insulating phases. For $\lambda < 6.5$, the system is in the MI phase with the configuration [1 1 1 1 ...]. For $\lambda > 13.1$, the system re-enters into an insulator phase, with the configuration [2 0 2 0 ...], which we call SLMI-II. For $6.5 < \lambda < 13.1$, the system resides in the SF phase.

The model at $U = 15$ behaves similar to that for $U = 10$. At $\rho = 1/2$, the system starts off in the gapless SF phase for low values of λ (< 2.2), as evident from Figs.(3.8) and (3.9), and also Table 3.4. As λ becomes greater than 2.2, the system enters the gapped SLMI-I phase, with vanishing SF density, and an occupancy of [1 0 1 0 ...]. At

Table 3.3: $U = 10.0$

λ	ρ	μ	ρ_1^s	ρ_2^s	n_1	n_2
0.2	0.48	0.00	0.30	0.29	0.53	0.44
0.2	1.00	2.00	0.00	0.00	1.00	1.00
0.2	2.00	14.50	0.00	0.00	2.00	2.00
2.2	0.50	1.20	0.00	0.00	1.00	0.00
2.2	1.00	3.00	0.00	0.00	1.00	1.00
2.2	2.00	15.00	0.00	0.00	2.00	2.00
6.2	0.50	0.50	0.00	0.00	1.00	0.00
6.2	1.00	7.50	0.00	0.00	1.00	1.00
6.2	1.50	12.00	0.00	0.00	2.00	1.00
10.2	0.50	0.19	0.00	0.00	1.00	0.00
10.2	1.00	9.97	0.65	0.32	1.51	0.47
10.2	1.50	12.16	0.00	0.00	2.00	1.00
14.2	0.50	0.10	0.00	0.00	1.00	0.00
14.2	1.00	10.70	0.00	0.00	2.00	0.00
14.2	1.50	15.60	0.00	0.00	2.00	1.00

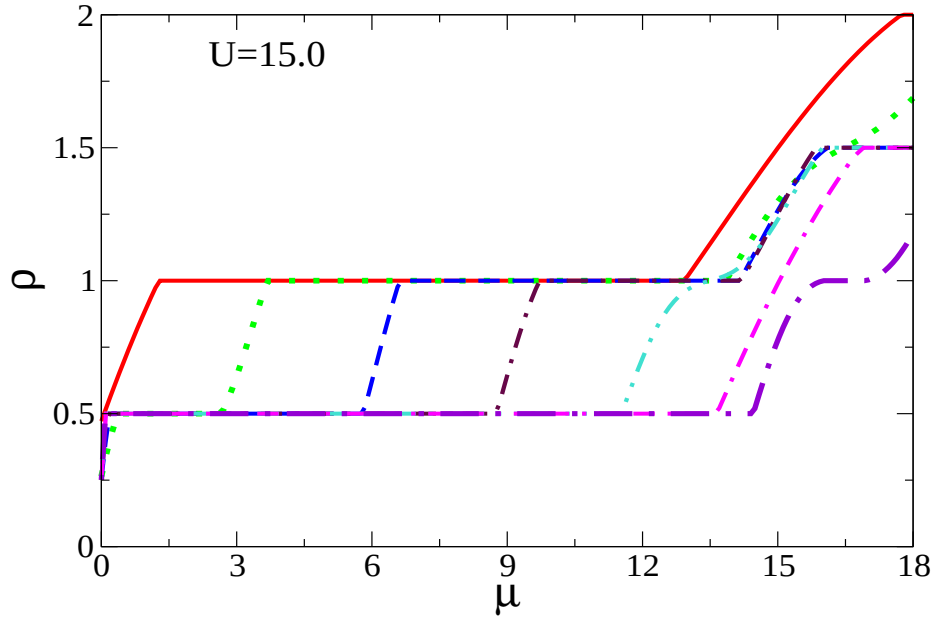

Fig. 3.8: Variation of average density of a unit cell ρ as a function of the chemical potential μ for U=15, but for different values of λ, varying from 0.2 (red solid curve) to 18.2 (violet large dot dashed curve) at intervals of 3.0

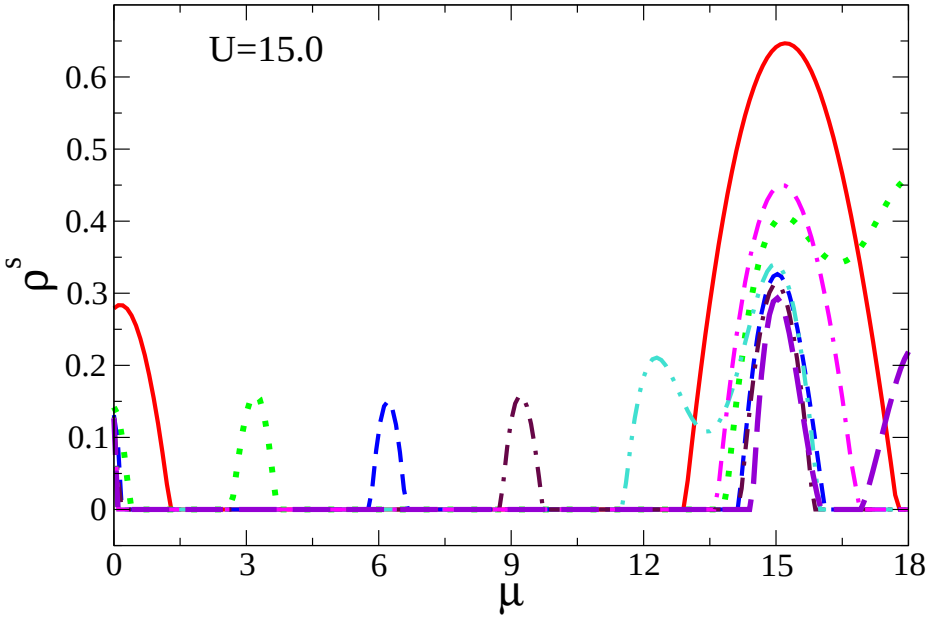

Fig. 3.9: Variation of average superfluid density of a unit cell as a function of μ for the same set of parameters as in Fig. 3.8.

$\rho = 3/2$, the system undergoes a transition from SF to SLMI-III at $\lambda = 4.8$, with a configuration of [2 1 2 1 ...]. At $\rho = 1$, the system stays in the MI phase for $\lambda = 0$, since the value of U is greater than U_c. It remains in the MI phase till λ is increased to a value of 11.7, after which it enters the SF phase. Further increase of λ beyond 18.1 takes the system to SLMI-II phase, with the configuration [2 0 2 0 ...].

Table 3.4: U=15.0

λ	ρ	μ	ρ_1^s	ρ_2^s	n_1	n_2
0.2	0.52	0.10	0.28	0.28	0.57	0.47
0.2	1.00	1.30	0.00	0.00	1.00	1.00
0.2	2.00	17.80	0.00	0.00	2.00	2.00
6.2	0.50	0.18	0.00	0.00	1.00	0.00
6.2	1.00	6.66	0.00	0.00	1.00	1.00
6.2	1.50	16.11	0.00	0.00	2.00	1.00
15.2	0.50	0.10	0.00	0.00	1.00	0.00
15.2	1.02	15.10	0.60	0.30	1.55	0.49
18.2	0.50	0.09	0.00	0.00	1.00	0.00
18.2	1.0	16.00	0.00	0.00	2.00	0.00
18.2	1.50	19.08	0.00	0.00	2.00	1.00

3.3 Density Matrix renormalisation Group Method Analysis

In this section, we present the analysis of the Bose-Hubbard model for ultracold atoms in an optical superlattice described in Eq. 3.1 using the DMRG method. To obtain the ground-state wavefunction and the energy eigenvalues of this model for a system of N bosons in a lattice of length L, with on-site interactions, tunneling and the relative energy shifts between neighbouring sites due to the superlattice potential, we use the finite size DMRG (FSDMRG) method with open boundary conditions [17, 18]. As investigated earlier, this method works quite accurately for the one-dimensional Bose-Hubbard model [18, 19, 20, 21, 22].

For all our computations, we have taken four bosonic states per site, that is a maximum of three bosons can be accommodated at a single site. The weights of the states neglected in the density matrix for either right block or left block is less than 10^{-6}. In order to improve the convergence, at the end of each DMRG step, we use a finite-size sweeping procedure given in [17, 18, 19, 20]. To obtain the ground state wavefunction, $|\Psi_{LN}\rangle$ and the associated energy, E_{LN}, for densities ranging from 0.24 to 1.25, we start the process with 4 sites and 4 atoms. We then increase the number of sites and atoms by two at every DMRG step, until we have 24 atoms. After this, we keep the number of atoms fixed, and increase the number of sites to 100, by adding 2 sites at a time in each DMRG step. At the end of each step, sweeping is done from left to right, and vice-versa across the entire lattice. This is continued until the energy value converges. The superlattice potential breaks the symmetry between the system and the environment. Therefore it is necessary to perform the calculations separately on each of the blocks at each DMRG iteration. Once the length, $L = 100$ is reached, we keep it fixed, and increase the number of atoms one at a time, and perform the complete DMRG sweep for the convergence of the energy. This iterative procedure is continued till the number of atoms reach the value of

125. Such a process will yield the ground state wave function and the energy for a range of densities from 0.24 to 1.25. We fix the hopping amplitude, $t = 1.0$ and the on-site repulsive interaction, $U = 10$, and vary the superlattice potential, λ from 0 to 15 for our simulations.

Using the ground state wavefunction, $|\Psi_{LN}\rangle$ and the energy, E_{LN}, the following physical quantities of interest are evaluated, to identify the various phases of the system.

- The chemical potential of a system of density, $\rho = N/L$, is defined as

$$\mu = \frac{\delta E_L(N)}{\delta N} \tag{3.4}$$

  The gapped and gapless phases of the system can be determined from the behaviour of ρ as a function of μ.

- The on-site density, $\langle n_i \rangle$ is defined as

$$\langle n_i \rangle = \langle \Psi_{LN} | \hat{n_i} | \Psi_{LN} \rangle \tag{3.5}$$

  This will give information about the on-site density distribution in the various phases.

- The momentum distribution defined as the Fourier transform of the single-particle density matrix

$$n(k) = \frac{1}{L} \sum_{p,q} e^{ik(p-q)} \langle \hat{a_p^\dagger} \hat{a_q} \rangle \tag{3.6}$$

  is a signature of the presence of the SF phase in the system.

- The structure function defined as the Fourier transform of the density-density correlation function

$$S(k) = \frac{1}{L} \sum_{p,q} e^{ik(p-q)} \langle \hat{n_p} \hat{n_q} \rangle \tag{3.7}$$

probes the presence of any density-wave order in the system and also the effects of the superlattice potential on the Brillouin zone boundaries.

3.3.1 Results

To get a reasonable idea of the various gapped and gapless phases in the system, we plot ρ as a function of μ, defined in Eqn.(3.4) as shown in the 3-d graph of Fig.(3.10), for a fixed value of $U = 10.0$, but with λ varying from 0 to 15. The presence of the gapped phases are revealed by the plateaus with the gap G_L being equal to the width of the plateau, i.e. $G_L = \mu_L^+ - \mu_L^-$, where μ_L^+ and μ_L^- are the values of the chemical potential at the upper and lower knees of the plateau, respectively. The value of U considered is much larger than the critical $U_c \sim 3.4$ as predicted by previous DMRG calculations. So at $\rho = 1.0$, we expect the system to be in the MI phase. Indeed we do see that in Fig.(3.10), where at $\lambda = 0.0$, there exists only one plateau at $\rho = 1.0$. The MI phase survives for small values of λ. As the strength of the superlattice potential, λ is increased, two interesting features become evident from the plots :

- a new plateau appears at $\rho = 1/2$
- the width of the plateau at $\rho = 1$ starts shrinking

These features are more clearly seen from the 2-d plots of ρ vs μ for different values of λ as shown in Fig.(3.11). For $\lambda = 0.2$, the gapped phase exists only at $\rho = 1.0$ and is gapless at other densities including $\rho = 1/2$. As λ is increased beyond 0.8, two gapped

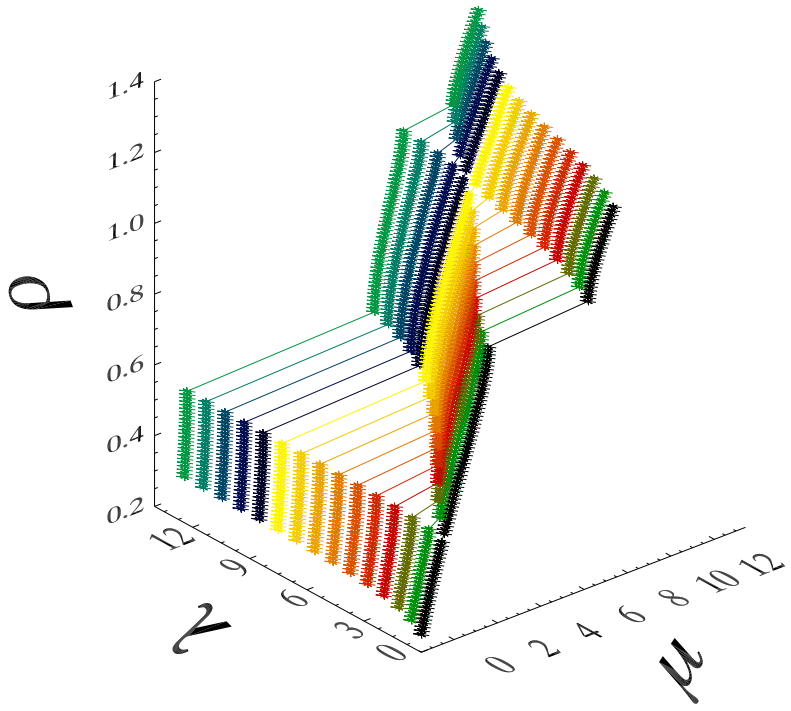

Fig. 3.10: Density ρ is plotted against the chemical potential for various values of λ at a fixed $U = 10$ and $t = 1$.

phases appear. One at $\rho = 1/2$ and the other at $\rho = 1.0$. The gapped phase at $\rho = 1/2$ appears because of the transition from SF to SLMI-I phase, with alternate sites being occupied by one atom. For the region between $\lambda = 0.8$ and 9.6, the system exhibits two gapped phases, one at $\rho = 1/2$ and the other at $\rho = 1$. The gap at $\rho = 1/2$ keeps on increasing steadily as λ is increased, and remains finite throughout. On the other hand, as mentioned earlier, the gap at $\rho = 1$ shrinks gradually with increasing λ, and vanishes completely at $\lambda = 9.6$. This marks the transition from the gapped MI phase to the gapless SF phase. It should be noted that this SF region appears for $\lambda \approx U$ values. A further increase of λ beyond 10.4 causes the gap to reappear, marking the transition to the SLMI-II phase with alternate sites being occupied by 2 atoms. The reason for the existence of the SF window inspite of the high value of U is quite interesting. It arises due to the competition between U and λ. When U is larger than λ, the MI phase is stabilised with a configuration [1 1 1 1 ...], and when λ is greater than U, λ dominates and this forces the system to enter the SLMI-II phase with [2 0 2 0 ...] configuration. But when their values are comparable, no particular configuration is attained, resulting in a random distribution of atoms in the lattice, thus leading to the SF phase. Fig.(3.12) shows this effect in a schematic way. At all incommensurate densities the system remains in the SF phase for all values of λ.

For a different perspective on the appearance of the various quantum phases, we consider the dependence of the on-site average number density distribution, $\langle n_i \rangle$, on the site index, i. Fig.(3.13) shows the plot of atom distribution in the lattice for $\rho = 1/2$. For values of λ less than 0.8, the number occupancy remains flat at the value of 0.5. However, as λ is increased, density oscillations set in slowly in the system. At higher values of λ, a clear [1 0 1 0 ...] occupancy configuration is observed from Fig.(3.13). This confirms the presence of the SLMI-I phase. Fig. 3.14 shows the distribution of atoms in the lattice for $\rho = 1$. For low values of λ, the plot shows that all the sites have an equal number of atoms, equal to 1, signifying the MI phase. Increasing λ induces some oscillations in

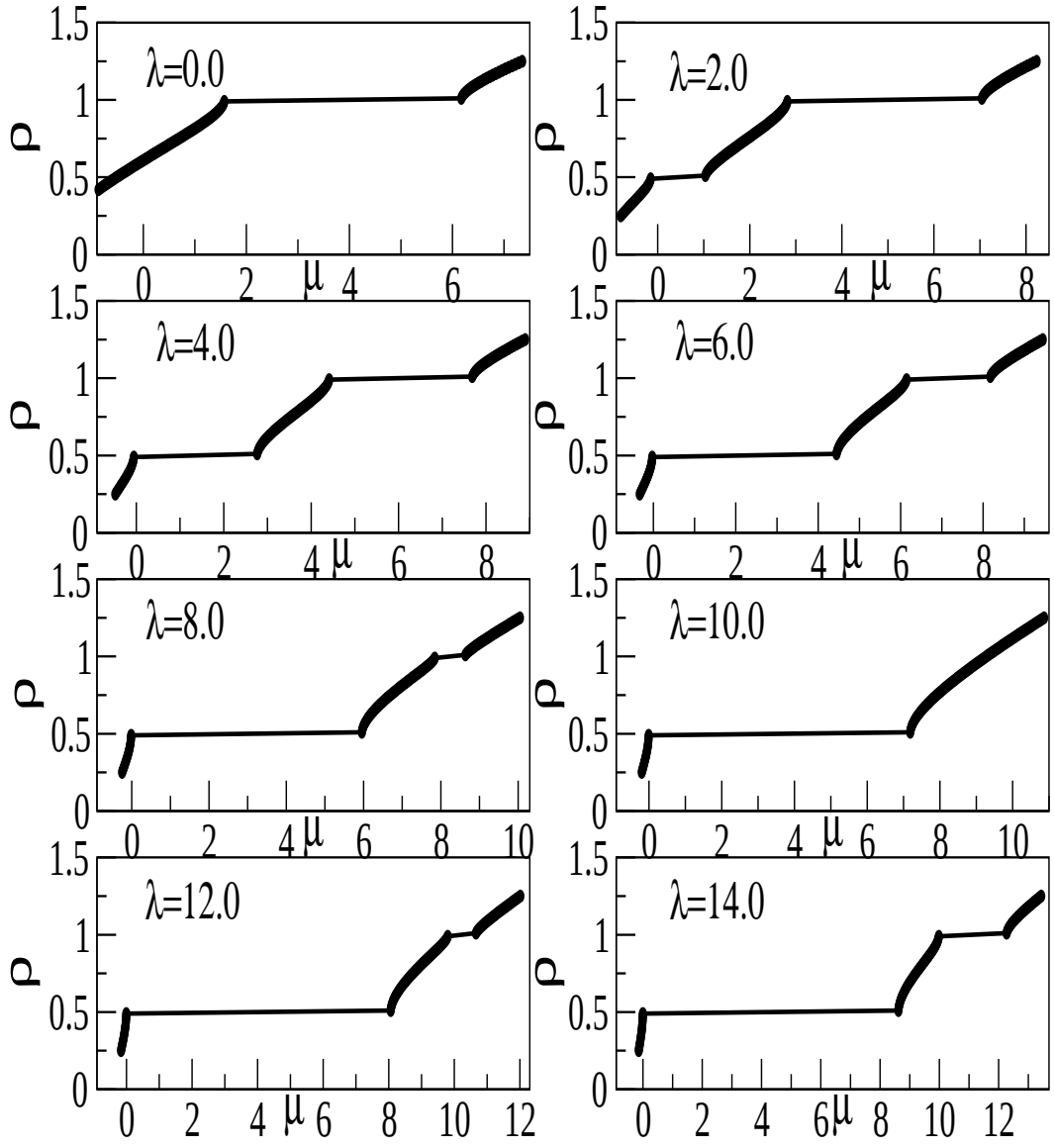

Fig. 3.11: The chemical potential, μ is plotted against density ρ for various values of λ, and $U = 10$.

the system, but it is still in the MI phase. Even for $9.6 \leq \lambda \leq 11.4$, when the system enters the SF region, there are density oscillations, varying from 1.5 (maximum) to 0.5 (minimum) values. This is signficantly different from a [2 0 2 0 ...] configuration. As λ is increased further, the system enters the gapped SLMI-II phase, with the occupancy configuration slowly tending towards a [2 0 2 0 ...] structure, signifying the onset of the SLMI-II phase.

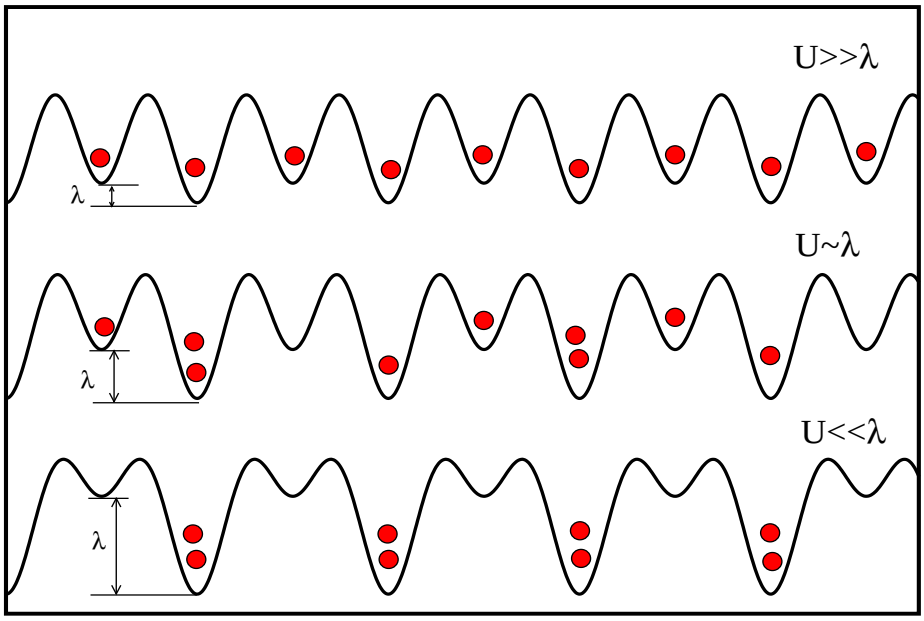

Fig. 3.12: Schematic representation of the phases appearing for various values of λ.

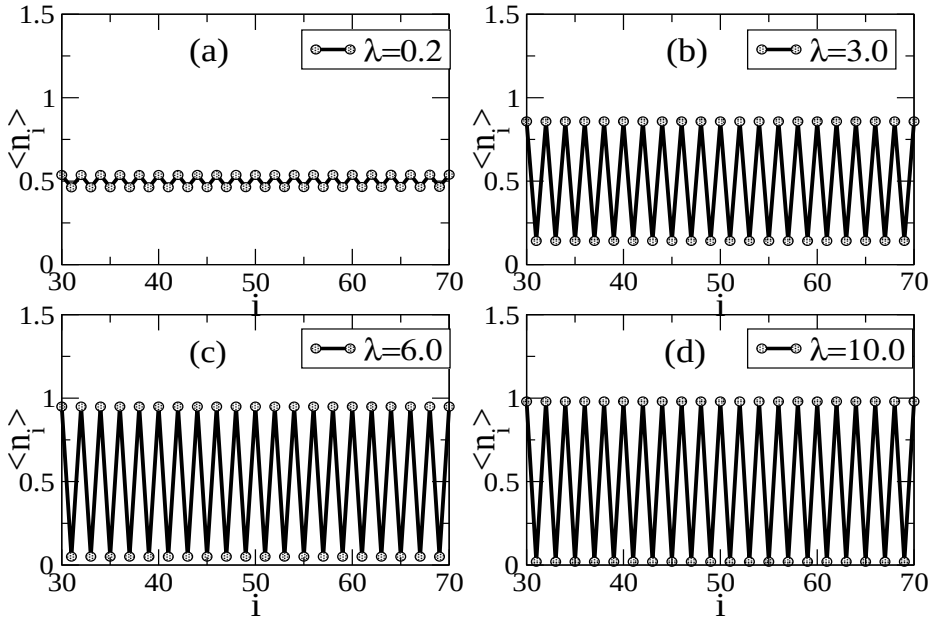

Fig. 3.13: On-site number density plotted against lattice site index at density, $\rho = 0.5$.

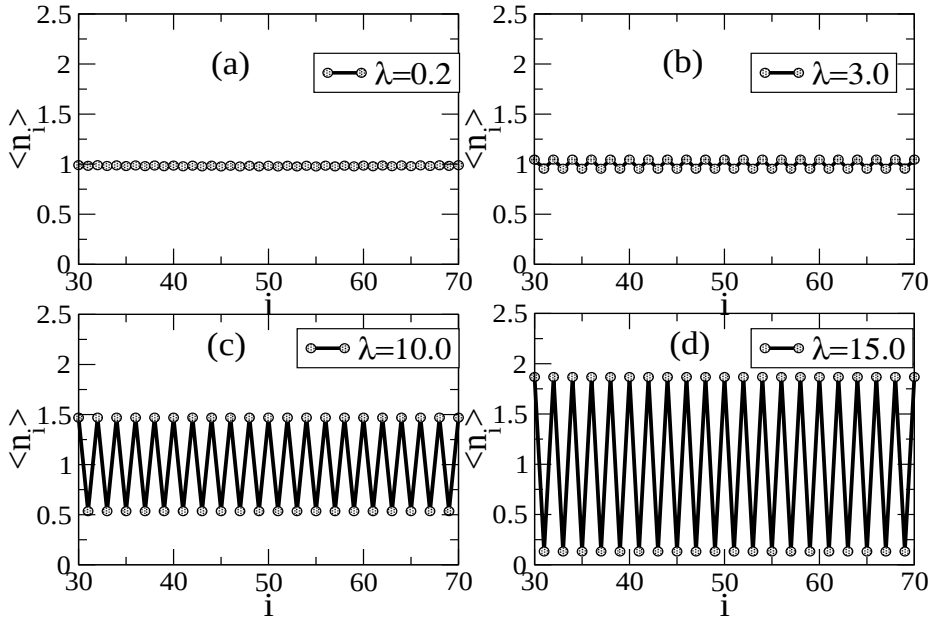

Fig. 3.14: On-site number density plotted against lattice site index at density, $\rho = 1.0$.

We now turn to the momentum distribution defined in Eqn.(3.6). The value of $n(k)$ at $k = 0$, which denotes the population in the $k = 0$ momentum eigenstate, is a signature of the SF phase, where it has a relatively large value. It is clear from Fig.(3.15) that for $\rho = 1/2$, $n(k = 0)$ has a high value for low values of λ. But as λ is increased, $n(0)$ falls off to values very close to zero, implying a transition from SF to some gapped phase. For $\rho = 1$, $n(0)$ is small for low λ values, since the system is in the MI phase. As λ approaches closer to the value of U, $n(0)$ starts increasing, and takes on a large finite value, indicating a transition from MI to SF phase. Further increase of λ makes $n(0)$ drop back to values close to zero, corresponding to the transition to the gapped SLMI-II phase. At an incommensurate density, for example $\rho = 0.7$, the value of $n(0)$ is always finite, supporting the fact that the system remains in the SF phase for all values of λ.

The structure function as defined in Eqn.(3.7) is plotted in Fig.(3.16). In the regular optical lattice, where the periodicity is one lattice site, the structure function peaks at $k = \pm 2\pi$ in the MI phase. However, for a 2- period optical superlattice, since the periodicity is two, the Brillouin zone gets halved. Hence in the MI phase for an optical

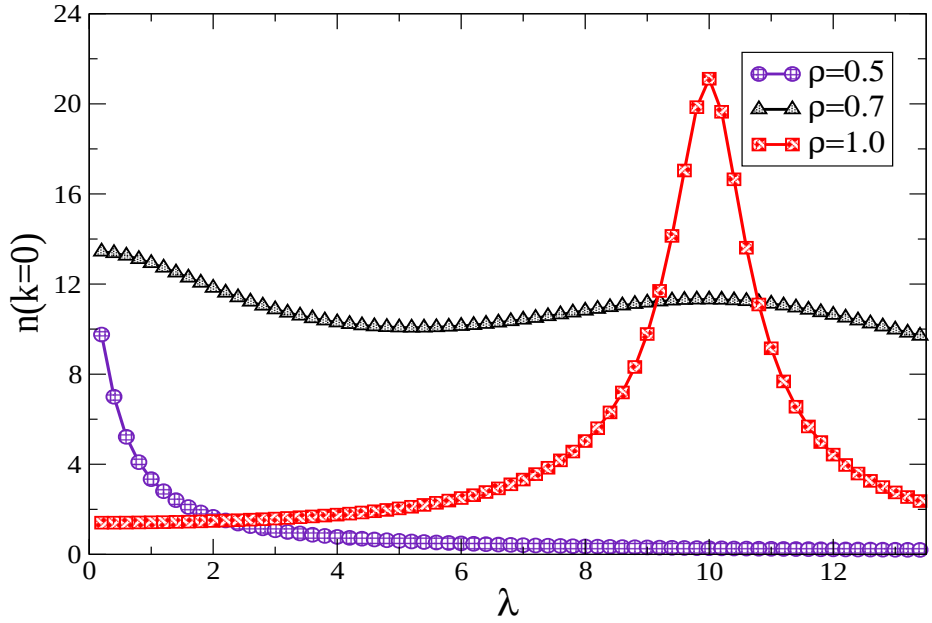

Fig. 3.15: $n(k=0)$ against various values of λ for densities, $\rho = 0.5, 0.7$ and 1.0.

superlattice, we expect to observe the peaks of $S(k)$ at $k = \pm\pi$. From Fig.(3.16), we can see two well defined peaks at $k = \pm 2\pi$ for $\rho = 0.5$, at a very large value of λ, implying the presence of the SLMI-I phase. For $\rho = 0.7$, which is an incommensurate density, there are two peaks at $\rho = 0.7$ for $\lambda \geq 2.0$. This is a consequence of density oscillations setting in the system due to the superlattice potential (Fig.(3.17)). Fig.(3.18) shows the behaviour of $S(k)$ for $\rho = 1.0$. For lower values of λ, there are no peaks at $k = \pm\pi$. But as λ increases, the peaks start appearing. The emergence of the peaks imply the influence of the superlattice potential, which changes the Brillouin zone boundaries.

Fig.(3.19) shows the plot of $S(k = \pi)$, for three different densities, as a function of λ. For $\rho = 0.5$, $S(\pi)$ starts from very close to zero, increases steadily, and then becomes constant. For $\rho = 1$, there is no peak initially. As λ increases, even in the MI phase, we see a finite value of $S(\pi)$, indicating the onset of the effect of the superlattice potential. Once λ crosses the value of $U(= 10)$, the value of $S(\pi)$ increases rapidly, showing the existence of the SLMI-II phase. For $\rho = 0.7$, $S(\pi)$ is close to zero for low values of λ, and then increases after λ becomes greater than some value, implying the existence of some

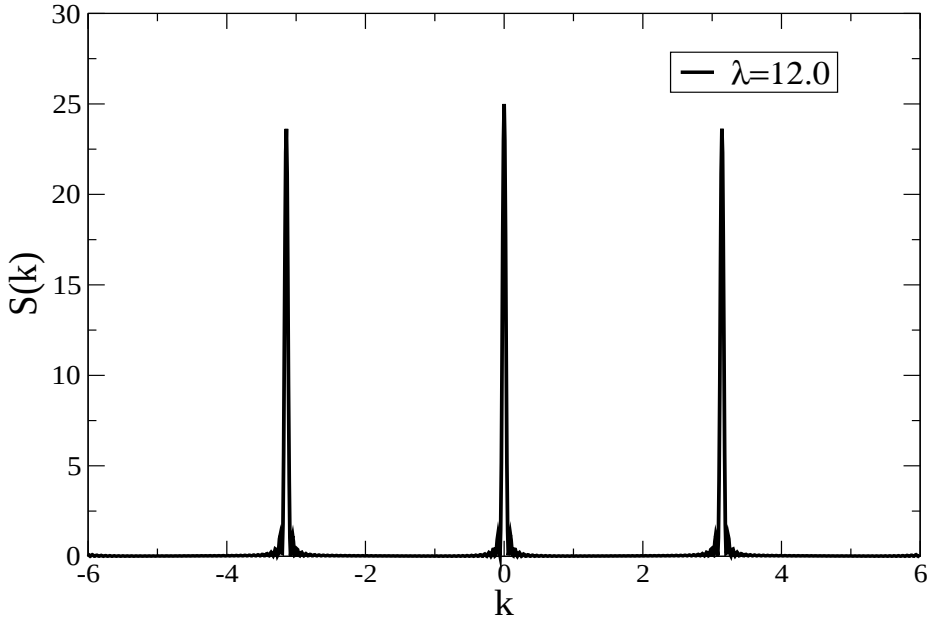

Fig. 3.16: Structure function, $S(k)$ versus the momentum, k, for density 0.5.

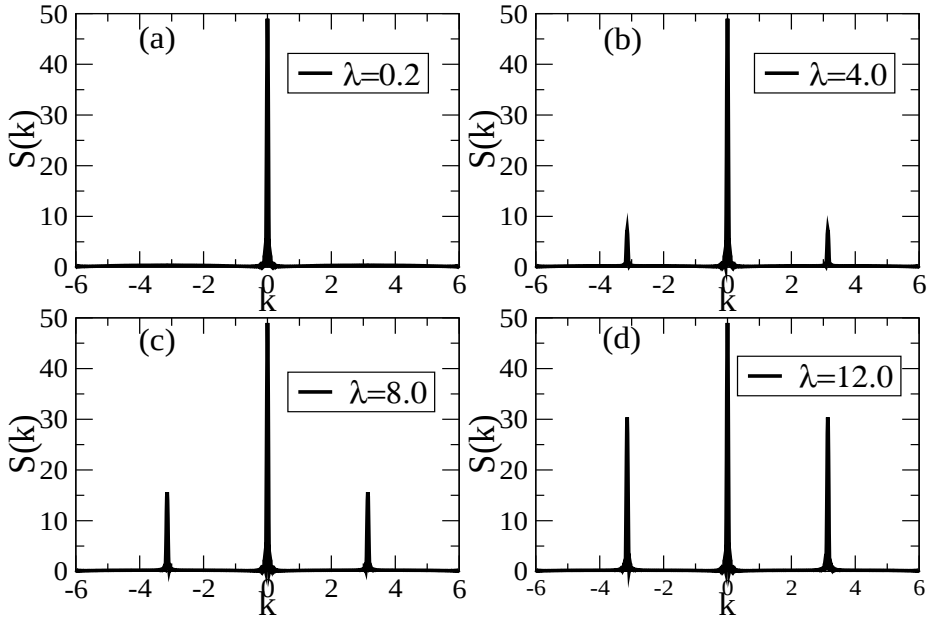

Fig. 3.17: Structure function, $S(k)$ versus the momentum, k, for density 1.0.

density modulations in the system.

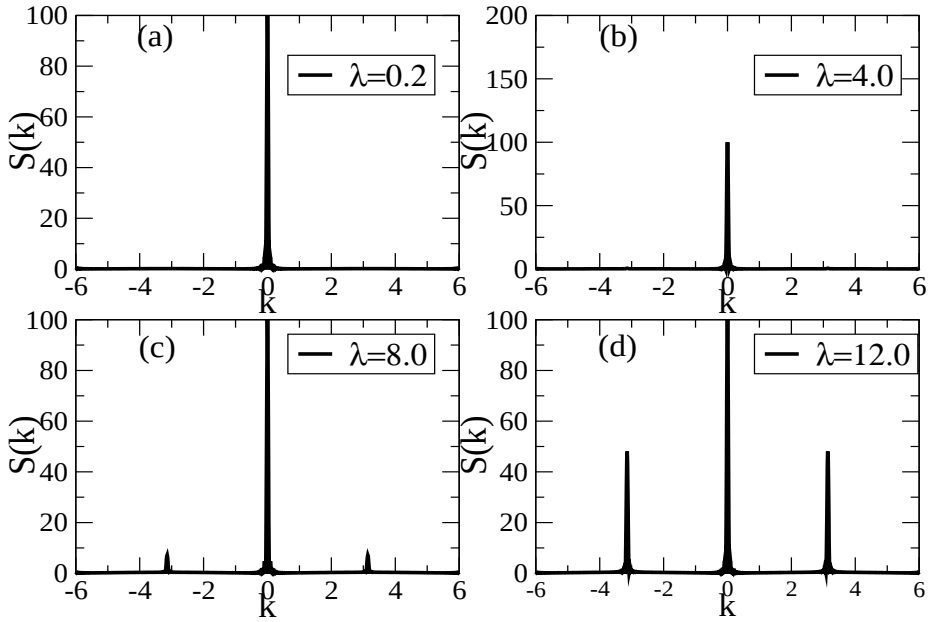

Fig. 3.18: Structure function, $S(k)$ vs the momentum, k, for density 0.7 for different values of λ.

The phase diagram in the μ-λ plane for $U = 10$ is shown in Fig.(3.20). μ_L^+ is defined as the energy cost when an atom is added to the system, i.e. $\mu_L^+ = E_L(N+1) - E_L(N)$, whereas μ_L^- is defined as the energy cost to remove an atom from the system, i.e. $\mu_L^- = E_L(N) - E_L(N-1)$. In order to get a correct phase diagram, we need to have accurate values of the chemical potential (both μ_L^+ and μ_L^-) in the thermodynamic limit, i.e. $L \to \infty$. For this purpose we plot the chemical potential versus the inverse of length $(1/L)$, and then extrapolate to length tending to infinity $(1/L \to 0)$. We plot these chemical potential values in Fig.(3.20) for densities 0.5 and 1.0, for a range of λ.

We further performed rigorous calculations to find the phase diagram in the U-λ plane to obtain the transition points accurately. The critical points were determined using the scaling relation of the Gap, which is defined as :

$$G_L = \mu_L^+ - \mu_L^- \tag{3.8}$$

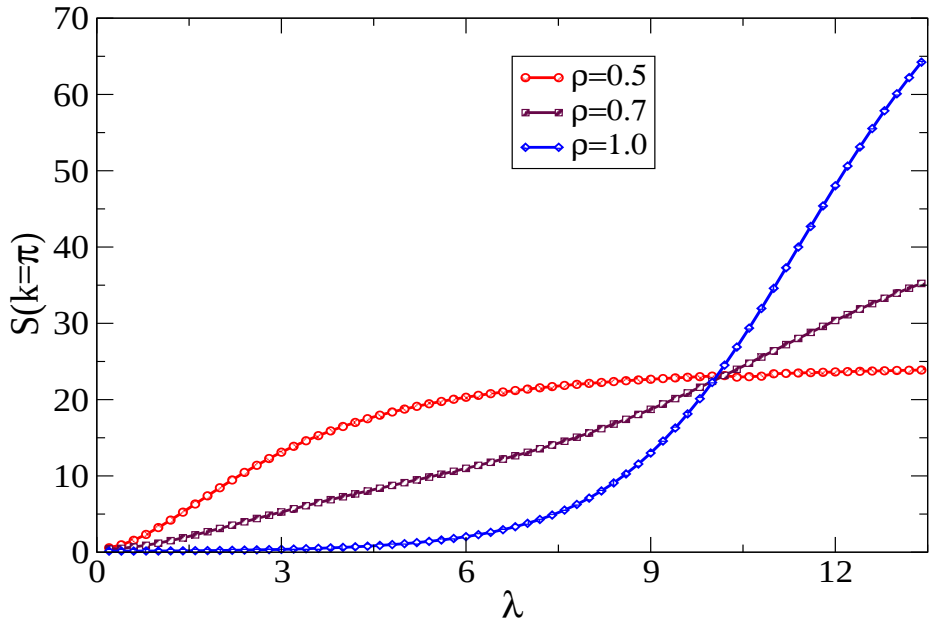

Fig. 3.19: S($k = \pi$) versus λ for three different density values, $\rho = 0.5, 0.7$ and 1.0.

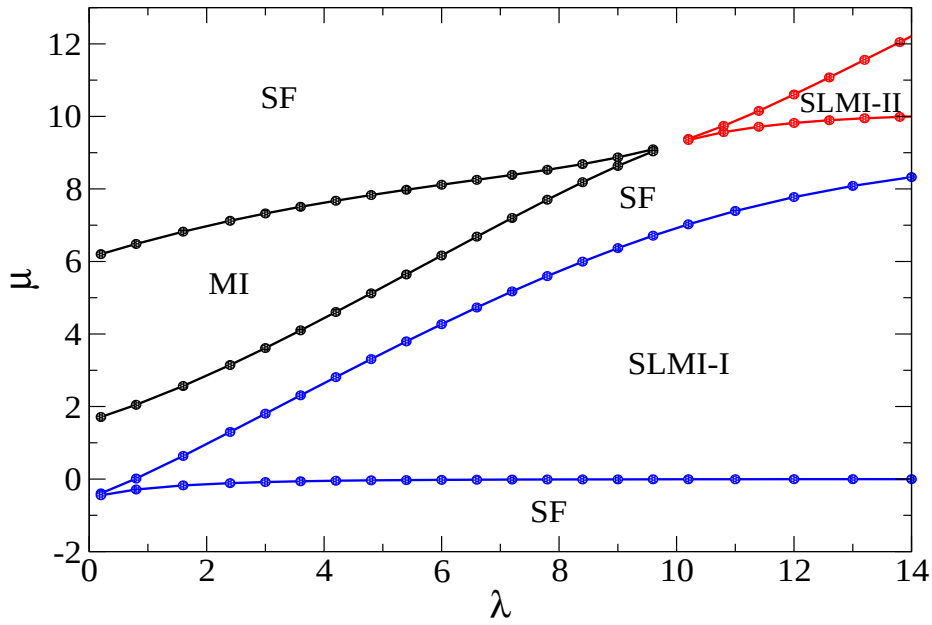

Fig. 3.20: Phase diagram for the system of optical superlattice in the $\mu - \lambda$ plane for $U = 10$.

In the gapless phase, the gap scales as $G_L \propto 1/L$ because of the finite-size effects, whereas in the insulating phase, it is $G_L \propto$ constant. Thus if simulations are carried out for various values of lengths of the system, L, and LG_L is plotted against λ, then in the SF phase, curves for various L will coalesce, whereas in the insulating phase, they will branch out. One such case is depicted in Fig.(3.21). We thus identify the critical points by checking the value of LG_L for $L = 140$ and 200, and see if the difference is less than 4%. Fig.(3.22) thus shows the complete phase diagram for $\rho = 1$.

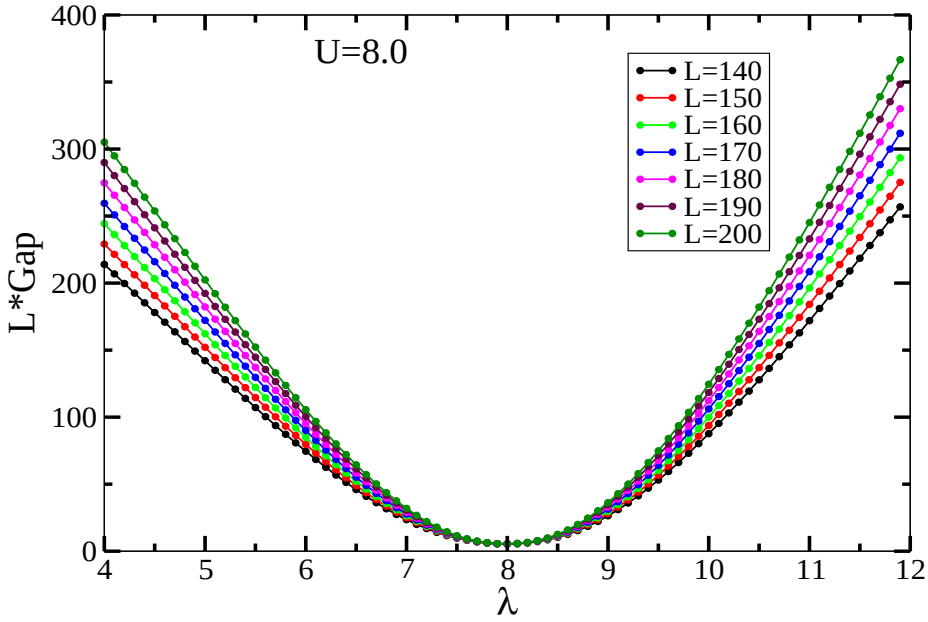

Fig. 3.21: Plot of L*Gap as a function of λ for $U = 8$

3.4 Three-Body on-site interaction in Optical Superlattice

The system of ultracold bosons with three-body interactions loaded in an optical superlattice can be best described by the following hamiltonian

$$H = -t \sum_{\langle i,j \rangle} a_i^\dagger a_j + \frac{U}{2} \sum_i n_i(n_i - 1) + \sum_i \lambda_i n_i + \frac{W}{6} \sum_i n_i(n_i - 1)(n_i - 2) \qquad (3.9)$$

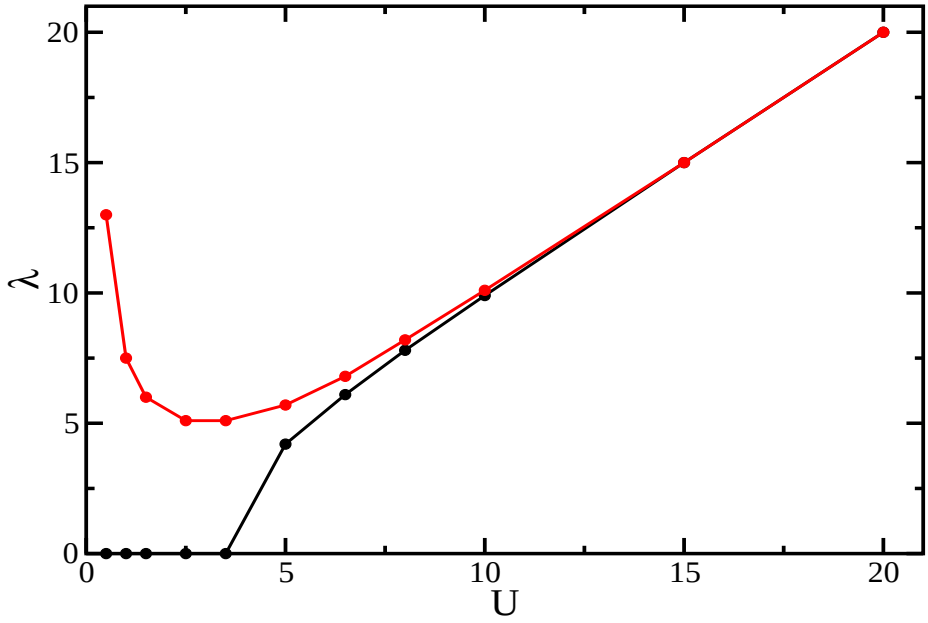

Fig. 3.22: Phase diagram for the system of optical superlattice in the $\lambda - U$ space for $\rho = 1$.

where W is the on-site three-body interaction amplitude. Zhang *et al.* had earlier found the insulating lobes being extended for optical lattice in the presence of three-body interactions, using decoupling mean-field theory [23]. Using two body collisions of atoms confined to the lowest vibrational state of the optical lattice, effective three- and higher-body interactions can be generated [24]. In earlier works, the effect of three-body interactions on the insulating lobes in an optical lattice were studied using mean-field and functional integral approaches [25].

On the experimental side, Will *et al.* [26] have detected and precisely measured the on-site three- and higher-body interaction strengths by observing the collapse and revival of the superfluid matter waves in a deep optical lattice. Nägerl *et al.* [27] have been able to accurately determine the on-site interaction energies including multibody interaction shifts. In another work, Greiner *et al.* [28] have determined the three-body interaction strengths by using occupation-sensitive photon-assisted tunneling. We now present the results of the effects of including the three-body interactions on various phases exhibited by ultracold bosonic atoms in an optical superlattice using FS-DMRG method.

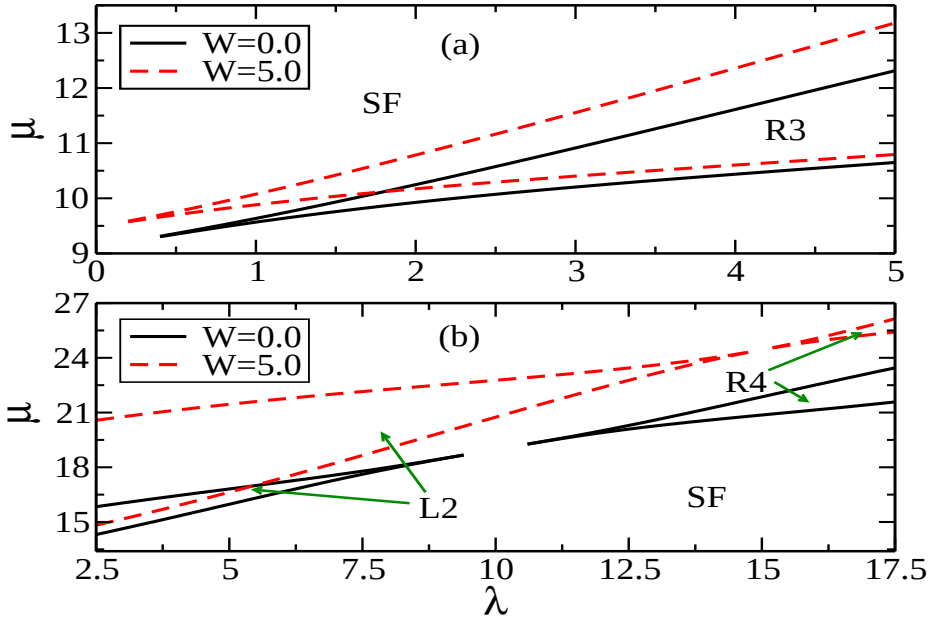

Fig. 3.23: Phase diagram for the system of ultracold bosonic atoms with on-site three-body interactions in an optical superlattice for two different densities (a) $\rho = 1.5$ and (b) $\rho = 2.0$

We plot the phase diagram for two different densities, $\rho = 1.5$ and 2 to see the effects of three-body interactions as shown in Fig.(3.23). Of course, at lower densities, there will be no effects of W, since the probability of three or more atoms being found at one site is negligible. For $\rho = 1.5$, in the absence of three-body interactions, the system undergoes a phase transition from the SF phase to the SLMI phase with configuration [2 1 2 1 ...] at $\lambda \sim 0.3$. However, at finite W (=5.0), the above transition occurs at $\lambda \sim 0.15$, signifying the enlargement of the insulating lobes (Fig.(3.23a)). At $\rho = 2.0$, in the absence of W, the system exhibits three phases for $U = 10.0$. For $\lambda < U$, the system is in the MI phase with [2 2 2 2 ...] configuration. It then undergoes a transition to the SF phase when λ becomes comparable to U (9.4). The system undergoes another quantum phase transition from SF phase to the SLMI phase with configuration [3 1 3 1 ...] as λ is increased beyond 10.6. But in the presence of W (=5.0), the SF window is shifted to a λ value which is comparable to $U + W$ as shown in Fig.(3.23b). The SF window not only shifts to a new λ value, but also shrinks when compared to that of $W = 0.0$.

We now propose an alternate method to observe three-body effects in an optical

lattice and superlattice. The effect of W is very small compared to the two-body interaction. From Eqn.(3.9), it is clear that the three-body energy scales as n^3. Therefore in order to observe the effect of three-body interaction in the experiments, it is necessary to study the SF-MI transition at higher densities. In the seminal experimental work by Greiner *et al.* [29], the SF-MI transition was observed by probing the excitation spectrum resulting from a particle-hole excitation. Such an excitation was provided by the potential gradient to the system in MI phase. Two narrow resonance peaks were seen in the plot of excitation probability versus the applied potential gradient. The first peak corresponds to the MI shell at density one. The appearance of the second peak may be due to the MI shell at density two. In the MI phase at density two, the particle-hole excitation at a given site would populate one of the neighbouring site with three atoms. In such a case, the atoms will experience the effects of W, along with that of U. In general, when there are n atoms in each site, the system is in MI phase with density n, and the excitation gap is given by $\Delta = U + (n-1)W$ for the optical lattice, and $\Delta = U + (n-1)W + \lambda$ for the optical superlattice. Therefore, by measuring the values of the potential gradients for higher-order peaks, and taking the difference between them for different values of n, it would be possible to determine the value of W.

3.5 Conclusions

We now summarize the findings from both the mean-field and DMRG approaches to the Bose-Hubbard model for ultracold atoms in a one dimensionl optical superlattice. The results can be broadly classified into two categories, one concerning density, $\rho = 1/2$, and the other for $\rho = 1$.

For $\rho = 1/2$, we see that for $\lambda = 0$, the system is always in the SF phase, no matter what the value of the on-site interaction, U is. As λ increases, the system undergoes a transition from the gapless SF phase to a gapped insulating phase, which we call as

the SLMI-I phase. This phase has the occupancy configuration [1 0 1 0 ...], displaying a density-wave character.

For $\rho = 1$, we further categorize our results into two parts, depending on the value of U. If U is less than the critical U_c for the SF-MI transition in the BH model, then the system will be in SF phase for $\lambda = 0$. As λ is increased, it goes to the gapped SLMI-II phase with a configuration of [2 0 2 0 ...] phase. However, if $U > U_c$, then the system will be in MI phase for $\lambda = 0$ with configuration [1 1 1 1 ...]. As λ is incremented, the system goes to the SF phase when $\lambda \approx U$. A further increase of λ drives the system into the SLMI-II phase. This window of SF diminishes as the value of U is increased, since a large U will tend to localise the atoms.

For the incommensurate density, $\rho = 0.7$, as expected that the system always remains in the SF phase. However, we also find density modulations induced by the superlattice potential, coexisting with this SF phase.

Thus our extensive analysis of the Bose-Hubbard model for a 1D optical superlattice has revealed novel quantum phases using two different theoretical methods, which agree with each other qualitatively to a large extent.

We also investigated the effects of three-body effects in optical superlattice at higher densities, and found the extension of the insulating lobes at $\rho = 1.5$. At $\rho = 2$, the SF window is found to be shifted to λ value which is comparable to $U + W$. The presence of W has also shrunk the SF window. We have also proposed a possible experimental scenario to find the values of W.

References

[1] V. G. Rousseau, D. P. Arovas, M. Rigol, F. Hebert, G. G. Batrouni, and R. T. Scalettar, Phys. Rev. B **73**, 174516 (2006).

[2] R. Roth and K. Burnett, Phys. Rev. A **68**, 023604 (2003).

[3] F. Schmitt, M. Hild, and R. Roth, Phys. Rev. A **80**, 023621 (2009).

[4] B.-L. Chen, S.-P. Kou, Y. Zhang, and S. Chen, Phys. Rev. A **81**, 053608 (2010).

[5] F. Schmitt, M. Hild, and R. Roth, eprint arXiv:1005.3129v1 [cond-mat.quant-gas].

[6] G. Roux, T. Barthel, I. P. McCulloch, C. Kollath, U. Schollwöck, and T. Giamarchi, Phys. Rev. A **78**, 023628 (2008).

[7] S. Piel, J. V. Porto, B. Laburthe Tolra, J. M. Obrecht, B. E. King, M. Subbotin, S. L. Rolston, and W. D. Phillips, Phys. Rev. A **67**, 051603 (R) (2003).

[8] J. Sebby-Strabley, M. Anderlini, P. S. Jessen, and J. V. Porto, Phys. Rev. A **73**, 033605 (2006).

[9] P. Cheinet, S. Trotzky, M. Feld, U. Schnorrberger, M. Moreno-Cardoner, S. Fölling, and I. Bloch, Phys. Rev. Lett. **101**, 090404 (2008).

[10] K. Sheshadri, H. R. Krishnamurthy, R. Pandit, and T. V. Ramakrishnan, Europhys. Lett. **22**, 257 (1993).

[11] D. Jaksch, C. Bruder, J. I. Cirac, C. W. Gardiner, and P. Zoller, Phys. Rev. Lett. **81**, 3108 (1998).

[12] D. van Oosten, P. van der Straten, and H. T. C. Stoof, Phys. Rev. A **63**, 053601 (2001).

[13] W. Krauth, M. Caffarel, and J. P. Bouchaud, Phys. Rev. B **45**, 3137 (1992).

[14] D. S. Rokhsar and B. G. Kotliar, Phys. Rev. B **44**, 10328 (1991).

[15] R. V. Pai, K. Seshadri, and R. Pandit, in *Current Topics in Atomic, Molecular and Optical Physics*, edited by C. Sinha and S. Bhattacharyya (World Scientific, Singapore, 2007), p. 105.

[16] T. Mishra, R. V. Pai, S. Ramanan, M. S. Luthra, and B. P. Das, Phys. Rev. A **79**, 013625 (2009).

[17] S. R. White, Phys. Rev. Lett. **69**, 2863 (1992); Phys. Rev. B **48**, 10345 (1993).

[18] U. Schollwöck, Rev. Mod. Phys. **77**, 259 (2005).

[19] T. D. Kuhner, S. R. White, and H. Monien, Phys. Rev. B **61**, 12474 (2000).

[20] R. V. Pai and R. Pandit, Phys. Rev. B **71**, 104508 (2005).

[21] T. D. Kuhner, S. R. White, and H. Monien, Phys. Rev. B **61**, 12474 (2000).

[22] L. Urba *et al.*, J. Phys. B **39**, 5187 (2006).

[23] Bo-lun Chen, Xiao-bin Huang, Su-Peng Kou, and Yunbo Zhang, Phys. Rev. A **78**, 043603 (2008).

[24] P. R. Johnson, E. Tiesinga, J. V. Porto, and C. J. Williams, New J. Phys. **11**, 093022 (2009).

[25] Kezhao Zhou, Zhaoxin Liang, and Zhidong Zhang, Phys. Rev. A **82**, 013634 (2010).

[26] Sebastian Will, Thorsten Best, Ulrich Schneider, Lucia Hackermüller, Dirk-Sören Lühmann, and I. Bloch, Nature **465**, 197 (2010).

[27] M. J. Mark, E. Haller, K. Lauber, J. G. Danzl, A. J. Daley, and H.-C. Nägerl, Phys. Rev. Lett. **107**, 175301 (2011).

[28] R. Ma, M. E. Tai, P. M. Preiss, W. S. Bakr, J. Simon, and M. Greiner, Phys. Rev. Lett. **107**, 095301 (2010).

[29] M. Greiner, O. Mandel, T. Esslinger, T. W. Hänsch and I. Bloch, Nature **415**, 39 (2002).

Chapter 4

Quantum Phases in Frustrated Ladder Systems

4.1 Introduction

In the previous chapter, we presented the results obtained for a system of ultracold bosonic atoms loaded in an optical superlattice, and determined the phase diagram. We found the existence of the superfluid (SF), Mott insulator (MI) and the superlattice induced Mott insulator (SLMI) phases. We now turn our attention to a system of ladders, and present the findings on two of different configurations. We first consider a zig-zag ladder with hardcore bosons loaded in it, followed by a regular two-legged ladder, which has hopping amplitudes that lead to an effective flux of π in each of the plaquettes. Both these systems display geometric frustration leading to novel quantum phases.

4.2 Triangular lattice with Superlattice Potential

In this section, we present our results for a system of hard-core bosons in a zig-zag ladder, with different potential depths in the two legs. This essentially maps onto a 1-d optical superlattice, with nearest and next-nearest hopping as shown in Fig.(4.1). The hamiltonian describing such a system can be written as :

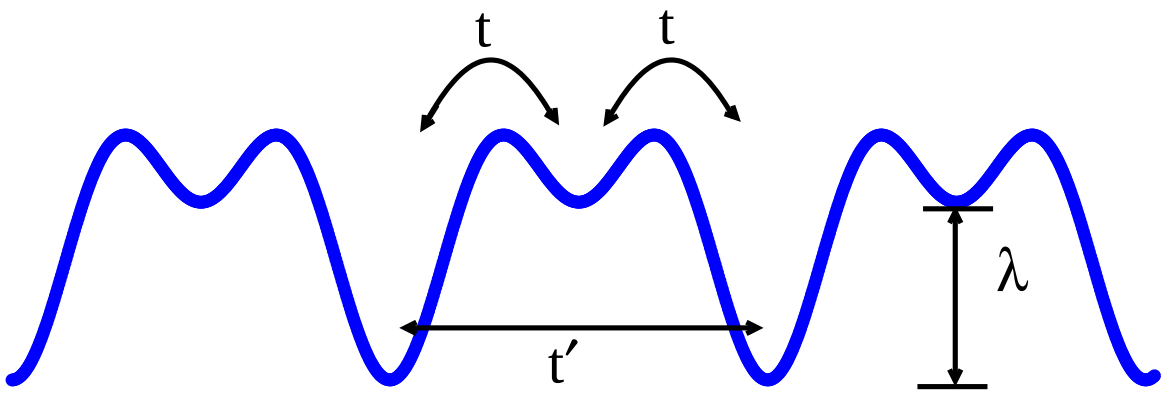

Fig. 4.1: Schematic diagram of an one-dimensional two-period optical superlattice with nearest and next-nearest hopping

$$\begin{aligned} H &= -t\sum_i (a_i^\dagger a_{i+1} + h.c.) - t'\sum_i (a_i^\dagger a_{i+2} + h.c.) \\ &\quad + \sum_i \lambda_i n_i \end{aligned} \tag{4.1}$$

where $a_i^\dagger$ and a_i are creation and annihilation operators respectively for hard core bosons at site i, and $n_i = a_i^\dagger a_i$ is the boson number operator at site i. To avoid multiple occupancies of the lattice sites we use the constraint that $a_i^{\dagger 2} = a_i^2 = 0$. Here t is the hopping amplitude for tunneling to the nearest neighbouring site, t' is the probability amplitude to tunnel to the next-nearest neighbour and λ_i is the superlattice potential. In the present work, we have considered a two-period superlattice, with $\lambda_i = \lambda$ for i being odd and $\lambda_i = 0$ for i being even. We study the system for a wide range of t' and λ while fixing the value of $t = 1$.

Recent experimental developements have resulted in the creation of various lattice geometries, using suitable arrangements of laser beams, such as optical superlattices [1], triangular lattices [2], Kagome lattices [3], etc. Using Feshbach resonance, the interatomic interactions can be tuned and controlled to a very high degree of precision [4], and these interactions can be made attractive or repulsive . The magnitude and sign of intersite hopping can now be controlled very accurately using shaking techniques [5, 6]. These remarkable advances on the experimental front motivate us to perform theoretical studies

of ultracold atoms in different lattice geometries and look for novel quantum phases.

Phases with density wave like configurations were theoretically predicted in a system of ultracold bosons in an optical superlattice [7, 8, 9, 10, 11, 12]. They are referred to as superlattice induced Mott insulator (SLMI) phases and have different densities depending on the occupation number of the atoms in a unit cell [13, 14]. The competition between frustration arising from lattice geometry and interactions has been widely studied [15, 16, 17], revealing rich physics with a variety of novel quantum phases exhibited by the superlattice system.

For the particular case for $t' = 0$, the model described in Eqn.(4.1) can be mapped exactly to a system of spinless fermions. Applying the Jordan-Wigner transformation [18],

$$a_i^\dagger = f_i^\dagger \prod_{\beta=1}^{i-1} e^{-i\pi f^\dagger f}, \quad a_i = \prod_{\beta=1}^{i-1} e^{-i\pi f^\dagger f} f_i^\dagger \tag{4.2}$$

Eqn.(4.1) can be mapped to

$$H = -t \sum_i (f_i^\dagger f_{i+1} + h.c.) + \sum_i \lambda_i f_i^\dagger f_i \tag{4.3}$$

where $f_i^\dagger$ and f_i are the creation and anihilation operators for the spinless fermions and $f_i^\dagger f_i$ is the number operator.

The above hamiltonian described in Eqn.(4.3) can be solved exactly to obtain the single particle eigenstates. Two bands arise due to the breaking of the translational symmetry of the lattice by the superlattice potential. The energy spectra of the two bands are given by

$$E_\pm(k) = \frac{\lambda \pm \sqrt{\lambda^2 + [4tcos(ka)]^2}}{2} \tag{4.4}$$

where a is the lattice spacing and k, the crystal momentum that runs from $\frac{-\pi}{2a}$ to $\frac{\pi}{2a}$. A plot of these spectra is shown in Fig.(4.2). From this figure and Eqn.(4.4) it can be seen that at half filling, the system exhibits a gap which is equal to the value of the superlattice potential. Finite values of λ takes the system into a gapped insulating

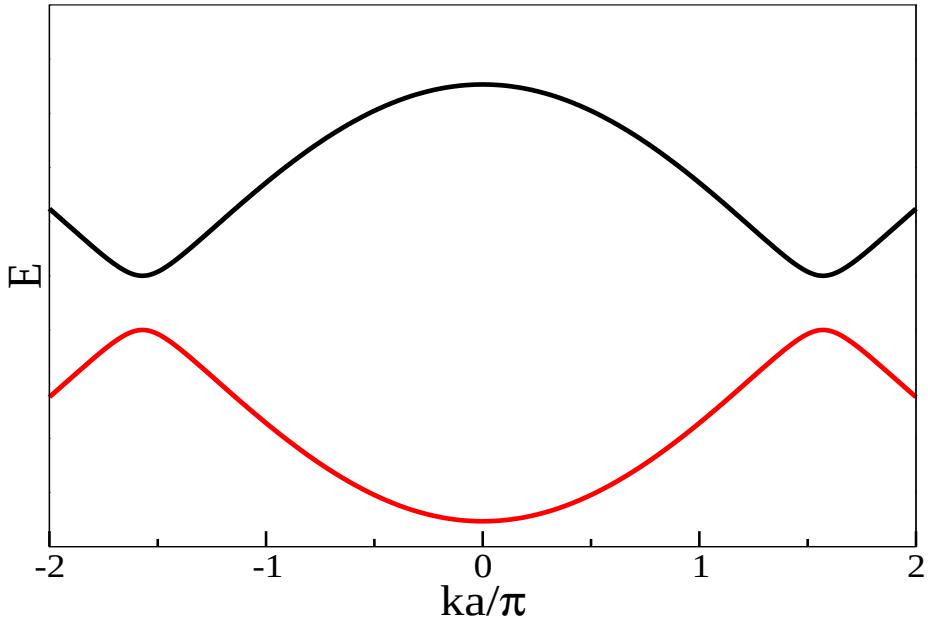

Fig. 4.2: Dispersion relation as computed from the Eqn.(4.4)

phase, which is a SLMI phase. The situation becomes more complex when t' is turned on, resulting in a model which cannot be solved exactly. Hence we take recourse to the numerical technique of density matrix renormalisation group (DMRG) method as described in Chapter 2 to determine the ground state energy and wavefunction. Positive t' ensures a greater likelihood of hopping for the atoms, whereas negative values of t' implies frustration, whereby hopping along one of the legs of the zig-zag ladder increases energy. In our work, we have considered both positive and negative values of t', in order to investigate the new quantum phases that could arise in the presence of a superlattice potential.

Due to the hard-core nature of the atoms, only zero or single occupancy in a single site will be allowed. This effectively results in $a_i^{\dagger 2} = 0$. For this scenario, the model can be exactly mapped into a zig-zag ladder, with different inter- and intra-chain hopping strengths. The presence of a superlattice potential means that the two legs of the ladder are at different depths. Eqn.(4.1) can be mapped onto a spin 1/2 Hamitonian through

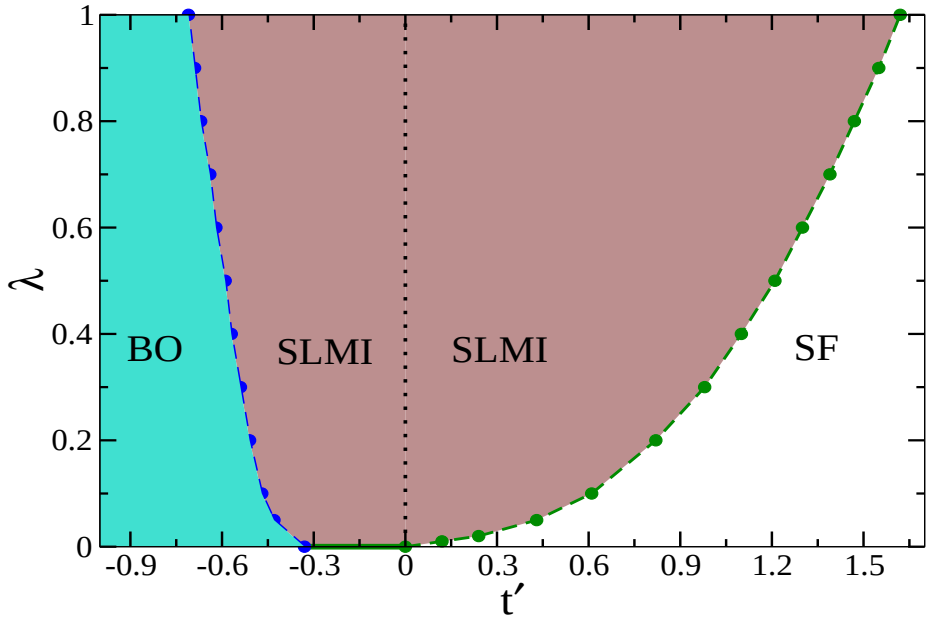

Fig. 4.3: Phase diagram for a system of hard-core bosons with nearest-neighbour hopping in an optical superlattice, at a filling factor of half

the following substitution :

$$S_i^+ = a_i^\dagger, S_i^- = a_i \tag{4.5}$$

$$S_i^z = (n_i - 1/2) \tag{4.6}$$

The hamiltonian then takes the form:

$$\begin{aligned} H &= \frac{1}{4}\sum_i [-2t(S_i^x S_{i+1}^x + S_i^y S_{i+1}^y)] \\ &\sum_i [-2t'(S_i^x S_{i+2}^x + S_i^y S_{i+2}^y)] + \sum_i \lambda_i (S_i^z + 1/2) \end{aligned} \tag{4.7}$$

4.2.1 Method

As mentioned before, to obtain the ground state properties of the model represented by Eqn.(4.1), we employ the finite-size DMRG with open boundary conditions [19, 20], which is suitable for one-dimensional systems. In all our computations, we studied systems up to a length of 300 sites, and retained the 128 highest eigenstates corresponding to the density matrix. The weight of the discarded states were less than 10^{-6}.

For the purpose of obtaining the ground state phase diagram, several physical quantities were evaluated as listed below :

- To distinguish between the gapped and gapless phases, the energy gap is given by

$$G_L = E(L, N+1) + E(L, N-1) - 2E(L, N). \tag{4.8}$$

  In Eqn.(4.8), $E(L, N)$ is the ground-state energy of a system with L sites and N bosons.

- For detecting the BO phase, we look at the bond order parameter given by

$$O_{BO} = \frac{1}{L}\sum_i (-1)^i B_i \tag{4.9}$$

  where $B_i = \langle b_i^\dagger b_{i+1} + b_{i+1}^\dagger b_i \rangle$ is the bond energy.

- The SLMI phase is characterised by the structure factor, given by the Fourier transform of the density-density correlation function

$$S(k) = \frac{1}{L}\sum_{i,j} e^{i(i-j)k} \langle n_i^\dagger n_j \rangle \tag{4.10}$$

- The momentum distribution is given by

$$n(k) = \frac{1}{L}\sum_{i,j} e^{i(i-j)k} \langle a_i^\dagger a_j \rangle \tag{4.11}$$

Before proceeding onto the results obtained with the parameters considered in our FS-DMRG simulations, we would like to mention that the set of parameters assumed in our computations are sufficient to obtain accurate results for this model. This is evident from the computation of energy gap as shown in Eqn.(4.8) for the system when $t' = 0$ given by Eqn.(4.3). An exact analytical treatment of Eqn.(4.3) shows that this gap will be equal to the superlattice potential, λ considered in our work. We compared the gap values obtained from numerical computations, and found $|G - \lambda| \sim 10^{-5}$

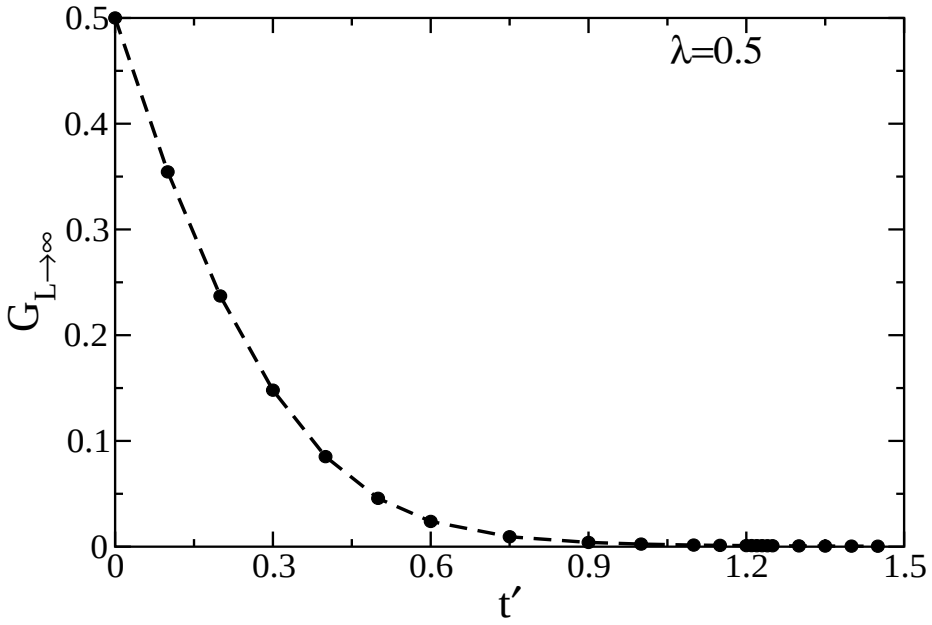

Fig. 4.4: Thermodynamic value of G plotted against t' for $\lambda = 0.5$ to locate the transition point.

4.2.2 Results

We now discuss in details the findings of our computations. For $t' = 0$, the system goes from a gapless SF to a gapped SLMI phase for any finite value of λ. This behaviour can be attributed to the fact that the atoms being hard core in nature, a small value of λ will create a difference in potential depths in the two legs of the zig-zag ladder. As a result, the atoms occupying the deep lattice site, i.e. one of the legs of the ladder, will be energetically favourable, giving rise to the distribution of [0 1 0 1 0 1]. The situation becomes interesting when t' is turned on. We investigate the system for both positive and negative values of t', and for a range of values of λ at half filling.

The phase diagram of the system described by Eqn.(4.1) is shown in Fig.(4.3). We divide our results into two sections depending on the sign of t', duly presented in the next two subsections.

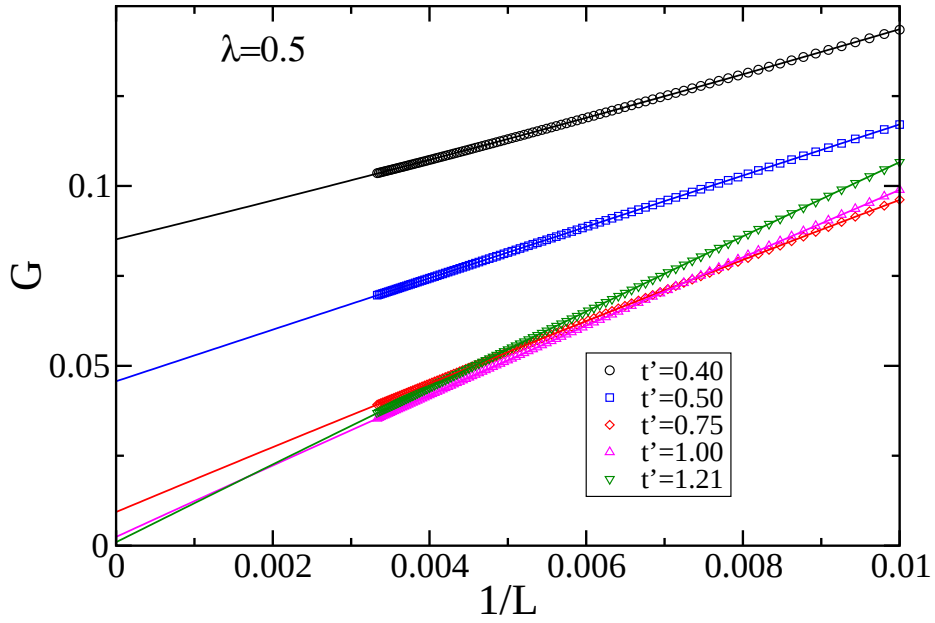

Fig. 4.5: Gap, G, plotted against $1/L$, along with the extrapolation for different values of t' for $\lambda = 0.5$

4.2.2.1 Positive t' scenario

For positive values of t', in the absence of a superlattice potential, the system is an unfrustrated triangular ladder described by a simple $t - t'$ model. Any finite value of t' drives the system into the gapless phase. However for non-zero values of λ, the system goes to the SLMI phase for small values of t'. Now fixing λ, if one increases t', the SLMI order in the system gradually disappears, leading to a gapless SF phase. This can be understood in the following way. In the SLMI phase, alternate sites are occupied. Because of the large value of t', one such atom may hop to the next nearest site which is already occupied. Because of the hard-core nature of the atoms, the latter atom will hop to its nearest neighbour, which incidentally is a free site. And this process can continue leading to a delocalisation of the wavefunction, which will then correspond to a SF phase. The signature employed to detect this transition is the energy gap, G.

A finite size scaling of the gap, G_L is performed by fitting with a quadratic polynomial in $1/L$. It is then extrapolated to $L \to \infty$ to get the thermodynamic limit of G. The

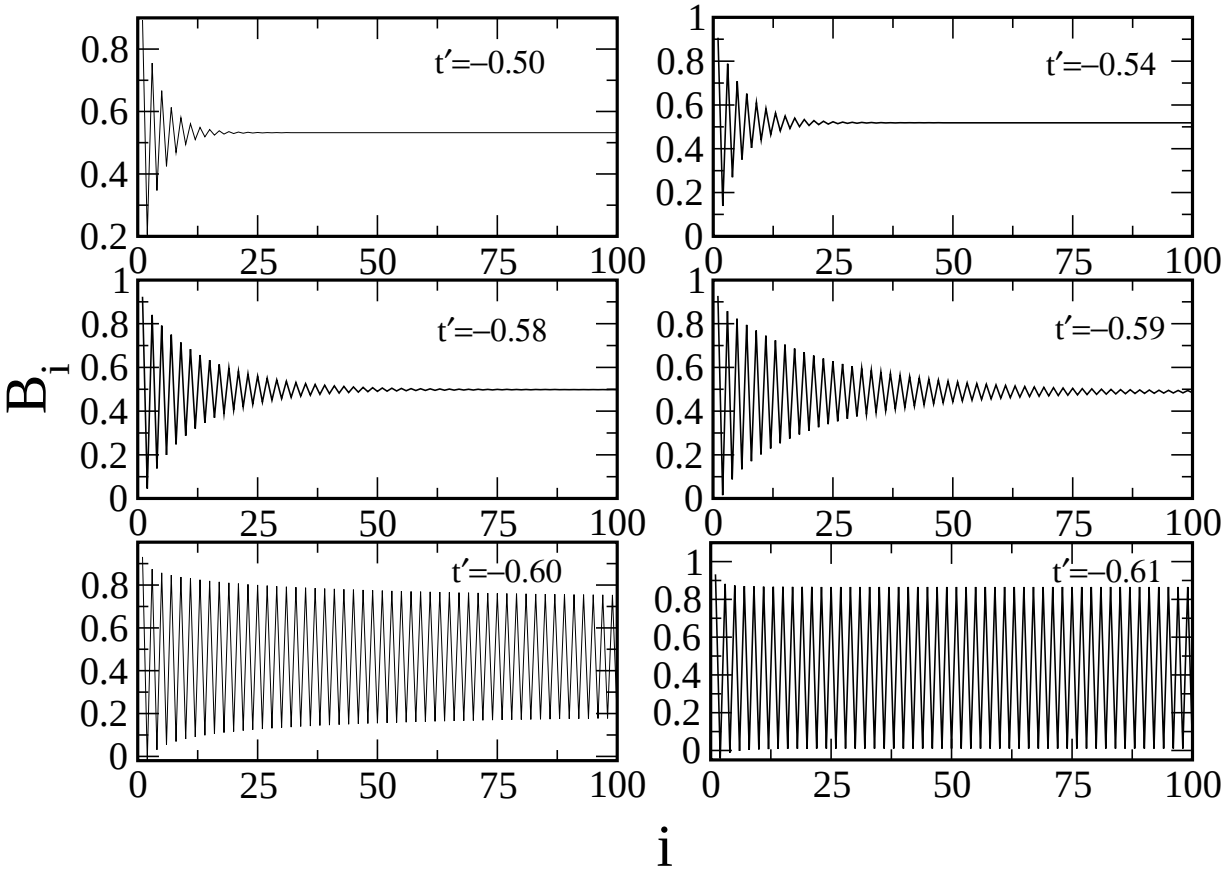

Fig. 4.6: B_i is plotted against i for $\lambda = 0.5$.

range of L considered for the above fitting were from 100 to 300. The extrapolated values of G as a function of t' for $\lambda = 0.5$ is shown in Fig.(4.4). This clearly shows the gap to fall down gradually signifying the transition to belong to the Berezinskii-Kosterlitz-Thouless (BKT) universality class. In Fig.(4.5), the finite size scaling of the gap, G_L, for different values of t' are plotted, along with the extrapolated functions. As the transition point approaches, the fitted function tends to 0, indicating the onset of the SF phase. We impose the criterion that $G_{L\to\infty} \sim 10^{-3}$ to determine the critical point for the gapped to the gapless phase transition.

4.2.2.2 Negative t' scenario

The negative values of t' induces frustration in the system leading to interesting phases. In the absence of the superlattice potential, $\lambda = 0$, the system has been investigated

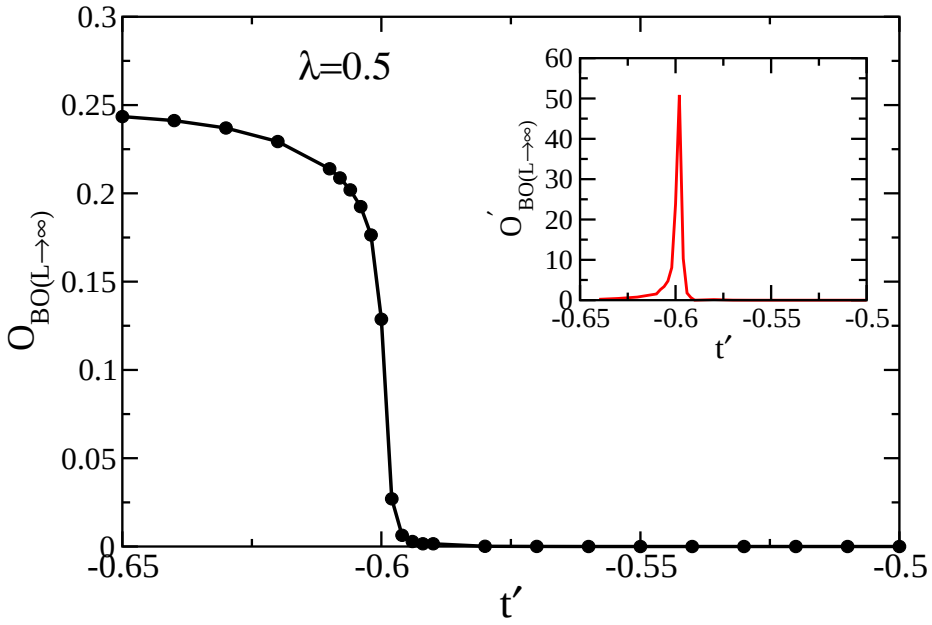

Fig. 4.7: Plot of thermodynamic values of the O_{BO} against t' for $\lambda = 0.5$. A discrete jump in the values can be observed around the transition point. Inset: The first derivative showing a peak at the transition point from SLMI to BO phase

extensively. It has been predicted that the system remains in the SF phase for small values of t'. For $|t'| > 0.33$, the system dimerises, with atoms getting localized between neighbouring sites. This phase is called the BO phase, which is gapless in nature, and the transition from SF to BO phase is of the BKT type. At $t' = -0.5$, the system exhibits a Majumdar-Ghosh type of state [17]. As discussed in the previous case, the system enters the SLMI phase for any small finite value of λ. Therefore on the negative t' side, there exists only a SF line which extends till $t' = 0.33$. For finite values of λ, the atoms begin to occupy in the lower potential wells thus entering the SLMI phase. However, if λ is fixed, and $|t'|$ is increased, then the atoms delocalise between neighbouring sites, thus entering BO phase. The BO phase is characterised by the periodic oscillations in the bond energy. In Fig.(4.6) we plot B_i as a function of lattice sites for various values of t' when $\lambda = 0.5$.

Fig.(4.6 a, b, c and d) show that for small values of $|t'|$, there is an exponential decay in the B_i with the lattice length. However, in Fig.(4.6 e), we see the setting in of long-range bond oscillations in the system. These oscillations are sustained throughout the

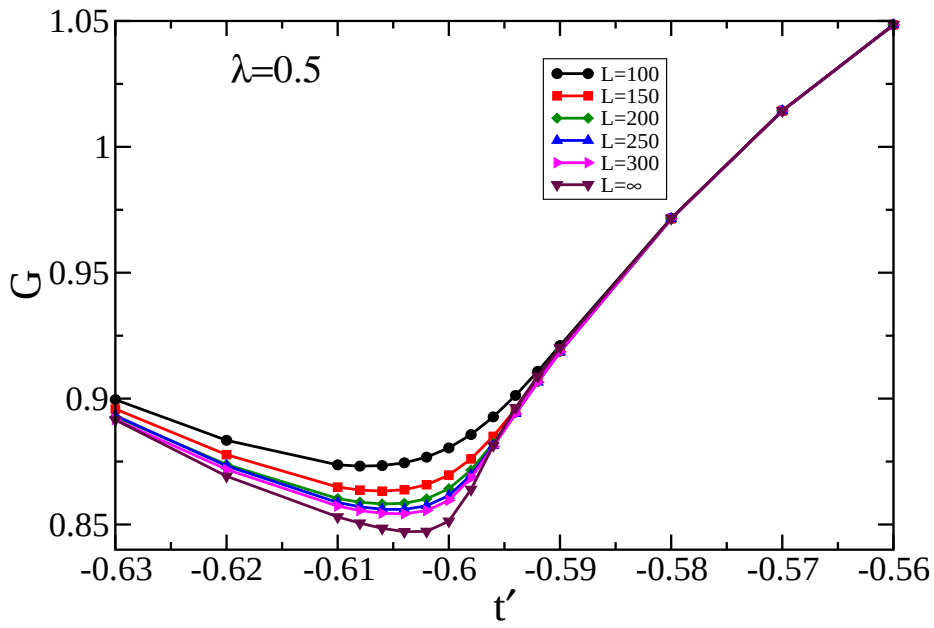

Fig. 4.8: Energy gap, G plotted for different lengths against t'. The minima implies the critical point.

entire lattice structure and become increasingly prominent as the value of $|t'|$ is increased. This clearly suggests the presence of the BO phase at lower values of t'. Now, having known the presence of these two phases, we proceed to locate the critical points. For this purpose, we compute the BO order parameter, O_{BO} as defined in Eqn.(4.9). To avoid the finite size effects, we extrapolate O_{BO} using a third order polynomial as a function of $1/L$. The thermodynamic value obtained in this way, for $1/L \to \infty$, is plotted for various t' in Fig.(4.7). The BO phase is characterised by a non-zero O_{BO}, whereas in the SLMI phase, it is zero. Fig.(4.7) clearly shows a discrete jump in its value implying a transition from the SLMI to the BO phase. The inset of the Fig.(4.7) plots the first derivative of O_{BO}. As expected, it shows a sharp maximum, the position of the peak giving us the transition point. A complementary approach for determining this phase transition is based on the behaviour of the gap G_L. In Fig.(4.8), we plot G_L as a function of t' for different values of length, L, including $L \to \infty$, obtained by a second order polynomial extrapolation. Along the λ axis, the gap is always finite. It decreases as we approach the critical point, and reaches a minimum at the transition point, followed by an increase

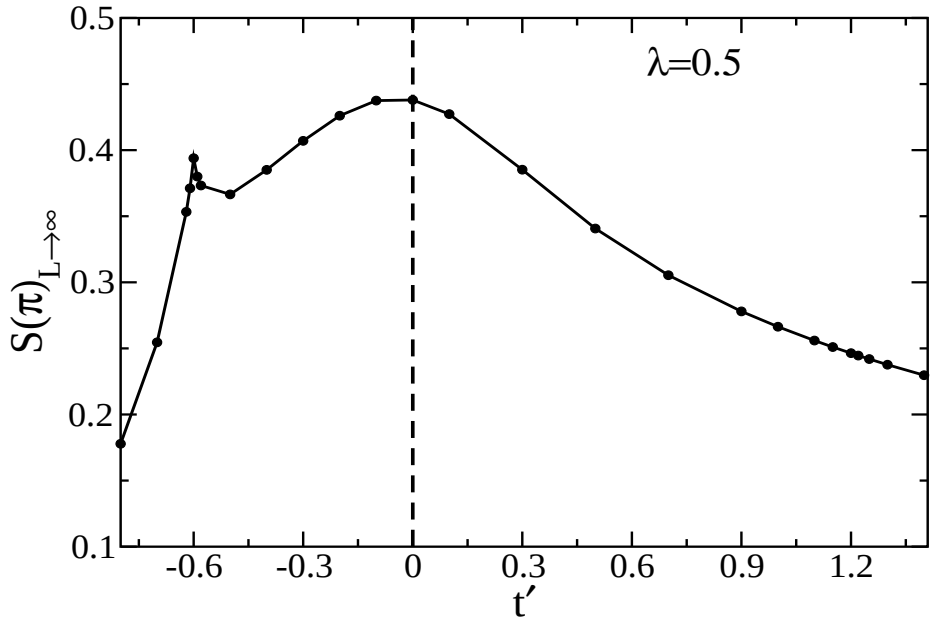

Fig. 4.9: Thermodynamic values of $S(\pi)$ is plotted for the entire range of t' for $\lambda = 0.5$

again as t' is increased. The minima shifts towards the actual critical point, as we consider larger lengths, L. In the thermodynamic limit, the minima or the critical point is located at $t' = -0.604$, which agrees with the value obtained from O_{BO} scaling.

The SLMI phase has the occupancy configuration of the form [1 0 1 0 1 0 ...]. As a result, the structure factor, $S(k)$, as defined in Eqn.(4.10) will display finite peaks at $k = \pm\pi$. But in the BO and SF phases, this peak value will decrease. As before, to correct for the finite size effects, we plot the thermodynamic values of $S(\pi)$ as a function of t' for two fixed values of $\lambda = 0.5, 0.05$ in Fig.(4.9) and Fig.(4.10) respectively. The thermodynamic values are obtained by a third order polynomial fit. Its value in the BO phase stays low. As t' approaches the critical point for the BO-SLMI transition, the value of $S(\pi)$ gradually increases. At the critical point, we observe a sharp peak, after which the latter decreases. As t' increases towards zero, $S(\pi)$ again increases steadily for $\lambda = 0.5$, whereas it decreases continuously for $\lambda = 0.05$. In both the cases the system now is in the SLMI phase. For positive values of t', both the plots for $\lambda = 0.5$ and 0.05 show a gradual decrease in the value of $S(\pi)$ as the system passes through the SLMI-SF phase transition.

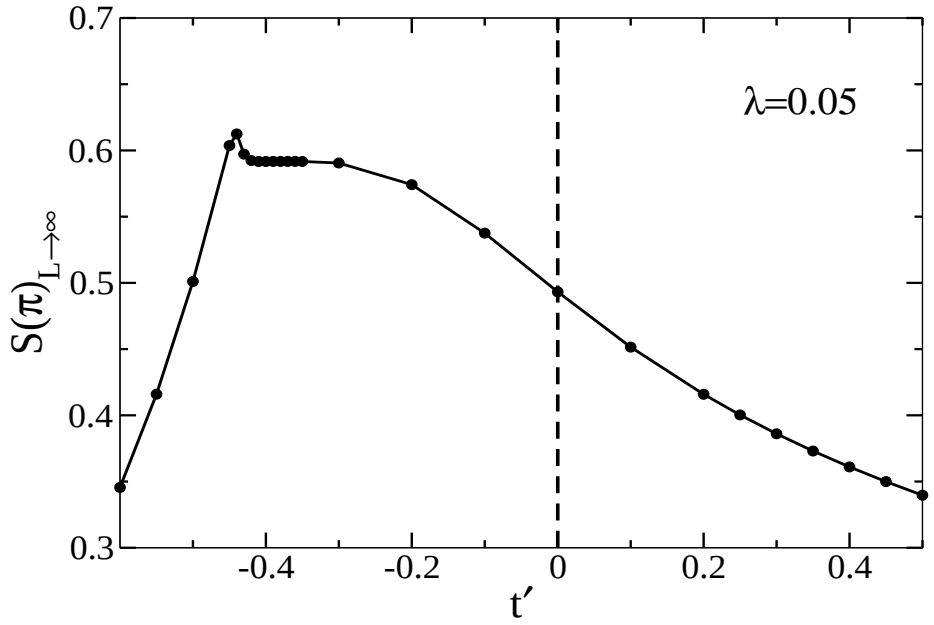

Fig. 4.10: Thermodynamic values of $S(\pi)$ is plotted for the entire range of t' for $\lambda = 0.05$

We now turn our attention to a physical quantity which can be directly observed in experiments. One such quantity is the momentum distribution which can be measured through the time-of-flight images. We numerically compute the momentum distribution, and plot it in Fig.(4.11). In the SLMI phase, it shows a broad peak at $k = 0$. But as the system enters the BO phase, we observe the appearance of two peaks, which shifts away from $k = \pm\pi$ (Fig. 4.11 a and b). For positive t' region, the population of atoms in the $k = 0$ state is very small, as indicated in Fig.(4.11 c). But as the system enters the SF region, $k = 0$ state fills up, resulting in a large peak as shown in Fig.(4.11 d).

It is convenient to analyse the model described by Eqn.(4.1) in two different regions : negative and positive next-nearest hopping amplitude, t'. For negative t' values, λ being zero, the system remains in SF phase for $t' \geq -0.33$. Smaller values of t' takes the system to the bond-ordered (BO) phase. Finite values of λ, drive the system into the SLMI phase since it is energetically favourable for the hard core bosons to occupy the lower potential wells. The transition to the BO phase for finite values of λ will now occur at a t' value smaller than -0.33 since it will require larger values of t' to break the SLMI order in the

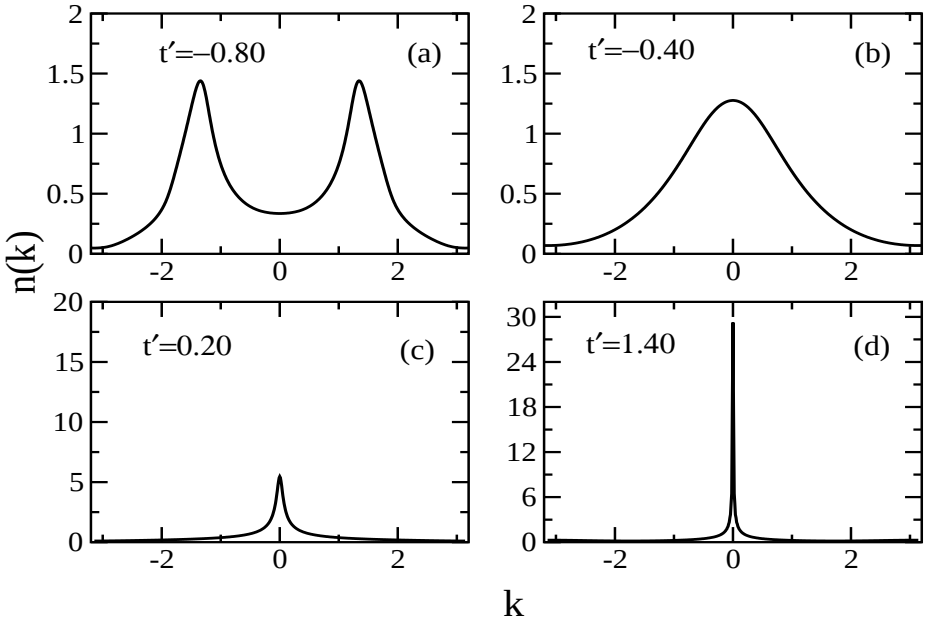

Fig. 4.11: Momentum distribution for different values of t' for $\lambda = 0.5$

system. In the positive t' region, for $\lambda = 0$, the system remains in the SF phase for all values of t'. But finite values of λ takes the system to the SLMI phase with alternate sites being occupied. Increasing t' results in atoms having higher hopping probabilities to the next-nearest sites ultimately leading to the transition to a SF phase.

4.2.3 Conclusions

In conclusion, we analysed a system of hard-core bosonic atoms at half-filling loaded in an optical superlattice, with finite nearest and next-nearest hopping amplitudes using the FS-DMRG method. Our findings suggest the existence of three phases, namely the BO phase, the SLMI phase and the SF phase, depending on the values of the superlattice potential and the next-nearest hopping amplitude.

4.3 Two-Leg Bose Ladder with π flux in each plaquette

Motivated by the recent developements in experiments where a uniform or staggered "synthetic magnetic field" for neutral atoms can be generated using two photon Raman transitions [21, 22, 23], thus permitting us to access large magnetic fields for bosons loaded in a lattice, we proceed to study the competition between strong correlations and frustration in the fully frustrated Bose-Hubbard (FFBH) model, with half a "magnetic flux" quantum per plaquette [24, 25, 26, 27]. Earlier works have studied the repulsive interactions quenching the "kinetic frustration", which led to the emergence of unconventional superlfuids [28, 24, 25, 26, 27], or quantum Hall liquids [29]. Such "kinetic frustration" can also be obtained by controlling the sign of the atom hopping amplitude using time-dependent shaking of the optical lattice, or populating higher bands of an optical lattice [28].

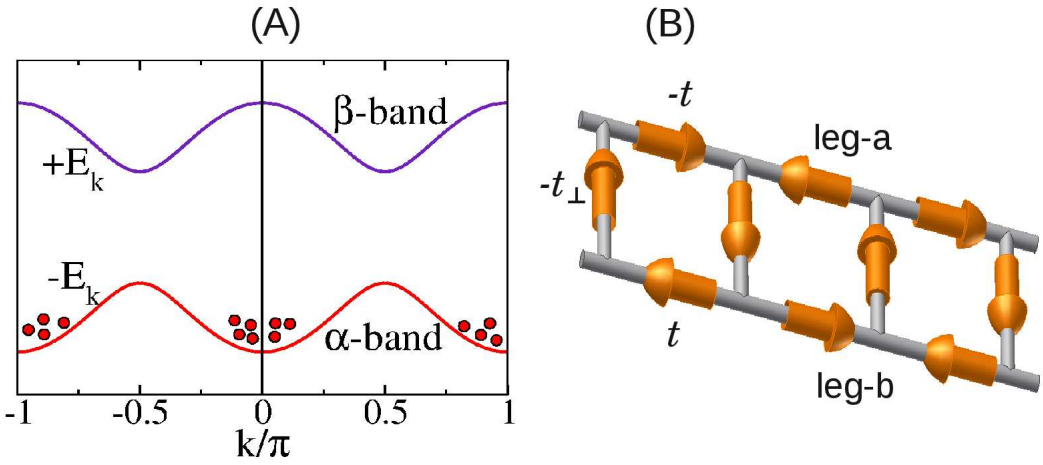

Fig. 4.12: (a) Dispersion of the FFBH model at $U = 0$, with two degenerate minima in the low-energy α band. Interactions force an equal number of bosons (on average) to condense into each of the two minima. (b) Alternating pattern of plaquette currents in the presence of chiral order.

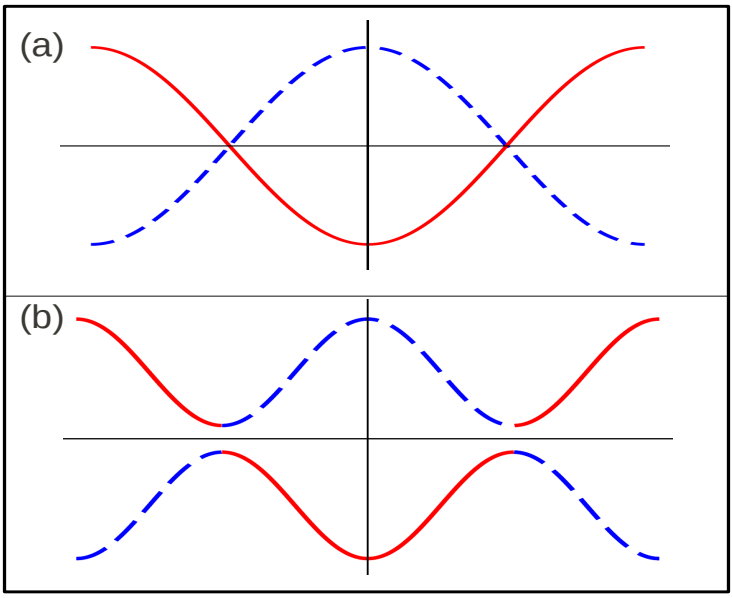

Fig. 4.13: The upper panel denotes the dispersion for $U = 0$ and $t_\perp = 0$ showing the degeneracy. The degeneracy is lifter by turning on $t_\perp$ as shown in the lower panel.

The hamiltonian of the FFBH model on a two-leg ladder is given by

$$\begin{aligned} H &= -t\sum_i (a_i^\dagger a_{i+1} + a_{i+1}^\dagger a_i) + t\sum_i (b_i^\dagger b_{i+1} + b_{i+1}^\dagger b_i) - t_\perp \sum_i (a_i^\dagger b_i + b_i^\dagger a_i) \\ &\quad + \frac{U}{2}\sum_i (n_{a,i}^2 + n_{b,i}^2) \end{aligned} \tag{4.12}$$

where a and b are the labels for the two legs of the ladder as shown in Fig.(4.12 b). The inter-chain hopping is denoted by $t_\perp$, and U denotes the on-site repulsive interaction. The opposite signs of the intra-chain hopping, t, contributes to an Aharonov-Bohm phase of π for a boson hopping around an elementary plaquette.

The single-particle dispersion relation ($U = 0$) for the model given by Eqn.(4.12) is given in Fig.(4.12 a). It exhibits two bands, with the lower (α) band having degenerate minima at momenta $k = 0, \pi$. This leads to a large number of many-body ground states to be degenerate. So a ground state of N bosons correspond to having N_1 bosons in one minimum, and the rest in the other one. The minimum at $k = 0$ ($k = \pi$) has a wavefunction that is located on leg-a (leg-b).

The dispersion relation can be viewed from a different perspective as well. For

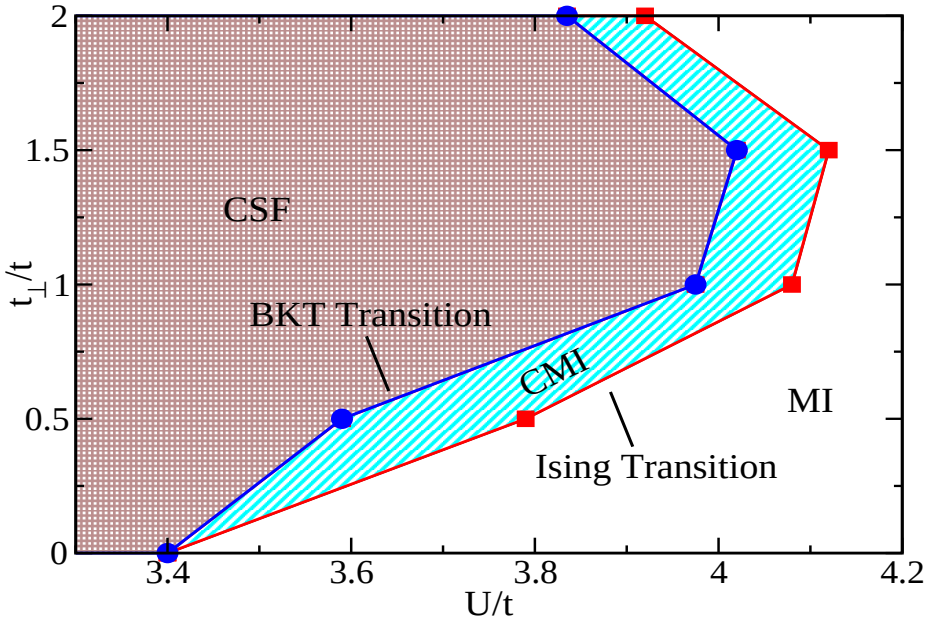

Fig. 4.14: The phase diagram for a 2-leg Bose ladder, with π flux per plaquette

$U = 0$, and $t_\perp = 0$, the dispersion is as shown in the upper panel of Fig.(4.13), with two bands (corresponding to each leg of the ladder) being inverted with respect to each other, and intersecting at $k = \pm\pi$. The band with the minimum located at $k = 0$ corresponds to leg-a, whereas the one with the maximum at $k = 0$ denotes leg-b. When $t_\perp$ is non-zero, the degeneracies at the points of intersection gets lifted. This leads to the formation of two bands with a gap as shown in the lower panel in Fig.(4.13). The two minima in the lower band located at $k = 0$ and π originate from the bands corresponding to each of the legs. The $k = 0$ minimum corresponds to bosons being localized in leg-a, whereas $k = \pi$ has bosons in leg-b. A single-particle condensate wave function for $U = 0$ can thus be written as a linear superposition of the states residing at the two minima.

In the presence of non-zero repulsive interaction, U, the system will avoid double oocupancy at a single site. Thus an equal distribution of bosons in both the legs will be favoured. Hence the single-particle condensate wave function has equal probability amplitudes in the states $|k = 0\rangle$ and $|k = \pi\rangle$ with a relative and global phase.

4.3.1 Methods

We used the FS-DMRG method [19] to compute the ground state properties of this system described by Eqn.(4.12). For convenience, we have mapped the 2-leg Bose-ladder into one single chain, carefully keeping track of the hopping parameters. We went upto system sizes of 200, which is equivalent to 100 rungs of the ladder system. The calculations were carried out at a filling factor of 1, with the size of the local Hilbert space in each site fixed to 6. 200 density matrix states were retained, with the error of the weights of the discarded states being less than 10^{-5}. The following relevant physical quantities were computed using the ground state wave function :

- Momentum distribution

$$n(k) = \frac{1}{L}\sum_{x,x'} e^{ik(x-x')}[\langle a_x^\dagger a_{x'}\rangle + \langle b_x^\dagger b_{x'}\rangle] \tag{4.13}$$

- Rung current structure factor

$$S_j(k) = \frac{1}{L^2}\sum_{x,x'} e^{ik(x-x')}\langle j_x j_{x'}\rangle \tag{4.14}$$

  where $j_x = i(a_x^\dagger b_x - b_x^\dagger a_x)$

4.3.2 Results

We first present the phase diagram exhibited by a system of ultracold bosons loaded in a 2-leg ladder following the hamiltonian given by Eqn.(4.12) in Fig.(4.14). As a result of the competition between the on-site interaction, (U), intra-chain hopping (t), and inter-chain hopping ($t_\perp$), three different quantum phases arise; the chiral superfluid (CSF), the chiral Mott insulator (CMI), and the regular Mott insulator (MI).

To understand the emergence of these phases, we study the phase diagram more carefully. When the repulsion (U) is small, the system exhibits a gapless SF region with

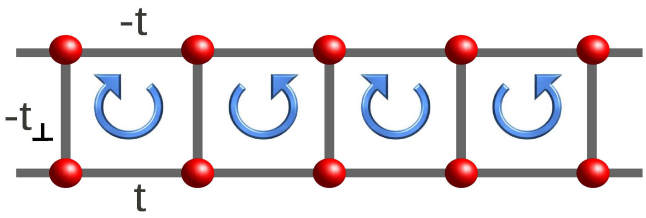

Fig. 4.15: The vortex and antivortex picture of CMI

a finite loop current order in each plaquette, which we call the chiral SF (CSF). For intermediate values of U, the system undergoes a transition from CSF to a phase which has a finite charge gap. This novel phase simultaneously supports staggered loop current

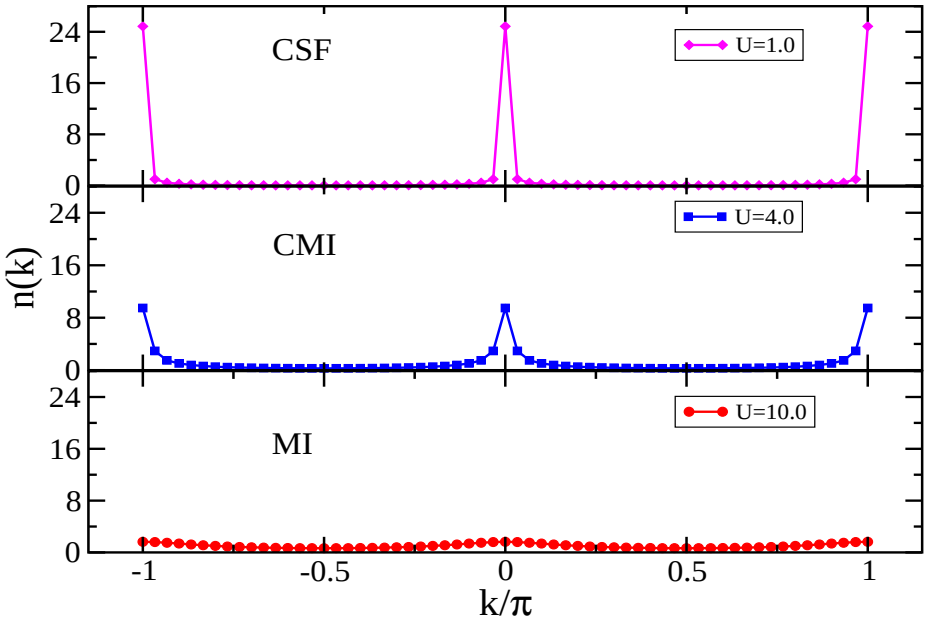

Fig. 4.16: The momentum distribution plotted for three different phases, all of them showing peaks at $k = 0, \pi$

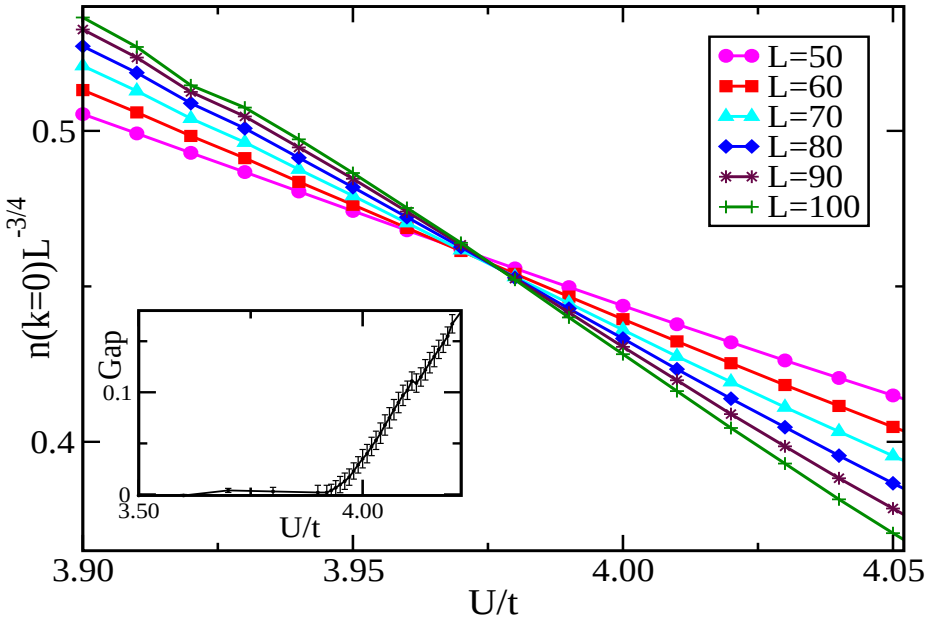

Fig. 4.17: $n(0)L^{-3/4}$ plotted as a function of U/t for different system sizes, showing a crossing point at 3.98 which we identify as the CSF-CMI transition point which is in the BKT universality class. The inset shows the charge gap opening up at this transition into the inuslator

and spontaneously breaks time-reversal symmetry. We have named this phase as the chiral Mott insulator (CMI). The transition from CSF to CMI belongs to the Berezenskii-Kosterlitz-Thouless (BKT) class. Further increase of U breaks this loop current order also, and the system undergoes an Ising transition to enter the regular MI phase.

An alternate physical picture of the CMI phase can be obtained if we consider the CSF phase, with staggered currents as a vortex crystal, where vortices and antivortices are nucleated by the presence of frustration, and locked into an "antiferromagnetic" pattern, due to strong intervortex repulsion as shown in Fig.(4.15). Large values of U causes this crystal to melt, thus delocalizing the vortices completely. This vortex superfluid is nothing but the regular MI phase. However, if a small number of defect vortices in the vortex crystal delocalize, they kill superfluidity, but still retain the background vortex crystallinity. This vortex supersolid is the dual description of CMI.

We now plot the momentum distribution in Fig.(4.16). As expected from the dispersion relation, we observe two peaks at $k = 0, \pi$ respectively in all the phases. We

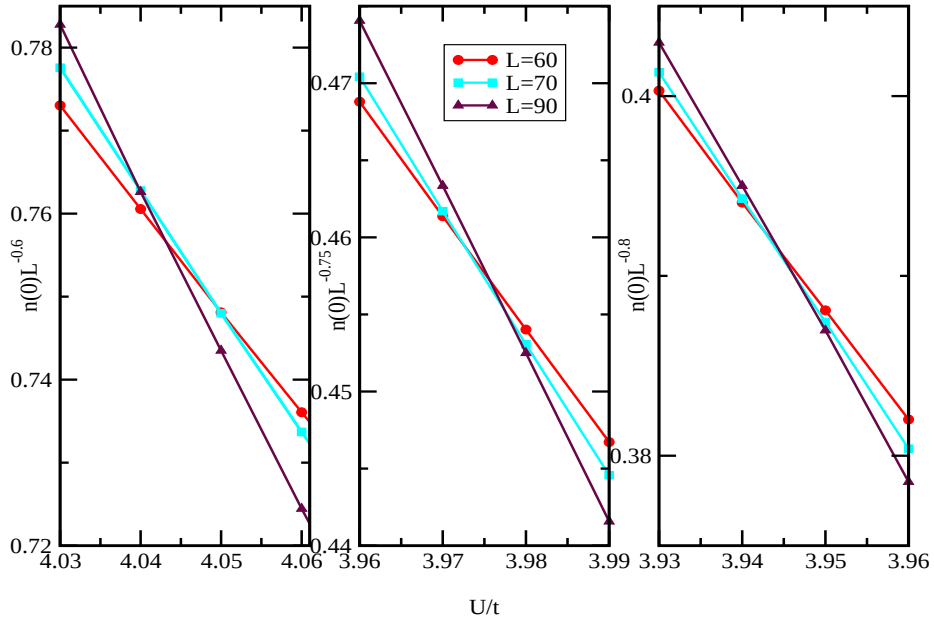

Fig. 4.18: $n(0)L^{-\alpha}$ as a function of U/t for three different values of α =0.6 (left), 0.75 (middle) and 0.8 (right) for different system sizes. The curves can be seen to cross sharply at $\alpha = 0.75$ and 0.8, but not at 0.6

plot the momentum distribution for U values corresponding to all the three phases. In the CSF phase, the two peaks are sharp and grow rapidly with system size. But in both the insulating phases, the peaks decrease in height, and a careful scaling analysis has shown that these peaks do not grow with system size. In the CMI phase, the peaks are still sharp in nature, but becomes distinctly broad in the MI phase.

It is known that at a BKT transition, the correlation function decays with distance following a power law as follows :

$$\langle a_x^\dagger a_{x'} \rangle = \langle b_x^\dagger b_{x'} \rangle \sim 1/|x - x'|^{1/4} \tag{4.15}$$

So $n(0)L^{-\alpha}$ with $\alpha = 3/4$ will be independent of the system length, L. Thus, to locate the critical point, we plot $n(0)L^{-3/4}$ for different L as a function of the tuning parameter, and the point where all the curves intersect each other is identified as the transition point from CSF to CMI phase. Fig.(4.17) plots $n(0)L^{-3/4}$ as a function of U/t with $t_\perp = t$. Curves for different lengths intersect at $U = 3.98(1)$, denoting the CSF-CMI transition. The inset of Fig.(4.17) shows the charge gap plotted against U/t. It becomes non-zero

at this point, signalling the onset of the insulating phase, thus providing a non-trivial consistency check for locating the critical point quite accurately.

To confirm that such an intersection is not obtained for $\alpha < 3/4$, we plot $n(0)L^{-\alpha}$ with $\alpha = 0.6$ and find that these curves for different lengths cross at significantly different U/t values as shown in Fig.(4.18) (left panel). Within the CSF phase, however we expect real-space correlations to decay slower than $1/|x - x'|^{1/4}$, so that curves of $n(0)L^{-\alpha}$ with $\alpha > 3/4$ are simply expected to cross at smaller U. This is shown in the Fig.(4.18) where the crossing point is much well defined for $\alpha = 0.75$ (middle panel) and $\alpha = 0.8$ (right panel)

Having located the CSF-CMI transition point accurately, we now turn to the CMI-MI transition. It is expected to belong to the Ising class, and so we use the scaling of rung current structure factor, $S_j(\pi)$ as shown in Fig.(4.19). If $S_j(k = \pi)$ scales linearly with the length, then it signifies a long-range staggered current order. We thus expect

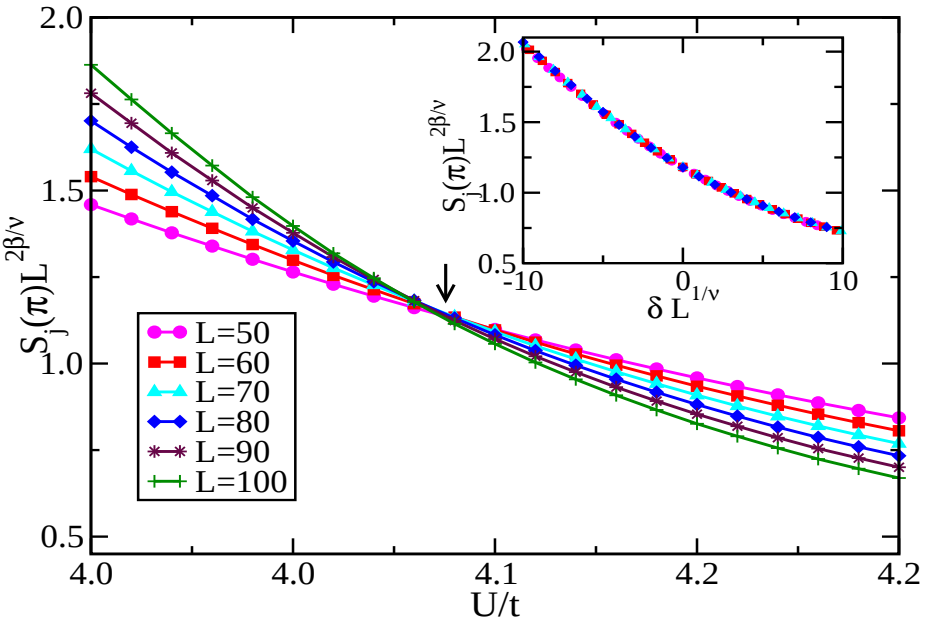

Fig. 4.19: Rung-current structure factor $S_j(\pi)L^{2\beta/\nu}$ vs U/t at $t_\perp - 1$. The intersection point yields the CMI-MI Ising transition at $U_c \approx 4.08t$. The inset shows $S_j(\pi)L^{2\beta/\nu}$ vs $\delta L^{1/\nu}$ with $\delta \equiv (U - U_c)/t$, for different U/t, leading to a scaling collapse for 2D Ising exponents $\nu = 1$ and $\beta = 1/8$

$S_j(k=\pi)$ to obey the critical scaling of the form

$$S_j(k=\pi)L^{2\beta/\nu} = f((U-U_c)L^{1/\nu}) \tag{4.16}$$

where U_c is the critical point for the CMI-MI transition, $f(..)$ is a universal scaling function, and $\beta = 1/8$ and $\nu = 1$ are the critical exponents for Ising-like transitions. As a result, curves of $S_j(k=\pi)L^{2\beta/\nu}$ for different lengths, L, are expected to intersect at the CMI-MI transition point, U_c. For $t_\perp = 1$, this crossing takes place at $U_c = 4.08$, as shown in Fig.(4.19). The inset of Fig.(4.19) plots the $S_j(k=\pi)L^{2\beta/\nu}$ as a function of $(U-U_c)L^{a/\nu}$. For $U_c = 4.08$, the plots show a complete collapse. Such an analysis, when performed for a range of values of $t_\perp/t$, allows us to map the critical points for the CMI-MI transition very accurately.

4.3.3 Conclusions

In Conclusion, we computed the phase diagram for the FFBH model for a 2-leg ladder, with π flux per plaquette, depicting three phases : CSF, CMI and MI phases. The CMI phase is sandwiched between the CSF and the MI phases. This remarkable phase is gapped and simultaneously supports staggered loop currents which spontaneously breaks time-reversal symmetry. The transition from CSF to CMI has been confirmed to be of the BKT type, whereas from CMI to MI belongs to the Ising class.

References

[1] P. Cheinet, S. Trotzky, M. Feld, U. Schnorrberger, M. Moreno-Cardoner, S. Foelling, I. Bloch, Phys. Rev. Lett. **101**, 090404 (2008).

[2] C. Becker *et al.*, New J. of Physics **12**, 065025 (2010).

[3] G.-B. Jo, J. Guzman, C. K. Thomas, P. Hosur, A. Vishwanath, and D. M. Stamper-Kurn, Phys. Rev. Lett. **108**, 045305 (2012).

[4] C. Chin *et al*, Rev. Mod. Phys. **82**, 1225 (2010).

[5] A. Eckardt, C. Weiss, and M. Holthaus, Phys. Rev. Lett. **95**, 260404 (2005).

[6] A. Zenesini, H. Lignier, D. Ciampini, O. Morsch, and E. Arimondo, Phys. Rev. Lett. **102**, 100403 (2009).

[7] Robert Roth, Keith Burnett, Phys. Rev. A **68**, 023604 (2003).

[8] V. G. Rousseau, D. P. Arovas, M. Rigol, F. Hèbert, G. G. Batrouni, R. T. Scalettar, Phys. Rev. B **73**, 174516 (2006).

[9] M. Rigol, A. Muramatsu, M. Olshanii, Phys. Rev. A **74**, 053616 (2006).

[10] I. Danshita, J. E. Williams, C. A. R. Sá de Melo, C. W. Clark, Phys. Rev. A **76**, 043606 (2007).

[11] Guo Huai-Ming, Liang Ying, Commun. Theor. Phys. (Beijing, China) **50**, 1142 (2008).

[12] Bo-Lun Chen, Su-Peng Kou, Yunbo Zhang, Shu Chen, Phys. Rev. A **81**, 053608 (2010).

[13] A. Dhar, T. Mishra, R. V. Pai and B. P. Das, Phys. Rev. A **83**, 053621 (2011).

[14] A. Dhar, M. Singh, R. V. Pai and B. P. Das, Phys. Rev. A **84**, 033631 (2011).

[15] A. Dhar, M. Majhi, T. Mishra, R. V. Pai, S. Mukerjee and A. Paramekanti, Phys. Rev. A (R) **85**, 041602 (2012).

[16] S. Greschner, L. Santos and T. Vekua, Phys. Rev. A **87**, 033609 (2013).

[17] T. Mishra, R. V. Pai, S. Mukerjee and A. Paramekanti, Phys. Rev. B **87**, 174504 (2013).

[18] P. Jordan, E. Wigner, Z. Phys. **47**, 631 (1928).

[19] S. R. White, Phys. Rev. Lett. **69**, 2863 (1992), Phys. Rev. B **48**, 10345 (1993).

[20] U. Schöllwock, Rev. Mod. Phys. **77**, 259 (2005).

[21] Y.-J Lin *et al.*, Nature (London) **462**, 628 (2009).

[22] M. Aidelsburger et al., Phys. Rev. Lett. **107**, 255301 (2011).

[23] K. Jimenéz-Garcia *et al.*, e-print arXiv:1201.6630.

[24] M. Polini, R. Fazio, A. H. MacDonald, and M. P. Tosi, Phys. Rev. Lett. **95**, 010401 (2005).

[25] V. M. Stojanović, C. Wu, W. V. Liu, and S. Das Sarma, Phys. Rev. Lett. **101**, 125301 (2008).

[26] L.-K. Lim, C. M. Smith, and A. Hemmerich, Phys. Rev. Lett. **100**, 130402 (2008).

[27] S. Sinha and K. Sengupta, Europhys. Lett. **93**, 30005 (2011).

[28] G. Wirth, M. Olschlager, and A. Hemmerich, Nat. Phys. **7**, 147 (2011).

[29] A. S. Sørensen, E. Demler, and M. D. Lukin, Phys. Rev. Lett. **94**, 086803 (2005).

Chapter 5

Time dynamics study of optical superlattices

5.1 Introduction

After studying the static part of the modified Bose-Hubbard model, taking into account the superlattice potential, we now turn our attention to the time-dependent scenario, where one parameter of the hamiltonian will be made a function of time. In particular, we would be interested in the effects of quasi-adiabatic dynamics of ultracold bosons loaded in a one-dimensional optical superlattice. Because of the recent developements in the experimental side, various parameters can be varied in time with sufficient control, such as the optical lattice depth or the magnetic field close to the Feshbach resonances [1]. Such exquisite experimental facilities has generated much interest to study both sudden and quasi-adiabatic quantum quenches.

Previous works have analysed the dynamical properties of BH model after a quasi-adiabatic crossing of the quantum critical point going from MI to SF and vice-versa [1, 2]. The evolution of various local observables such as density, compressibility, and on-site particle distribution were studied as a function of ramp time using numerical techniques[1, 2, 3, 4, 5, 6, 7, 8, 9, 10, 11, 12, 13, 14, 15, 16, 17, 18, 19, 20]. In both the cases, forma-

tion of topological defects were found. More recently, the effects of parabolic trapping potential were also taken into account [19, 20]. On the experimental side, quenches across the MI-SF quantum phase transition using ultracold atoms trapped in optical lattices were performed [21, 22, 23]. Using the time-of-flight measurements, excitations of the condensate formed after the quench were measured. It was observed that the degree of excitations and energy produced during the quench have a power-law dependence on the quench rate, suggesting the excitation process to be governed by Kibble-Zurek mechanism [24]. Moreover the redistribution of quasimomentum in a gas of atoms trapped in an optical lattice when the lattice depth is reduced was also investigated both experimentally and numerically [25]. Superposition of two optical lattices with different frequencies can give rise to the study of local relaxation dynamics if a sudden quench in the optical superlattice is performed.

The mechanism by which defects were formed in the case of classical phase transitions, by rapidly varying a thermodynamic parameter in order to drive the system out of equilibrium, in the context of the early universe was first studied by Kibble and Zurek [26, 27, 28]. More recently, this mechanism has been extended to quantum phase transitions [29, 30], for the case of adiabatic quenches across a transition point. Compared to classical phase transitons, the quantum phase transitions involve completely closed quantum mechanical evolution at zero temperature [31]. The quenches are performed by varying a parameter in the hamiltonian which will drive the system from one phase to another. The quantum evolution in some cases can be described to quite an extent by means of an effective two-level approximation with an avoided level crossing, within the Landau-Zener formalism [32, 33, 34]. This led to a number of theoretical studies on many-body systems, including quantum gases. Despite such efforts, many aspects involving the response of such systems to slow quenches needs further analysis. In fact, it is known that in the presence of non-isolated critical points or of extended critical regions, the validity of K-Z mechanism may not be that obvious. Although in some cases it is still

possible to predict the defect density by identifying a critical point or by using scaling arguments [9, 11, 12].

5.1.1 Kibble-Zurek Mechanism

The Kibble-Zurek mechanism (KZM) describes the non-equilibrium dynamics and the formation of topological defects in a system which is driven through a continuous phase transition across an isolated critical point between two gapped phases at a finite rate. This mechanism is attributed to Tom W. B. Kibble, who worked on the structure formation in early universe in the 1970's [27], and Wojciech H. Zurek, who carried forward this formalism to apply in the context of condensed matter systems [27]. The essence of the mechanism is an adiabatic-impulse-adiabatic approximation. This essentially means that during the very slow time evolution, when the system is far away from the critical region, is assumed to be adiabatic in nature, whereas in the close neighbourhood of the gapless critical point, we consider the system to be effectively frozen out, whereby the state will remain unchanged. As a result, the state after the transition has a finite correlation length $\hat{\xi} \sim \tau_Q^{\frac{\nu}{1+\nu z}}$, where τ_Q is a characteristic time of the adiabatic transition between the two phases and ν, z are the crtical exponents. This universal scale of length determines density of excitations or excitation energy above the ground state scales as an inverse power of the transition time, τ_Q [34].

It should be noted that the generalized KZM formalism is not only restricted to the above said scenario. Indeed it can be also extended to the case where one drives an infinite system into a gapped phase starting exactly at the critical point. It can also be applied to quantum phase transitions happening in space, and not time, i.e. the parameter in the hamiltonian driving the transition is time-independent, but inhomogeneous in space, so that different parts of the system are in different phases. The phase transition can also be driven in an inhomogeneous way such that some parts of the system cross the critical point earlier than the other.

KZM and the Landau-Zener (LZ) model of level crossing are closely related to each other. The adiabatic-impulse-adiabatic approximation, which forms the central theme in KZM, can be used to obtain approximate solutions of the LZ model in some limits of the parameters. There are certain classes of integrable models which can be mapped onto sets of independent LZ transitions. Such a treatment provides exact solutions supporting KZM and its generalisations. Time-dependent perturbation theory can also be the starting point to derive the KZM, although it only reproduces approximately the exact results in the integrable models.

Under a linear quench, KZM estimates the density of topological defects, and predicts that it obeys a power law in the quench rate. This prediction is universal in nature, and the power law exponent is given in terms of the critical exponents of the transition. The KZM generally applies to spontaneous symmetry breaking scenarios where a global symmetry is broken.

In this work, we consider a one-dimensional optical superlattice, with a periodicity of two sites, at integer density. Such a system at zero temperature will undergo a quantum phase transition between various phases, such as the conventional MI, SF and various superlattice induced Mott insulator (SLMI), which has a periodic modulation in the on-site occupancy [35, 36, 37]. We study the effects of a linear time variation of the superlattice potential such that the system crosses multiple critical points, beginning and ending in the insulator phases, thus passing through SF region. The problem of slow quenching becomes non-trivial in such a case where the system passes through a quantum critical point or/and a gapless superfluid region. Since the gap closes, the system is unable to stay in the equilibrium ground state of the instantaneous hamiltonian, no matter how slow the quench is performed. Near this non-adiabatic region, the correlation length and the relaxation time (the time taken for the system to relax to external perturbations) tends

to infinity. As a result, defects are formed which results in an excited state at the end of the time evolution. We are interested to study the defect formation in the final state after the quench is performed, and show a non-trivial scaling of the final excess energy as a function of the quench rate. We perform our studies in the realm of time-dependent density matrix renormalisation group method, in the formalism of matrix product states ansatz.

5.2 Model

The one-dimensional BH model modified for optical superlattice reads as follows :

$$H = -J \sum_{\langle i,j \rangle} a_i^\dagger a_j + \frac{U}{2} \sum_i n_i(n_i - 1) + \sum_i \lambda_i n_i \tag{5.1}$$

Here a_i and $a_i^\dagger$ are annihilation and creation operators respectively, signifying the hopping from one site to its neighbouring site, n_i is the number operator for a site i, and λ_i is the superlattice potential. For a two period optical superlattice, formed by the superposition of two optical lattices with one having double the frequency of the other, we can consider $\lambda_i = 0$ for odd sites and $\lambda_i = \lambda$ for even sites. In the absence of λ, the system underdoes a quantum phase transition from SF to MI at $U_c \approx 3.3$ as calculated using various numerical techniques. Now the presence of λ will shift the lattice depths at various sites, with repect to its neighbour.

At integer fillings, the system of ultracold bosons can exhibit various phases depending on the values of U and λ. For $U \leq U_c$, the system stays in SF phase for $\lambda = 0$. For a finite λ, the system goes to the SLMI phase with a configuration of [2 0 2 0 ...]. For $U \geq U_c$, the system stays on MI phase with one aton at each site for $\lambda = 0$. As λ is increased, the system enters the SF region when λ value becomes comparable to U value. A further increase in λ takes the system to SLMI phase, with a configuration of [2 0 2 0 ...]. The width of the intermediate SF region decreases as U value is increased as shown in Fig.(5.1).

We now vary λ linearly in time as :

$$\lambda(t) = \lambda_0 + (\lambda_f - \lambda_i).t/\tau \tag{5.2}$$

Here τ denotes the time of quench, while λ_0 and λ_f are the initial and final values

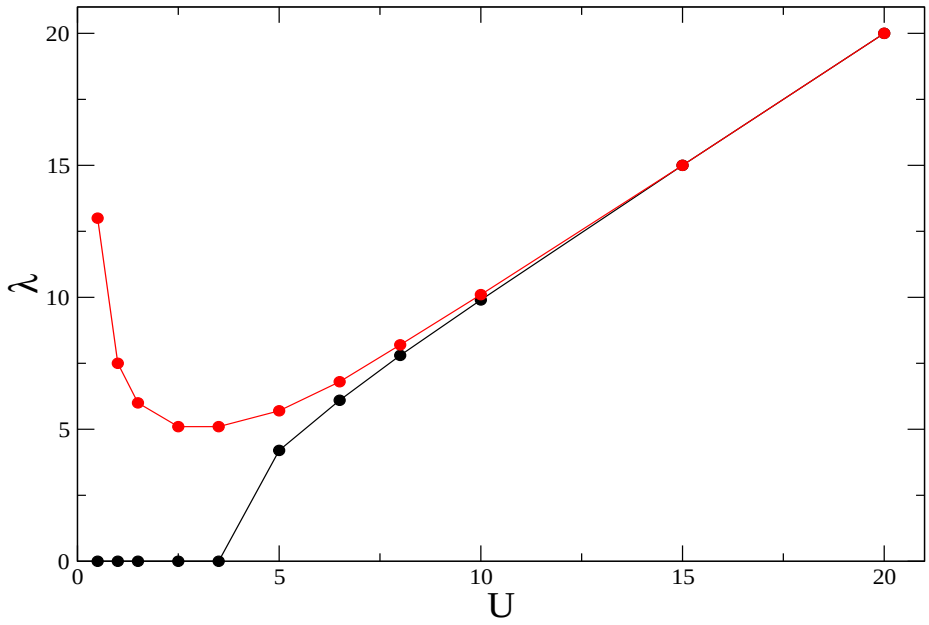

Fig. 5.1: Phase diagram of bosons in an optical superlattice with filling factor one

of the superlattice potential, λ before and after the quench, respectively. We fix the value of U, and choose accordingly λ_0 and λ_f such that the system starts off in the MI phase, passes through SF phase, and ultimately ends in the SLMI phase. This evolution scenario is true for all U values except for $U < U_c$, where the system starts in the SF phase and ends in SLMI phase. We perform the quench for various values of τ. Due to the presence of the gapless region, a finite number of defects will be formed in the final state after the time evolution, no matter how slow we perform the quench. Our primary aim is to see how the defect formation depends on τ, and in turn on U, since the width of the SF region depends on it as mentioned earlier.

The system wavefunction evolves according to the time-dependent Schrödinger equation as follows :

$$|\psi(t)\rangle = exp(-i \int_o^t H(t')dt')|\psi(0)\rangle \tag{5.3}$$

where $H(t')$ is the time-dependent hamiltonian according to which the system evolves, $|\psi(0)\rangle$ is the initial ground state of the hamiltonian with $\lambda = \lambda_0$. For our simulations,

we evaluated the final time evolved wavefunction, $|\psi(t)\rangle$ using the time-adaptive DMRG within the formalism of MPS. For numerical purposes, the integration is replaced by summation. We break up the time interval for evolution [0,τ] into many small slices, $(t, t+\Delta t)$ of time interval, $\Delta \ll 1$, approximating that $H(t)$ is constant during that small time-slice. The correponding time-evolution operator is $e^{-iH(t)\Delta t}$ is expanded using the sixth order Suzuki-Trotter (ST) decomposition. Let us spend some time to understand the ST decomposition in a bit more detail.

The first order ST decomposition is given by :

$$e^{-iHt} \approx (\prod_{1}^{L-1} e^{-iH(L,L+1)\Delta t})^n \tag{5.4}$$

where $n = \Delta t/t$, gives the discretization of time in small intervals Δt. $H(L, L+1)$ is the interaction hamiltonian (plus the local terms) between site L and $L+1$. Higher order decompositions can be performed by dividing the hamiltonian into two parts, F and G, defined by $F = \sum_{Leven} H(L, L+1)$, containing only the even bonds and $G = \sum_{Lodd} H(L, L+1)$, containing only the odd bonds. Since our hamiltonian consists of only nearest neighbour terms, F and G will commute. We can then have an even-odd expansion :

$$e^{-iHt} \approx (e^{-iF\frac{\Delta t}{2}} e^{-iG\Delta t} e^{-iF\frac{\Delta t}{2}})^n \tag{5.5}$$

This is the second order ST decomposition, in which the error is proportional to $(\Delta t)^3$. Similarly, higher order approximations can be applied. For an approximation of order p, the error involved is proportional to $(\Delta t)^{p+1}$. For a sixth order decomposition, we have

$$e^{-iHt} = \prod_{i=1}^{15} (e^{-iH_{(-1)^i c_i \Delta t}})^n + O(\Delta t)^7 \tag{5.6}$$

Here H_{odd}/H_{even} depends on i, and $H = H_{odd} + H_{even}$, and c_i are the coefficients.

Considering a time-step of $\Delta t = 0.05$, and a threshold in the weight of the discarded states as $\varepsilon = 10^{-9}$, by using a bond link dimension $m \leq 200$ states for all our simulations, in which we went to a system size of $L = 100$, and kept the size of the local Hilbert space of a particular site fixed to 4, that is, a maximum of three bosons can be accommodated at each site. In order to quantify the number of defects formed, we look at a quantity called residual energy, ΔE, which is the difference between the final energy of the system after evolution and the ground state energy of the final hamiltonian.

$$\Delta E = \langle \psi_f | H_f | \psi_f \rangle - \langle \psi_f^g | H_f | \psi_f^g \rangle \tag{5.7}$$

The above expression can be further simplified considering the entire eigen spectrum of the final hamiltonian, H_f. Let ψ_f^n denote the eigen functions of H_f, with $n = 0, 1, 2, ...$ The ground state eigenfunction corresponds to $n = 0$ which is also written as $n = g$ in the above equation. Since ψ_f^n forms a complete basis, the final wavefunction after time evolution can be expanded in this basis in the following way :

$$|\psi_f\rangle = \sum_n c_n |\psi_f^n\rangle \tag{5.8}$$

where c_n denotes the coefficients. Substituting this in the expression of residual energy, ΔE, we get,

$$\Delta E = \sum_n |c_n|^2 \langle \psi_f^n | H_f | \psi_f^n \rangle - \langle \psi_f^g | H_f | \psi_f^g \rangle \tag{5.9}$$

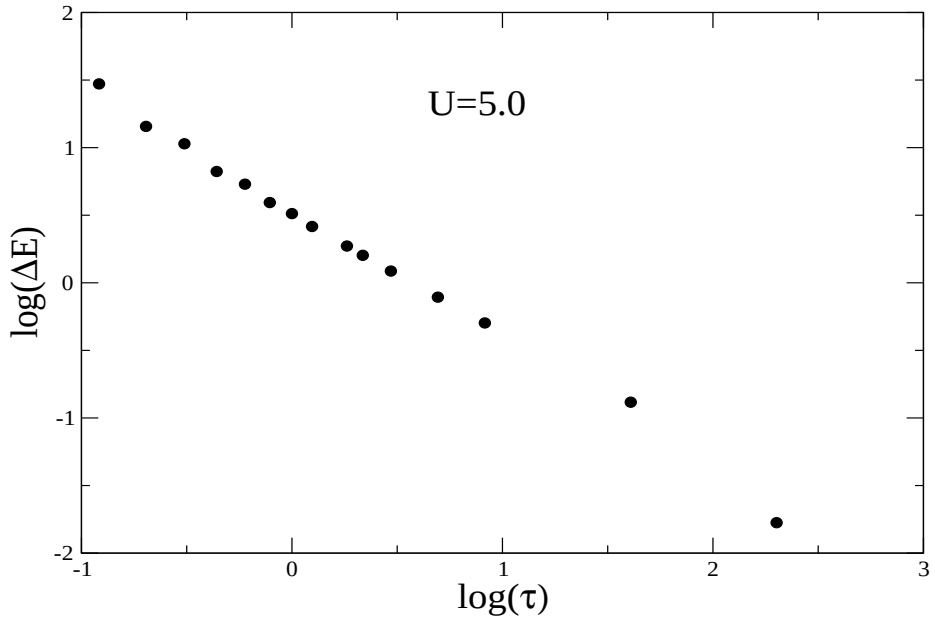

Fig. 5.2: Plot of residual energy vs $1/\tau$ for U=5.0

Separating the $n = 0$ part, and identifying $|\psi_f^n\rangle$ as eigenfunctions of H_f with eigenvalues E_f^n, we get

$$\Delta E = \sum_{n\neq 0} |c_n|^2 E_f^n + |c_0|^2 E_f^0 - E_f^0 \tag{5.10}$$

Since the states are normalised, $\sum_n |c_n|^2 = 1$, we therefore get

$$\Delta E = \sum_{n\neq 0} |c_n|^2 (E_f^n - E_f^0) \tag{5.11}$$

Hence it can be seen that the residual energy is a weighted sum of all the excitation energies. The number of defects, or in our case, the deviation from the final ground state is directly proportional to the residual energy.

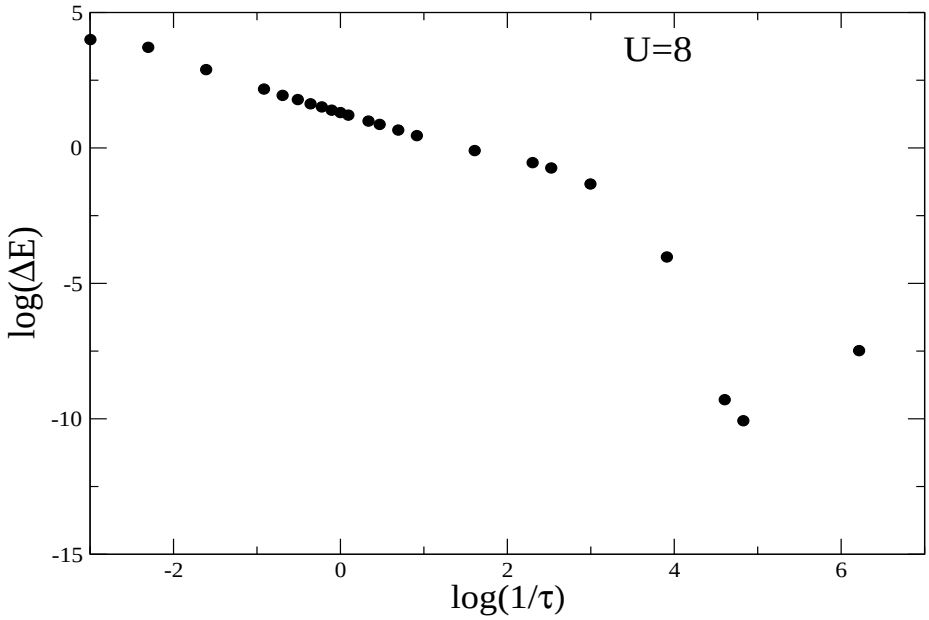

Fig. 5.3: Plot of residual energy vs $1/\tau$ for U=8.0

Table 5.1: List of λ_0 and λ_f for various U

U	λ_0	λ_f
2.5	0.0	8.0
5.0	2.5	7.5
8.0	5.5	10.5
10.0	7.5	12.5
15.0	12.5	17.5
20.0	17.5	22.5
25.0	22.5	27.5

5.3 Results

We now present the behaviour of the residual energy, ΔE, when the superlattice potential, λ is varied in time following Eqn.(5.2) with various rates. Particularly, we look for the scaling of ΔE as a function of τ for several values of on-site interaction, U, as shown in Figs.(5.3, 5.4, 5.5, 5.7). Table 5.1 lists the initial and final values of λ considered for each of the U values.

According to the K-Z mechanism, the residual energy typically follows a power law

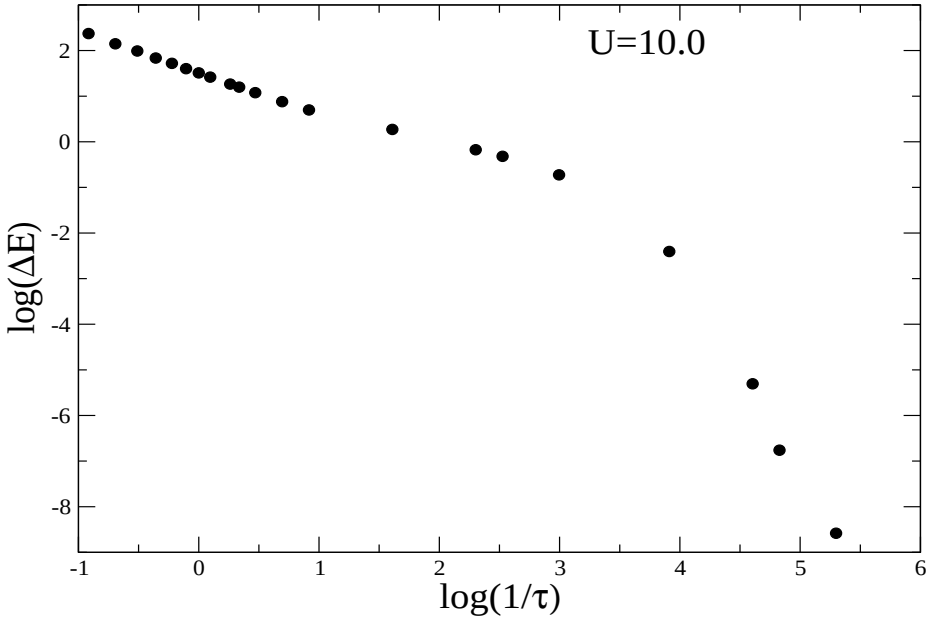

Fig. 5.4: Plot of residual energy vs $1/\tau$ for U=10.0

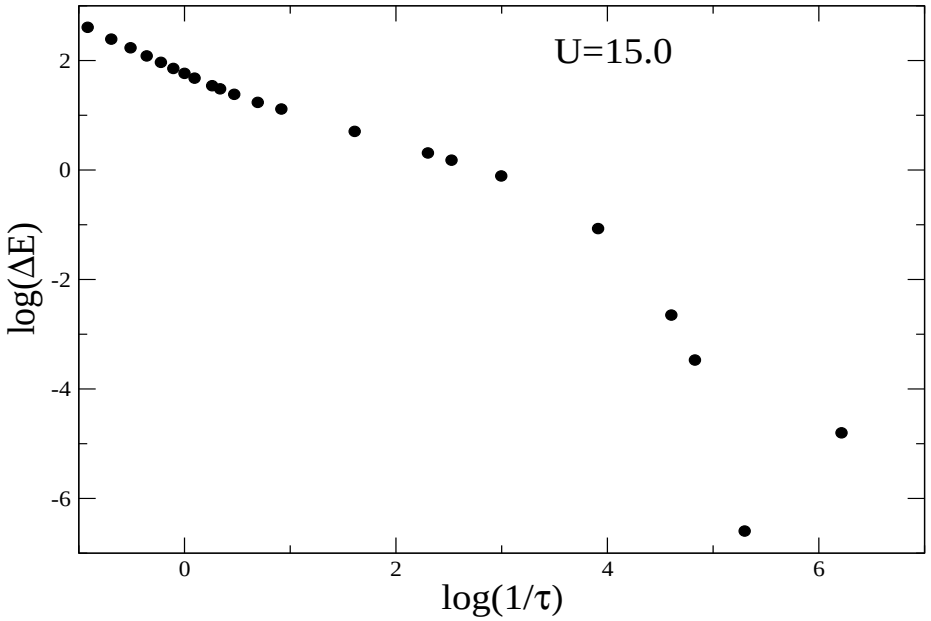

Fig. 5.5: Plot of residual energy vs $1/\tau$ for U=15.0

behaviour with the quench rate, τ as

$$\Delta E \sim \tau^{-\kappa} \tag{5.12}$$

where in some cases, the exponent κ can be predicted with high enough accuracy. Looking at the plots, we can identify three distinct regions as a function of τ. The very

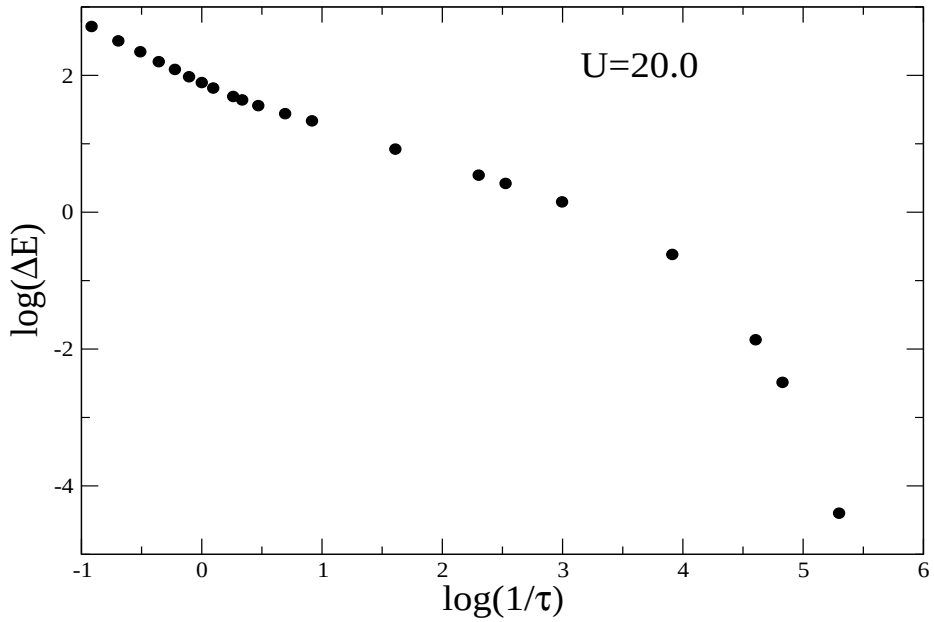

Fig. 5.6: Plot of residual energy vs $1/\tau$ for U=20.0

slow quench or the adiabatic limit ($\tau \gg 1$), which is characterised by a universal power law decay given by $\kappa = 2$. On the other side, when $\tau \ll 1$, it is the sudden quench, where the initial state is essentially frozen during such a fast quench, and the residual energy saturates with τ. The intermediate regime is the most interesting one, since it is crucially affected by the behaviour of the system about the critical points.

In recent years, KZ mechanism has been found useful to explain the dynamics of systems crossing isolated critical points. It also gives an accurate estimate of the scaling of the number of defects formed during the quench. Since residual energy is directly proportional to the number of defects formed, it provides a direct way to estimate κ in the intermediate regime. As an example, the exponent for 1D quantum Ising model turns out to be $\kappa^* = 0.5$, when one goes from one gapped phase to another passing through a critical point.

However the KZ formalism cannot be strictly applied to our case since the system goes from one gapped phase to another gapped phase, but passing through an extended gapless region, thus traversing through two critical points. Hence we expect different

Table 5.2: K-Z coefficients for various U

U	κ
2.5	0.98268
5.0	0.955161
8.0	0.932564
10.0	0.917662
15.0	0.866299
20.0	0.809662
25.0	0.752259

exponents in our problem. To extract the values of κ, we first identified the intermediate region, which will be different for various values of U considered, since the width of the SF phase varies with U. The results are reported in Fig.(5.7), and also listed in Table 5.2. We also tried to find the behaviour of κ with U, and found that it behaves as a power law also. In the large U limit, where the SF gap shrinks to a point, we find that κ approaches a value of 0.5, which is the same as the 1D quantum Ising model.

We also studied the dependence of the KZ coefficient on system size. For $U = 8.0$,

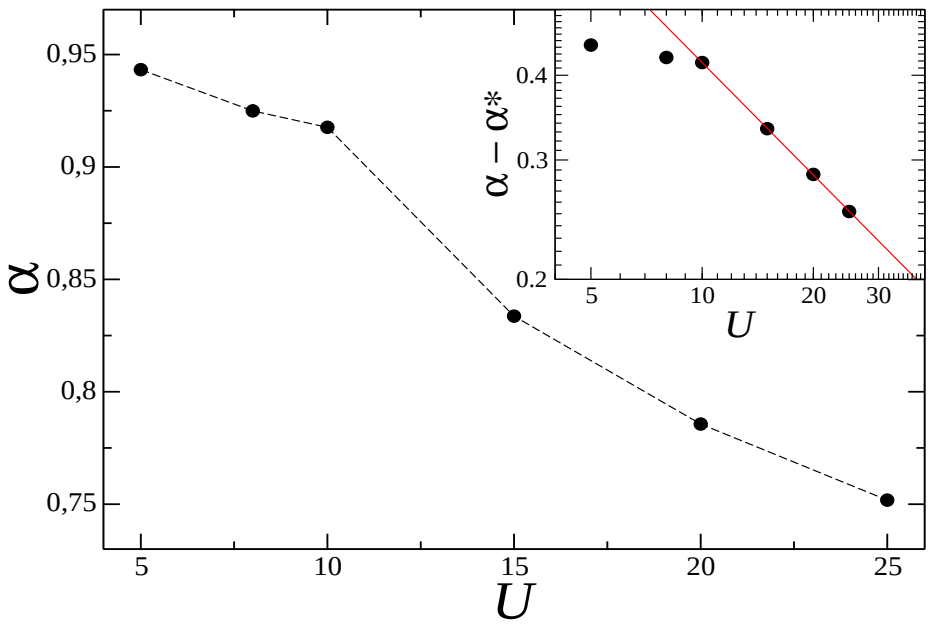

Fig. 5.7: Power law decay rate κ for the excess energy in the intermediate scaling region as a function of on-site interaction, U. The inset displays the same data in the log-log scale after a rescaling of $\kappa^* = 0.5$, while the straight line is the best fit to the numerical data for $U \geq 10$ correponding to $\kappa - \kappa^* = 1.485 \times U^{-0.551}$

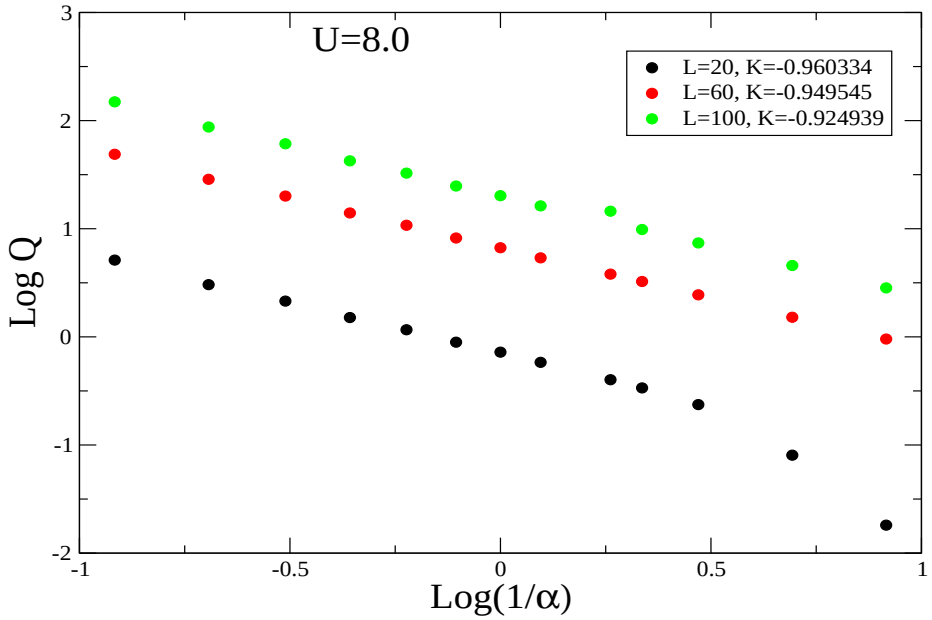

Fig. 5.8: Plots of residual energy as a function of τ for different system sizes

it resulted in a decrease of κ with increase in L, which is consistent with previous works, as shown in Fig.(5.8) [19].

5.4 Conclusions

In Conclusions, we have looked at the effects of quenching the superlattice potential as described in model (Eqn.(5.1)) linearly in time in the quasi- adiabatic regime. Such a quenching takes the system from the Mott insulator phase to the SLMI phase passing through a gapless SF region, thus crossing two critical points. The intermediate SF region width depends on the on-site repulsive interaction, U. Such a quenching process produces defects which depend on the rate of quench as well as U. Our analysis has shown a power law dependence of the residual energy on the quench rate, thus implying a Kibble-Zurek mechanism to be responsible for the production of defects. KZ coefficients at different values of U also show a power law behaviour, saturating at a value of 0.5, which coincides with the value for a Ising model when the system undergoes a quench from gapped to gapped phase, through a critical point.

References

[1] S.R. Clark and D. Jaksch, Phys. Rev. A **70**, 043612 (2004).

[2] R. Schützhold, M. Uhlmann, Y. Xu, and U.R. Fischer, Phys. Rev. Lett. **97**, 200601 (2006).

[3] J. Dziarmaga, Phys. Rev. Lett. **95**, 245701 (2005).

[4] R.W. Cherng and L. Levitov, Phys. Rev. A **73**, 043614 (2006).

[5] F.M. Cucchietti, B. Damski, J. Dziarmaga and W.H. Zurek, Phys. Rev. A **75**, 023603 (2007).

[6] L. Cincio, J. Dziarmaga, M.M. Rams, and W.H. Zurek, Phys. Rev. A **75**, 052321 (2007).

[7] T. Caneva, R. Fazio and G.E. Santoro, Phys. Rev. B **76**, 144427 (2007).

[8] T. Caneva, R. Fazio and G.E. Santoro, Phys. Rev. B **78**, 104426 (2008).

[9] F. Pellegrini, S. Montangero, G.E. Santoro, and R. Fazio, Phys. Rev. B **77**, 140404 (R) (2008).

[10] K. Sengupta, D. Sen, and S. Mondal, Phys. Rev. Lett. **100**, 077204 (2008).

[11] S. Deng, G. Ortiz, and L. Viola, Europhys. Lett. **84**, 67008 (2008).

[12] U. Divakaran, A. Dutta, and D. Sen, Phys. Rev. B **78**, 144301 (2008).

[13] A. Polkovnikov and V. Gritsev, Nature Phys. **4**, 477 (2008).

[14] C. De Grandi, R.A. Barankov and A. Polkovnikov, Phys. Rev. Lett. **101**, 230402 (2008).

[15] E. Canovi, D. Rossini, R. Fazio, and G.E. Santoro, J. Stat. Mech. P03038 (2009).

[16] V. Mukherjee and A. Dutta, Europhys. Lett. **92**, 37004 (2010).

[17] F.E. Zimmer and M. Haque, arXiv:1012.4492 (2010); arXiv:1110.0840 (2011).

[18] C. Trefzger and K. Sengupta, Phys. Rev. Lett. **106**, 095702 (2011).

[19] J.-S. Bernier, G. Roux, and C. Kollath, Phys. Rev. Lett. **106**, 200601 (2011).

[20] J.-S. Bernier, D. Poletti, P. Barmettler, G. Roux, and C. Kollath, Phys. Rev. A **85**, 033641 (2012).

[21] S. Fölling, S. Trotzky, P. Cheinet, M. Feld, R. Saers, A. Widera, T. Müller, and I. Bloch, Nature **448**, 1029 (2007).

[22] M. Cramer, A. Flesch, I.P. McCulloch, U. Schollwöck, and J. Eisert, Phys. Rev. Lett. **101**, 063001 (2008); Phys. Rev. A **78**, 033608 (2008).

[23] S. Trotzky, Y.-A. Chen, A. Flesch, I.P. McCulloch, U. Schollwöck, J. Eisert, and I. Bloch, Nature Phys. **8**, 325 (2012)

[24] D. Chen, M. White, C. Borries, and B. DeMarco, Phys. Rev. Lett. **106**, 235304 (2011).

[25] David C. McKay, Brian DeMarco, arXiv:1211.4772v1.

[26] T.W.B. Kibble, J. Phys. A: Math. Gen. **9**, 1387 (1976).

[27] W.H. Zurek, Nature **317**, 505 (1985).

[28] W.H. Zurek, U. Dorner, and P. Zoller, Phys. Rev. Lett. **95**, 105701 (2005).

[29] A. Polkovnikov, Phys. Rev. B **72**, 161201(R) (2005).

[30] B. Damski, Phys. Rev. Lett. **95**, 035701 (2005).

[31] S. Sachdev, *Quantum Phase Transitions*, Cambridge University Press, Cambridge (1999).

[32] L.D. Landau and E.M. Lifshitz, *Quantum Mechanics*, 3rd ed. ,Pergamon, New York (1991).

[33] C. Zener, Proc. R. Soc. A **137**, 696 (1932).

[34] J. Dziarmaga, Advances in Physics, vol. **59**, issue 6, pp. 1063-1189 (2010).

[35] V. G. Rousseau, D. P. Arovas, M. Rigol, F. Hebert, G. G. Batrouni, and R. T. Scalettar, Phys. Rev. B **73**, 174516 (2006).

[36] A. Dhar, T. Mishra, R. V. Pai and B. P. Das, Phys. Rev. A **83**, 053621 (2011).

[37] A. Dhar, M. Singh, R. V. Pai and B. P. Das, Phys. Rev. A **84**, 033631 (2011).

Chapter 6

Conclusions and Future Directions

6.1 Conclusions

We now summarize the findings that have been described in the previous chapters. This thesis has primarily aimed at the study of the behaviour of ultracold atoms when loaded in an optical superlattice. The search for novel quantum phases that can be exhibited by these systems is the principal motivation for the present work. This has been achieved by combining the power of quantum many-body theories with state-of-the art numerical methods.

We started by investigating a system of ultracold atoms in an optical superlattice in the context of the Bose-Hubbard model. In the absence of a superlattice potential, the system of soft-core bosons exhibit two distinct quantum phases at the filling factor of one. When the ratio of the hopping amplitude (t) to the on-site repulsive interaction (U) is small, the Mott insulator phase is found to exist, whereas in the opposite extreme, the superfluid phase is the preferred ground state. This quantum phase transition occurs at a critical value of (t/U). Turning on the superlattice potential breaks the translational symmetry of the system. Our analysis has shown that for on-site repulsive interaction amplitudes smaller than the critical value, the system stays in the gapless superfluid phase

in the absence of the superlattice potential. As the superlattice potential is increased, the system undergoes a transition to a gapped phase, which has a periodic variation in the number occupancy of the individual sites, of the form [2 0 2 0 ...]. The behaviour of the ultracold atoms becomes even more interesting when the on-site repulsive interaction amplitude is greater than the critical value. In the absence of the superlattice potential, the system resides in the gapped Mott insulator phase with all the sites being occupied by one atom. As the superlattice potential is increased, the gap gradually decreases, and ultimately vanishes when the superlattice potential becomes comparable in magnitude to the on-site repulsive interaction. This results in the emergence of the gapless superfluid phase. It should be noted that this superfluid phase exists even at large values of the repulsive interaction. Further increase of the superlattice potential reopens the gap with the system entering a gapped phase with a periodic variation in the number density of the form [2 0 2 0 ...]. This novel phase is peculiar to the superlattice potential, and hence we named it as superlattice induced Mott insulator. At density half, the system undergoes a transition from the superfluid phase to the gapped phase with configuration [1 0 1 0 ...]. At other incommensurate densities, the system remains a superfluid throughout, but with a finite density wave order [1, 2].

We had used the density matrix renormalisation group method and the mean field decoupling approximation to study the above mentioned problems in one and higher dimensions respectively. Both the approaches yielded results that are in qualitative agreement with each other. From the ground state wave functions and energies, we evaluated various physical quantities of our interest, which were used to distinguish between various quantum phases and characterise them. We presented a complete phase diagram for the system of optical superlattice at density one.

The introduction of the three-body on-site interaction in the above scenario significantly modifies the phase diagram. At lower densities, the three-body effects will not be there since the probability of having more than three atoms at a particular site is

extremely small. At higher densities, there is a marked signature of the presence of three-body effects. The insulating lobes get bigger in the phase diagram. Also the location of the presence of the intermediate superfluid phase gets displaced in the presence of three-body interaction [3].

Frustrated models embody rich physics, and we analysed two such cases in detail. The first model that was considered was an optical superlattice with the nearest and next-nearest hopping amplitudes being finite. This model can be mapped exactly into a zig-zag ladder with the two legs of the ladder having different potential depths. Hard-core bosons at half-filling, in the absence of a superlattice potential remains in the superfluid phase for positive values of the next-nearest hopping ampltude. Negative next-nearest hopping induces frustration in the system which results in a transition from the superfluid phase to a gapped bond ordered phase. Finite superlattice potential values in the absence of next-nearest hopping takes the system to the superlattice induced Mott insulator phase with a configuration of [1 0 1 0 ...]. On the positive next-nearest hopping region, the system undergoes a transition from this gapped phase to the gapless superfluid phase. On the other hand, for negative values of next-nearest hopping the system goes from the gapped superlattice induced Mott insulator phase to another gapped bond ordered phase [4].

The second model we considered was that of a two leg ladder, but with inter and intra-chain hopping such that an effective π flux per plaquette is induced. At high values of the on-site repulsive interaction, the system resides in the standard Mott insulating phase with a finite gap. At low values of the interaction, the system is in the superfluid phase with finite loop current order in each of the plaquettes. We call this phase as the chiral superfluid phase. For intermediate values of the interaction, the system chooses the ground state with a finite charge gap and also simultaneously supports a staggered loop current, thus spontaneously breaking time reversal symmetry. This remarkable novel quantum phase is called the chiral Mott insulator [5, 6].

Having explored the ground state properties of ultracold bosonic atoms in an optical superlattice using the Bose-Hubbard model, we also addressed the dynamics of this system. By considering the superlattice potential as a function of time, the system is allowed to evolve, and the properties are investigated after the time evolution. The choice of the initial and final values of the superlattice potential are made such that the system starts off in the Mott insulating phase, passes through the superfluid phase, and then becomes a superlattice induced Mott insulator. In this journey, the system passes through two quantum critical points, and hence the final evolved state is expected to have defects present in it. The number of defects formed is proportional to the residual energy, and it is observed to scale with the rate of quenching, following a power law behaviour. We therefore conclude that the Kibble-Zurek mechanism holds for this system in order to explain the generation of defects. An interesting observation we made was that the exponent of the power law depended on the width of the superfluid region.

6.2 Future Directions

The rapidly developing field of ultracold atoms has brought to the fore a wide range of important problems that can be explored in the future. Some of them are listed below.

- Ultracold molecules are becoming increasingly important especially now that it is possible to experimentally cool and trap them in optical lattices. The study of molecules with long-range interactions due to strong dipole moments can exhibit a number of novel quantum phases depending on internal states. Internal states include hyperfine and rotational degrees of freedom that can be controlled using external fields.

- The dynamics of ultracold molecules with long-range interactions will be worth investigating. At incommensurate densities, the supersolid phase exists in such systems. Hence it would be quite interesting to study the dynamics in such systems,

and to shed light on whether this dynamics would be regular or chaotic in nature. Investigating the validity of the Kibble-Zurek mechanism in such evolution secnarios will also be interesting, where analytical studies are not possible including non-integrable systems.

- Another problem which is of current interest is the role of quantum chaos and the outstanding question of the relation between chaos analogs in strongly-correlated systems, semiclassical chaos, and spatial entanglement. The latter is naturally tracked dynamically in the matrix product state method.

- Two dimensional optical lattices with long-range interaction can give rise to various types of charge density waves, by taking into account different nearest neighbour couplings. A detailed exploration of the elusive supersolid phase and its properties in a two dimensional optical lattice can be investigated.

- Quantum magnetism, especially the study of frustrated antiferromagnets have been at the cutting edge of condensed matter physics for decades, having implications from high temperature superconductors to spintronic devices. Cold atoms offer opportunities to create various frustrated spin models in triangular, or even Kagome lattices. In the past few years, quantum magnetism involving higher spins [SU(N)] has been a topic of considerable interest. It has been proposed that such SU(N) Hubbard model describing N-flavor fermions hopping on a lattice with flavor-independent on-site interactions can be achieved using ultracold alkaline-earth-metal atoms. We can consider a dimerized 2D optical lattice and triangular lattice with fermions of spin greater than 1/2, along with different hopping among neighbouring sites. The inclusion of harmonic trap in such a system will also give rise to interesting physics.

- The dynamics of the zig-zag ladder with optical superlattice where the system is quenched across different quantum critical points can be investigated, and the validity of the Kibble-Zurek mechanism can be checked.

- The projects described above involve bosonic atoms. It would be perfectly in order to focus on ultracold fermionc gases, and explore novel quantum phases and new types of quantum dynamics possible for systems with long-range interactions.

- The density matrix renormalisation group method and the matrix product states method yield very accurate results for one-dimensional systems, but fail to do so in higher dimensions. Hence, developing a method which would be suitable in higher dimensions could be a challenging project. One such candidate is the coupled cluster method, but to date, it has not been formulated for bosonic atoms in optical lattices. This method has been applied to spin systems in two dimensions, and has shown to reproduce fairly accurate results and provide new insights. This provides the impetus to develop suitable coupled cluster formalisms that could be fruitfully applied to ultracold bosonic and fermionic atoms in two and three dimensional optical lattices.

The last two decades have been a witness to an overwhelming progress in atomic, molecular and optical (AMO) physics. It can be undoubtedly said that ultracold atoms will be at the forefront of modern physics for the coming decades. As mentioned in the Introduction chapter in this thesis, it has a wide range of applications, starting from fundamental physics to industrial purposes. Till date eight physicists have been awarded the Nobel Prize in Physics, the latest being in 2012. This clearly implies the importance of the field of ultracold atoms. Because of great advancements in trapping of ultracold atoms and molecules in various optical lattice geometries, experimentalists have been able to reach regimes which were unthinkable even one decade ago. The high degree of controllability and tunability for various system parameters, together with the near defect free systems, have caused these systems to become testbeds for phenomena from various branches of physics. Along with the experimental progress, this is also the right moment for theoreticians to investigate different systems and predict novel quantum phases with

signatures which can be observed experimentally. The future directions proposed in this thesis is extremely relevant in the current scenario, and if pursued, would surely contribute a lot to the scientific community.

References

[1] A. Dhar, T. Mishra, R. V. Pai and B. P. Das, Phys. Rev. A **83**, 053621 (2011).

[2] A. Dhar, M. Singh, R. V. Pai and B. P. Das, Phys. Rev. A **84**, 033631 (2011).

[3] Manpreet Singh, Arya Dhar, Tapan Mishra, R. V. Pai, and B. P. Das, Phys. Rev. A **85**, 051604 (R) (2012).

[4] Arya Dhar, Tapan Mishra, R. V. Pai, Subroto Mukerjee and B. P. Das, arXiv:1307.4053.

[5] Arya Dhar, Maheswar Majhi, Tapan Mishra, R. V. Pai, Subroto Mukerjee, Arun Paramekant, Phys. Rev. A **85**, 041602 (R) (2012).

[6] **Arya Dhar**, Tapan Mishra, Maheswar Majhi, R. V. Pai, Subroto Mukerjee, Arun Paramekanti, Phys. Rev. B **87**, 174501 (2013).